Zeitschrift: IABSE reports = Rapports AIPC = IVBH Berichte

Band: 79 (1998)

Rubrik: Working session: Environmental actions on bridges. Papers and posters

Nutzungsbedingungen

Die ETH-Bibliothek ist die Anbieterin der digitalisierten Zeitschriften auf E-Periodica. Sie besitzt keine Urheberrechte an den Zeitschriften und ist nicht verantwortlich für deren Inhalte. Die Rechte liegen in der Regel bei den Herausgebern beziehungsweise den externen Rechteinhabern. Das Veröffentlichen von Bildern in Print- und Online-Publikationen sowie auf Social Media-Kanälen oder Webseiten ist nur mit vorheriger Genehmigung der Rechteinhaber erlaubt. Mehr erfahren

Conditions d'utilisation

L'ETH Library est le fournisseur des revues numérisées. Elle ne détient aucun droit d'auteur sur les revues et n'est pas responsable de leur contenu. En règle générale, les droits sont détenus par les éditeurs ou les détenteurs de droits externes. La reproduction d'images dans des publications imprimées ou en ligne ainsi que sur des canaux de médias sociaux ou des sites web n'est autorisée qu'avec l'accord préalable des détenteurs des droits. En savoir plus

Terms of use

The ETH Library is the provider of the digitised journals. It does not own any copyrights to the journals and is not responsible for their content. The rights usually lie with the publishers or the external rights holders. Publishing images in print and online publications, as well as on social media channels or websites, is only permitted with the prior consent of the rights holders. Find out more

Download PDF: 07.02.2026

ETH-Bibliothek Zürich, E-Periodica, https://www.e-periodica.ch

Working Session

Environmental Actions on Bridges

Papers and Posters

Leere Seite
Blank page
Page vide

Wind Tunnel Experiments with Active Control of Bridge Section Model

Henriette I. HANSEN
Ph.D. Student
Aalborg Univ.
Aalborg, Denmark

Henriette I. Hansen, born 1966, got her M. Sc. in Civil engineering in 1991 from Aalborg Univ. Before she started as a Ph.D.-student in 1993 she worked as a research engineer for Computational Safety & Reliability in Aalborg.

Palle THOFT-CHRISTENSEN
Prof. Dr
Aalborg Univ.
Aalborg, Denmark

Palle Thoft-Christensen, born 1936, got his M. Sc. in civil engineering in 1960 and his Ph.D. in mathematical plasticity theory in 1963 from the Technical Univ. of Denmark. His main research areas are structural reliability and optimisation.

Summary

This paper describes results of wind tunnel experiments with a bridge section model where movable flaps are integrated in the bridge girder so each flap is the streamlined part of the edge of the girder. This active control flap system is patented by *COWIconsult* [1] and may be used to increase the flutter wind velocity for future ultra-long span suspension bridges. The purpose of the wind tunnel experiments is to investigate the principle to use this active flap control system. The bridge section model used in the experiments is therefore not a model of a specific bridge but it is realistic compared with a real bridge. Five flap configurations are investigated during the wind tunnel experiments and depending on the actual flap configuration it is possible to decrease or increase the flutter wind velocity for the model.

1 Introduction

During the last decades the span length of suspension bridges has grown rapidly. During 1998 two very long suspension bridges are planned to be opened for traffic, namely the *Akashi Kaikyo Bridge* in Japan with span length 1,991 m and the *Great Belt Bridge* in Denmark with span length 1,624 m. Of future ultra-long span suspension bridges that may be constructed can be mentioned the Messina *Crossing* with the span length 3,300 m and the crossing of the *Gibraltar Straits,* see Brown [4].

To increase the span length the suspension bridge can be optimised with regard to materials, deck shape and cables as described by Brown [4), Gimsing [7], Astiz [3], Ostenfeld [10] and Ostenfeld & Larsen [11]. Another possibility may be to introduce the *intelligent bridge,* where active control systems are used to limit the vibrations. A step in this direction is to introduce passive control systems, e.g. viscoelastic damping elements, tuned mass dampers and eccentric masses, as described by Ostenfeld & Larsen [11]. In advanced aircrafts actively controlled surfaces are moved relatively to the main surfaces (wings, flaps or ailerons) on which they exert control [11]. The control surfaces are moved by hydraulics based on measurements from sensors attached to the main surfaces. The same principle could be applied to bridges as patented by *COWIconsult* [1].

2. Wind Loads

For ultra-long span suspension bridges the main aeroelastic effect of concern is flutter, see Astiz [3] and Larsen & Walther [9]. In flutter the motion-induced wind load is dominating the wind load. Flutter occurs at a critical wind velocity at which the energy input from the motion-induced wind load is equal to the energy dissipated by structural damping, see Dyrbye & Hansen [5]. The critical wind velocity is called the flutter wind velocity.

The motion-induced wind loads on a streamlined bridge deck with integrated flaps can be described by aerodynamic derivatives. For new bridge designs these coefficients must be estimated by wind tunnel tests or by numerical flow simulations. For flexible bridges the cross-sectional shape of the bridge deck is the most dominating factor on the wind loads, see Scanlan [12). Therefore, bridge section models are used to estimate the aerodynamic derivatives. During preliminary bridge design the aerodynamic derivatives may be approximated by the values for a flat plate. Theodorsen [13] has derived the force and moment on a flat plate with a trailing flap. This context can be extended to include the leading flap by assuming that the rotation of the leading flap has no effect on the circulation. The results of the wind tunnel experiments are compared with the theoretical results for a flat plate with both leading and trailing flaps.

3. Test Set Up

Experiments have shown that the critical wind velocity for a streamlined girder is much higher than for a rectangular girder, see Ostenfeld & Larsen [11]. The bridge section model is therefore made streamlined with the flaps as the streamlined part. The cross-sectional shape of the model equipped with flaps is shown in figure 1. The width of the model exclusive flaps is B, the height of the model is $0.15\,B$ and each of the flaps has the length $0.25\,B$.

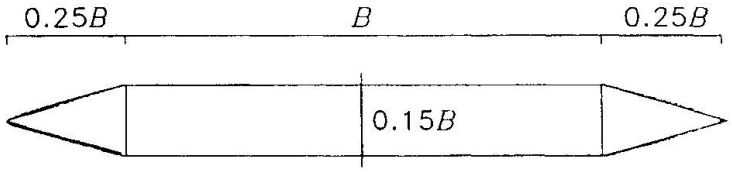

Figure *1: Cross-sectional shape of bridge*

The selected scaling factors and the parameters for the model are shown in table 1 and 2, respectively,

Scaling factor	Symbol	Value
Length	λ_L	1/40
Wind velocity	λ_V	1/4
Mass density of surroundings	λ_ρ	1

Table 1: Selected scaling factors.

Parameter	Symbol	Value
Width of model inclusive flaps	B	0.937 m
Mass per unit length	m	17.94 kg/m
Mass moment of inertia per unit length	I	0.589 kg m^2/m
Circular frequency for bending	ω_z	5.2 rad/s
Circular frequency for torsion	ω_α	10.1 rad/s
Structural damping in bending	ζ_z	0.012
Structural damping in torsion	ζ_α	0.008

Table 2.- Parameters for bridge section model.

The model is connected to a horizontal extension rod in each side which is going through the wind tunnel wall. The suspension system is the same in both sides. The extension rod is connected to an arm with dummy masses that can be moved on the arm so the model can represent the correct mass and mass inertia. Each side of the arm is suspended in a helical spring. The springs can be moved on the arm so the stiffness corresponding to the torsional motion of the model can be adjusted. Finally the extension rod is connected to a windward drag wire and a leeward drag wire. A simplified illustration of one side of the suspension system is shown in figure 2.

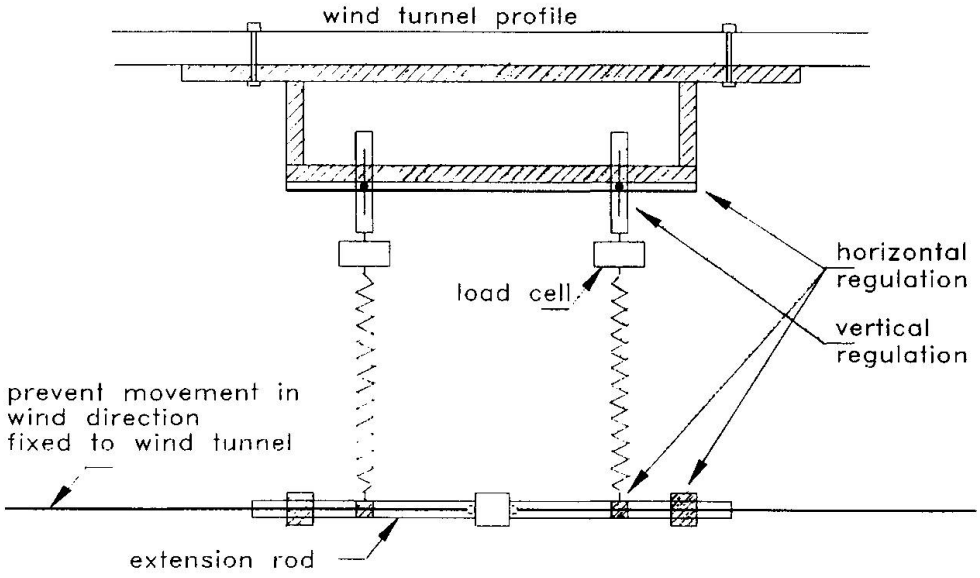

Figure 2: Simplified suspension system.

The active flap control system consists of:

- Load cells to measure the position of the model.
- Calculation of flap positions based on the position of the model and the flap configuration.
- Servo system with servo amplifiers, servo motors and reduction gears to regulate the flaps via cables between the gears and the flaps. This system consists of two separate parts as the flaps can be regulated independently.

4 Wind Tunnel Experiments

The positive definitions of the vertical position z, the torsional angle α, the angle of the leading flap α_l and the trailing flap α_t are shown in figure 3. U is the mean wind velocity.

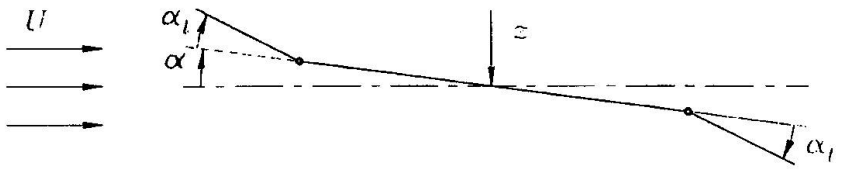

Figure *3: Definition of positive directions.*

The torsional motion can be described by

$$\alpha(t) = A_\alpha(t)\cos(\omega'_\alpha t) \tag{1}$$

where t is the time, $A_\alpha(t)$ is the amplitude of the envelope curve for the torsional motion and ω'_α is the circular eigenfrequency for the damped torsional motion. The actual flap position for e.g. the trailing flap can be described by

$$\alpha(t) = a_t A_\alpha(t)\cos(\omega'_\alpha t - \varphi_t) \tag{2}$$

here a_t is the amplification factor and φ_t is the phase angle for the trailing flap. In the same way the actual flap position for the leading flap can be described by the amplification factor a_l and the phase angle φ_l.

$$\alpha(t) = a_l A_\alpha(t)\cos(\omega'_\alpha t - \varphi_l) \tag{3}$$

The amplification factors and phase angles for the flap configurations are shown in table 3.

Flap configuration	Amplification		Phase angles	
	a_t	a_l	φ_t [rad]	φ_l [rad]
0	0	0	-	-
1	1.9	-2.0	4.5	4.5
2	3.4	-3.6	4.6	4.6
3	2.0	-2.0	1.5	1.5
4	3.4	-3.6	1.5	1.5

Table 3: Amplification factors and phase angles for each flap configuration.

A damping experiment follows the procedure:

1. Justification of wind velocity.
2. The model is given a 'standardised' initial displacement by pulling a rope that is connected to the horizontal arms of the model.
3. Start of the program that measures the position of the model every 12 m.

4. The flaps are started slowly at the first upcrossing of the torsional motion with the desired flap configuration. The actual positions of the flaps are measured and new values are specified every 12 m.
5. The results are stored and used to estimate the damping of the model from the free vibration following the initial displacement.

The damping ratio for the torsional motion as a function of the wind velocity is estimated based on the wind tunnel experiments. The damping ratio can also be estimated by the Air Material Command method, see e.g. Fung [6]. The damping ratio $g(U)$ defined in the AMC method as twice the necessary structural damping is replaced by -0.5 $g(U)$ + 0.008 to be compared with the experimental damping ratios.

The damping ratios estimated based on the experimental data are compared to the theoretical damping ratios by using the AMC method and the aerodynamic derivatives for a flat plate for flap configurations 0-4, see figure 4.

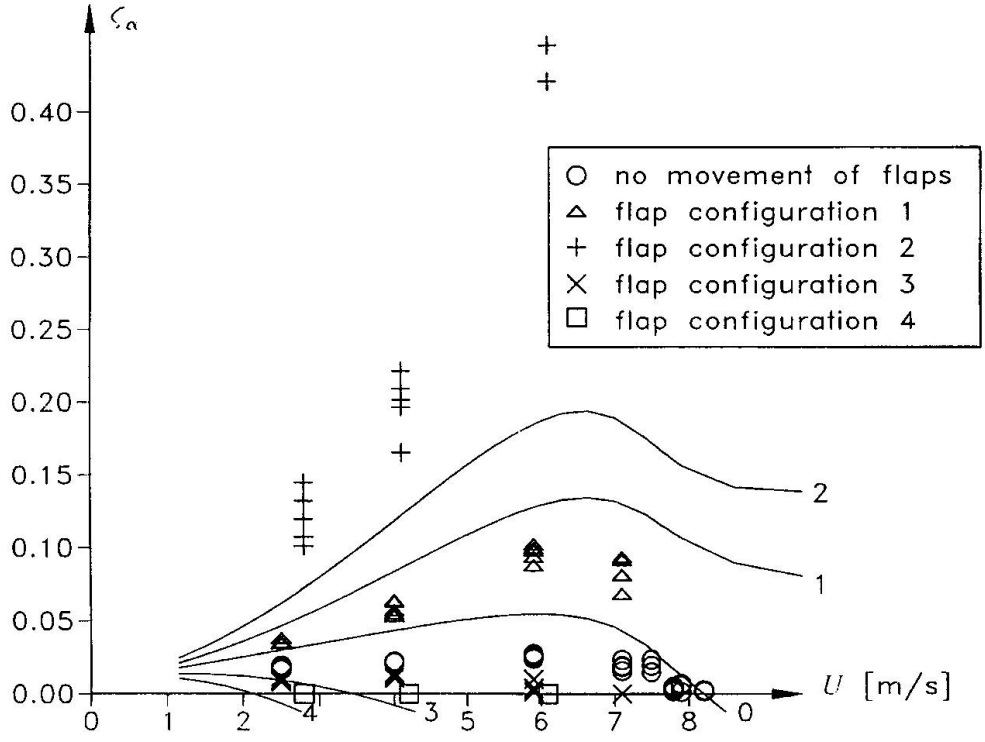

Figure 4: Theoretical (solid lines) and experimental damping ratio for torsional motion with wind for flap configuration 0-4. The number in the end of a solid line denotes the actual flap configuration.

As seen in figure 4 the experimental damping ratio is smaller for flap configurations 0 and 1 than the theoretical damping ratio but the shape of the curve is almost the same. For flap configuration 2 the experimental damping ratio exceeds the theoretical one. For flap configurations 1 and 2 the theoretical curves show that no binary flutter will occur. Unfortunately, it was not possible during the wind tunnel experiments to perform experiments with wind velocities above the relatively low divergence wind velocity (8.5 m/s) without the risk to damage the model.

5. Conclusions

The wind tunnel experiments show that it is possible by using very simple closed-loop control algorithms for the active flap control system to increase or decrease the flutter wind velocity for the bridge section model. The control algorithms are not optimised with regard to the amplification factors and phase angles, it is therefore expected that the effect of the flaps can be even better.

6. Acknowledgement

The present research was supported by The Danish Technical Research Council within the research program Safety and Reliability.

Bibliography

[1] European Patent *Specification. A System and a Method of Counteracting Wind induced Osc2'llations in a Bridge Girder.* EP 0 627 031 B1. Bulletin 1996/24.

[2] *Proceedings of the 15th Congress of IABSE.* Copenhagen, Denmark, June 16-20, 1996.

[3] M.A. Astiz. *Wind Related Behaviour of Alternative Suspension Systems.* In [2], p.1079-1090.

[4] W.C. Brown. *Development of the Deck for the 3300 m Span Messina Crossing.* In [2], p. 1019-1030.

[5] C. Dyrbye and S.O. Hansen. *Wind Load on Structures.* John Wiley & Sons, 1996.

[6] Y.C. Fung. *An Introduction to the Theory of Aeroelasticity.* John Wiley & Sons, 1955.

[7] N.J. Gimsing. Large Bridges of the Future. In [8], p. 295-304.

[8] A. Larsen, editor. *Aerodynamics of Large Bridges,* Proceedings of the First International Symposium on Aerodynamics of Large Bridges, Copenhagen, Denmark, 1992.

[9] A. Larsen and J.H. Walther. *A New Computational Method for Assessment of the Acroelastic Stability of Long Span Bridges.* In [2], p. 93-98.

[10] K.H. Ostenfeld. *Comparison between different Structural Solutions. The Great Belt Project.* In [2], p. 1063-1078.

[11] K.H. Ostenfeld and A. Larsen. *Bridge Engineering and Aerodynamics.* In [8], p. 3-22.

[12] R.H. Scanlan. *Wind Dynamics of Long-Span Bridges.* In [8], p. 47-57.

[13] T. Theodorsen. *General Theory of Aerodynamic, Instability and the Mechanism of Flutter,* p. 22-31. AIAA Selected Reprint Series, Vol. V, Aerodynamic Flutter. American Institute of Aeronautics and Astronautics, 1976. NACA Rep. No. 496 (1935).

Wind Vibrations and Damping Systems for Stay Cables

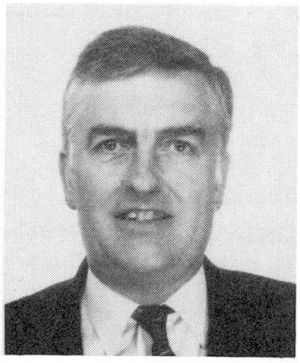

Jean FUZIER
Scientific Dir.
Freyssinet International
Vélizy, France

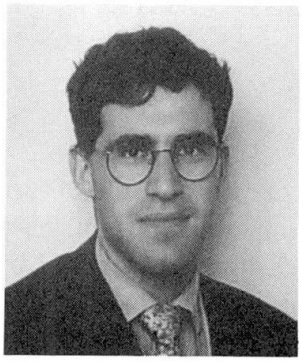

Jérôme STUBLER
Technical Dir.
Freyssinet International
Vélizy, France

Summary

The large-amplitude cable vibrations which have occurred in several major cable-stayed bridges remind us that the dynamics of cable structures are fundamental to their design. During the last past years several research programs have been performed and significant progresses have been made. The dynamic behaviour of the cables themselves have been considered together with the calculation of the dampening characteristics of the cables and the additional measures which are used to limit the amplitude vibrations. Several devices have been developed, installed and tested. An excellent correlation with the theoretical assumptions has been achieved.

1. Introduction

The main sources of cable vibrations are, on one hand, the wind which creates periodic or irregular lift and drag forces and on the other hand, the movements of the cable attachments on the pylon and on the deck due to the action of traffic loads or of the wind on the structure itself.

Several research programs and analyses have been carried out on this subject (References : [1], [2], [4] and [5]).

2. Vibrations phenomena

2.1 Vortex shedding

This movement is due to oscillating pressures in the wake of the cable. To have a vortex shedding exciting a stay cable, the frequency shall coincide with one of the natural frequencies of the stay cable since this type of vibration follows the *von Karman* law : $N = C\ V / D$ (V = wind speed / D = duct diameter / C varies from 0.16 to 0.22). This is possible but as the stay cable fundamental frequency is comprised between 2 and 0.5 Hz, the coincidence will always take

place on high harmonics. Also several studies give a limit to the amplitude of the vibrations which can reach a cylinder subject to vortex shedding. This amplitude is close to 40 % of the diameter of the cylinder.
Consequently vortex shedding can excite stay cables with high frequencies but low amplitudes. These vibrations are likely to generate fatigue at the anchorage zones but are little noticeable for the bare eye.

2.2 Galloping

Galloping oscillations are movements of large amplitude in a direction transverse to the wind. They are related to the modification of the transverse force coefficient with the wind angle of incidence. The angle change is originated by the movement of the stay cable which creates a change in the apparent angle of incidence. Sometimes interaction between cables can initiate what is called wake galloping.

2.3 Rain and wind vibrations

This phenomenon has been observed several times (References : [3], [5] and [6]). During rainy days a water rivulet can be formed on the surface of the sheath ; a wind (6 to 12 m/s speed) showing an angle with the cable vertical plane between 20 to 60 degrees may create such vibrations which could be considered as a particular galloping.

2.4 Effort of the structure vibrations

Cable vibrations can also be caused by dynamic forces acting on other parts of the structure (deck and pylon). The intrinsic structural damping of the stay cable is so low that a small movement of the deck and/or pylon suffices for creating a large movement of the stay cable.
Recent studies show that the amplitude of the movement of the stay cable can be up to 30 to 100 times the amplitude of the movement of deck and/or pylon but that the amplitudes can't increase with no limits.
Experience shows that risks are limited in case the fundamental frequency of the deck is close to that of the stay cable, the amplitude of the vibrations being small. To the contrary risks become high when the stay cable fundamental frequency is close to the double of the fundamental of the deck.

3. Damping characteristics of a stay cable

3.1 Damping factor definition

If a_{n+1} and a_n represent two consecutive amplitudes of vibration of a system left free to vibrate without any external excitation, $l_n (a_{n+1} / a_n)$ is the « logarithmic decrement » or the damping ratio.

β, the damping factor, is defined as $\beta = 1 / 2 \pi \; l_n (a_{n+1} / a_n)$.

Stay	Natural damping factor β
- Grouted stay	0.08 to 0.13 %
- Locked coil	0.15 to 0.3 %
- HDPE duct with galvanized strands and filled with wax	0.1 to 0.18 %
-HDPE duct with individually protected Freyssinet strands	0.12 to 0.20 % *

* The damping factor β may be written $\beta = -6 \times 10^{-4} \times L + 0.24$ (**L** = length of the stay cable in m).

3.2 Measurement of the damping factor

When the stay vibrates under any excitation, its damping effect results from the energy dissipation within the stay itself or thanks to specific dampers where the energy is consumed by friction or by lamination of a confined material. Using an accelerometer and an automatic recording system, the damping characteristics of any stay cable can be obtained. In the same manner it is possible to predict with accuracy the effect the installation of a damper with given characteristics will have on the damping factor. The numerical models which are used are confirmed by experiments on site.

3.3 Prediction of the damping factor

A detailed calculation model has been developed to evaluate the β factor provided by the various types of damping systems. A universal damping curve has been established allowing an accurate tuning of the damper. This curve permits to predict the behaviour of each stay cable in the wind.

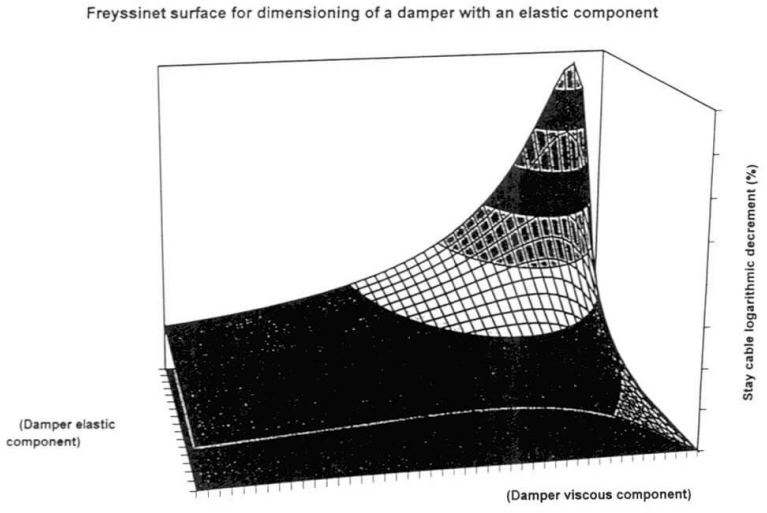

4. Range of available technologies

4.1 Circular duct with helical ribs

Several approaches have been made in JAPAN with longitudinal ribs or artificial roughness created on the duct [6]. The system which has been developed for the Normandie Bridge incorporates a double helical rib on the HDPE duct (patented). Extensive testing programmes were carried out in both laboratories : at the CSTB (NANTES), 1992-1993, for the Normandie Bridge and at the Danish Maritime Institute in 1997. This system keeps the stay cable stable by preventing the apparition of the water rivulet under certain wind conditions ; it does not increase the drag factor of the cable while maintaining the required aesthetical appearance of the stays.

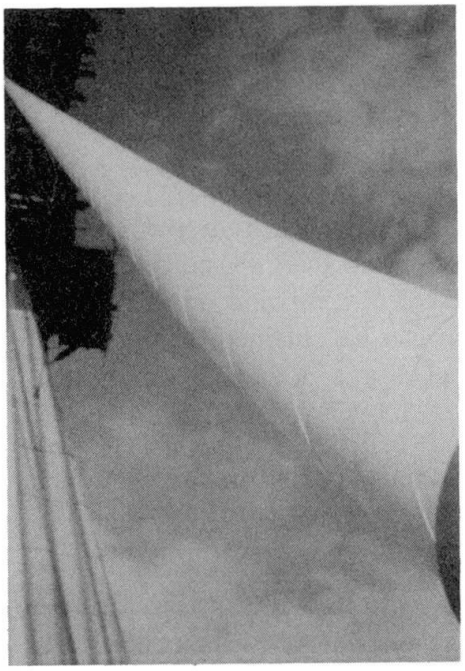

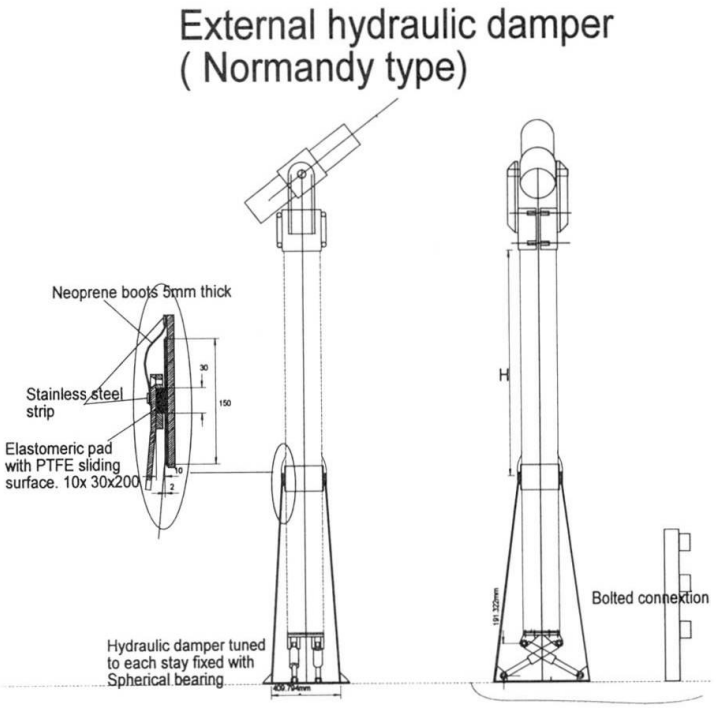

4.2 Damping ropes

The natural frequency of the stays can be modified by means of transversal cables connected to them. This solution which is effective although expensive and delicate to install has been used for some large bridges. It is recommended when the vibration frequencies of the deck or pylon are close to the frequencies of the stay cables. For the Normandie Bridge , the main vibration period for vertical bending would have been of the same magnitude as the vibration period of the longer cables, 4.5 seconds. The cross ropes reduce the periods of the cables to 1.25 second and less (Ref. [4]). Four ropes connect all cables in each plane of stays. Their tension was selected to avoid slackening effects. They consist of a bundle of stainless steel wire ropes fully embedded in HDPE and other dampening plastic material. They went through a testing programme for fatigue and damping capacity. A steel collar provides the fixation of the ropes on each stay and facilities for any orientation.

4.3 External Hydraulic Damper (EHD)

This damper is specifically designed to each project. The damping capacity can be tuned to obtain the required logarithmic decrement. However it requires a regular maintenance and it is not always meeting the aesthetics objective of the designer.

4.4 Internal Elastomeric Damper (IED)

A cast piece of special rubber with high damping characteristics and a specially designed shape is placed between the stay cable and the guide tube (deck and pylon). If the damping characteristics need to be increased, viscous oil can be placed in a special chamber. This is a very compact system with virtually no maintenance. It can provide sufficient damping for cables as long as 150 m (500'). This damper is completely invisible from the deck. It must be remembered that sometimes the word « damper » is used improperly to designate an annular sleeve generally made of normal elastomer placed around the stay cable near its extremities. The support of this sleeve is connected to the structure. This device can be effective to « dampen » the bending stresses at the anchorage but not at all the cable vibrations. It should rather be called an elastic support or guide.

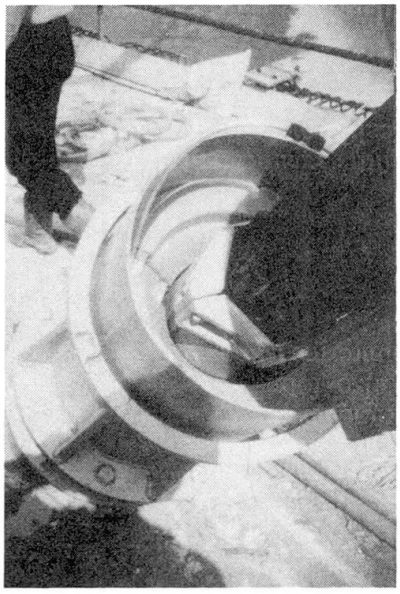

Internal Elastomeric Damper

4.5 Internal Hydraulic Damper (IHD)

This system is very convenient for cables longer than 150 m. Used in parallel with the IED, it increases the damping characteristics of the whole system. It has the same advantage : not visible and nearly no maintenance.

5. Conclusion

Several tests have been conducted on various cable-stayed bridges with different mechanical concept, stiffness and materials. This has permitted to validate the vibration calculation model and to establish a universal damping curve. A damping ratio, a logarithmic decrement, in the order of 3 to 4 % is sufficient to provide in most cases a satisfactory behaviour of the cable stays.

6. References

[1] Prof. M. IRVINE (Australia) : **Cable Structures and Structural Dynamics**

[2] Davenport A.G. (1995) : **The Dynamics of Cables in Wind**, Proceedings of the International Symposium on Cable Dynamics, Liege, Belgium / October 19-21.

[3] Saito T., Matsumoto M. and Kitazawa M. (1994) : **Rain-Wind Excitation of Cables on Cable-Stayed Higashi-Kobe Bridge and Cable Vibration Control**, Proceedings of Conference on Cable-Stayed and Suspension Bridges, Deauville, France, 12-15 Oct. 1994, pp 507-514.

[4] Virlogeux M. (1995) : **Design of Cables for Cable-Stayed Bridges : the example of the Normandie Bridge**, Proceedings of the International Symposium on Cable Dynamics, Liege, Belgium / October 19-21.

[5] Irwin Peter A. : **Wind Vibrations of Cables on Cable-Stayed Bridges**, Proceedings of ASCE Structures Congress, Portland, Oregon / October 14-16, 1997.

[6] Matsumoto, Hikami and Kitazawa (1994) : **Cable vibration and its aerodynamic / mechanical control**, Proceedings of Conference on Cable-Stayed and Suspension Bridges, Deauville, France, 12-15 Oct. 1994.

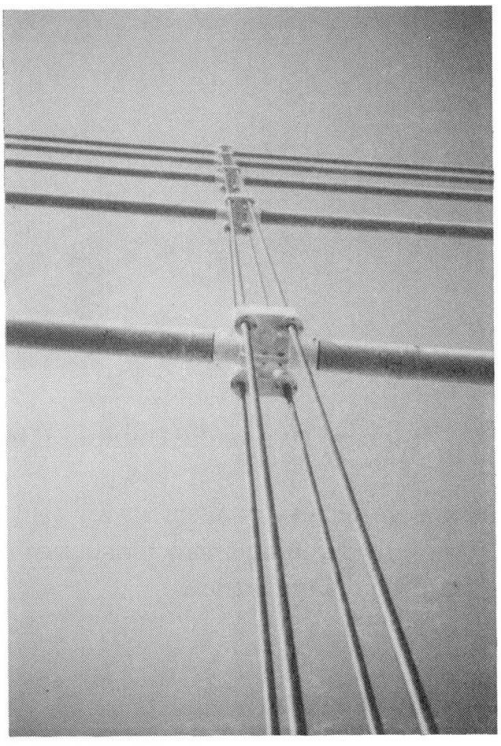

Normandie Bridge : Damping ropes and hydraulic dampers

Coupled Flutter Behavior of Ultra Long-Span Suspension Bridges

Masami IWAMOTO
Assist. Prof.
Nagoya Inst. of Technology
Nagoya, Japan

Yasuyuki MORIZONO
Research Eng.
Chodai Co. Ltd
Tsukuba, Japan

Masatsugu NAGAI
Prof.
Nagaoka Univ. of Technology
Nagaoka, Japan

Ken-ichi MAEDA
Prof.
Tokyo Metropolitan Univ.
Hachioji, Japan

Yozo FUJINO
Prof.
Univ. of Tokyo
Tokyo, Japan

Summary

The realization of ultra long-span bridges with center span length of 2,500 to 3,000 m depends on the aerodynamic stability. In order to develop ultra long-span suspension bridges with streamlined stiffening box-girders that have excellent structural characteristics, the torsional stiffness should be improved within the limits of the advantage in cost. This study dealt with two cable systems: mono-duo shaped main cable and rigid hanger frame, the latter of which is a newly proposed auxiliary hanger system. In order to investigate the aerodynamic characteristics of the proposed cable systems, a multi-mode flutter analysis was performed using four analytical models based on a trial design of ultra long-span suspension bridge with center span length of 2,500 m. The results demonstrated that rigid hanger frames and mono-duo shaped main cables are effective on the aerodynamic stability.

1. Introduction

The Akashi-Kaikyo Bridge with center span length of 1,990 m will be opened for service soon, and a part of the channel-crossing-road project that was developed as a next-generation project is proceeding to the implementation stage. Thus, an era of ultra long-span bridges whose span length considerably exceeds that of the Akashi-Kaikyo Bridge is about to begin. Under this circumstance, the research and development of ultra long-span suspension bridges with center span length ranging from 2,500 to 3,000 m has recently been underway. For the realization of such bridges, detailed investigations will be conducted using actual examples.

To construct ultra long-span suspension bridges successfully, it is important to ensure the aerodynamic stability of the bridges, in addition to realizing high economic performance. Therefore, major research subjects are the increase of the torsional stiffness of girder cross sections as well as that of the entire bridge and the improvement of the aerodynamic characteristics of girders.

In order to apply suspension structures with streamlined stiffening box-girder to ultra long-span bridges, we have performed a research focused on cable systems that increase the torsional stiffness of the entire bridge (Maeda, Iwamoto and Fujino et al. 1996, 1997). In the research, we investigated wind-resistant countermeasures through the use of mono-duo shaped main cable system and auxiliary hanger cable systems, based on the results of Astiz and Andersen (1990) and Ostenfeld and Larsen (1992) about the influence of auxiliary cable systems on flutter critical wind velocity.

The aim of this paper is to clarify the applicability as wind-resistant countermeasures for ultra long-span bridges of two cable systems: mono-duo shaped main cable and rigid hanger frame, the latter of which is a newly proposed auxiliary hanger system. We investigated in detail the changes in the characteristics of natural vibration modes due to these cable systems. Then, we conducted a multi-mode coupled flutter analysis and compared the results with the values calculated from the conventional basic two-mode analysis. In addition, we attempted to find the dominant modes other than the basic two modes that affected the critical wind velocity.

2. Wind-Resistant Countermeasures

Figure 1 shows the concept of mono-duo shaped main cable system used in this study. Conventional suspension bridges have the relative displacement of both sides of the main cable in the bridge axis direction at the tower top due to symmetric torsional deformation. On the other hand, mono-duo shaped main cable system restricts the relative displacement, leading to the increase in the torsional stiffness of the entire bridge. This restriction effect is the main effect. The effect resulting from the reduced polar moment of inertia of the main cable compared to that for conventional suspension bridges is relatively small.

Figure 2 shows the newly proposed auxiliary hanger systems named rigid hanger frames. The rigid hangers have bending stiffness and include hanger cables. They are installed concentratedly at several locations in the center span. We investigated the three types of rigid hanger frames shown in *Fig. 2* and confirmed that there is almost no difference in their effects. Therefore, hereafter we deal with the rigid frame c).

3. Analytical models

In this study, we used four types of analytical models shown in *Fig. 4* based on an example design, the general design plan of which is shown in *Fig. 3* and sectional values of structural members listed in *Table 1*. The four models contain a conventional model (PARA model), a basic mono-duo model (MONO model) and two rigid hanger frame models (PARA-RIGID and MONO-RIGID) in which rigid hanger frames are

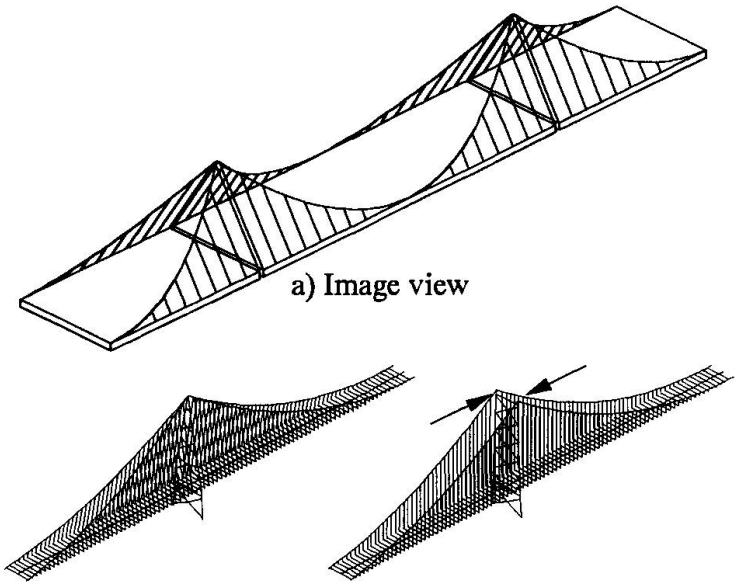

a) Image view

b) Displacement at tower top

Fig. 1 Concept of mono-duo shaped main cable

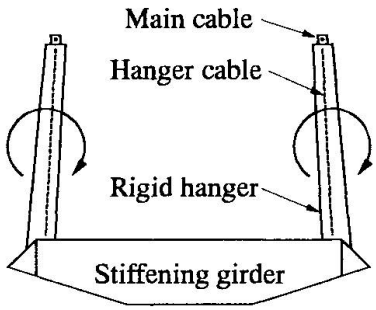

a) Rigid hanger

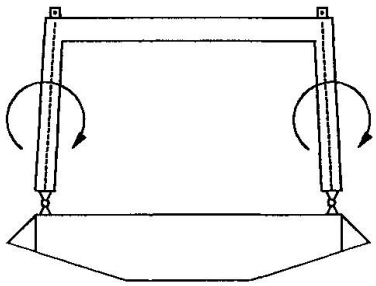

b) Hinged frame

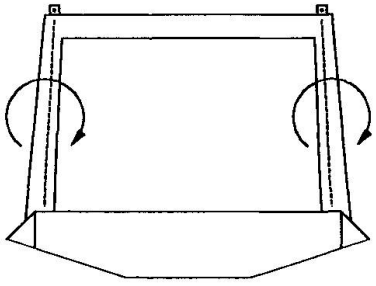

c) Rigid frame

Fig. 2 Rigid hanger frames

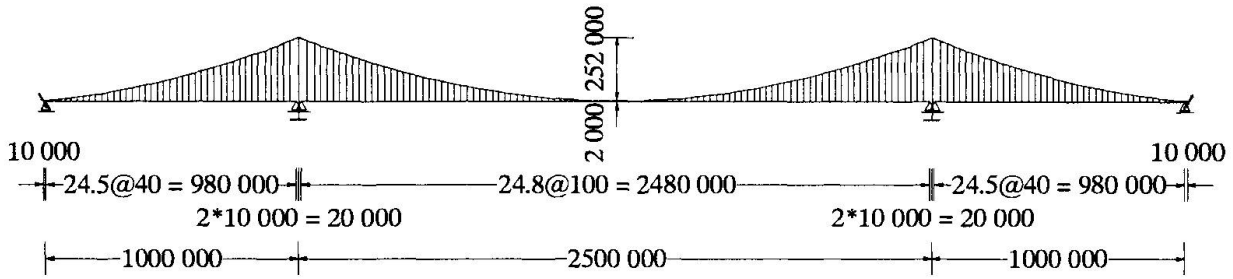

Fig. 3 Trial design

Table 1 Sectional values of structural members

Main cable	A_C	0.5564 m^2/cable
Hanger cable	A_H	0.006 m^2/cable
Center stay	A_S	0.2 m^2/cable
Stiffening Girder	A_G	1.3 m^2
	$I_{G,in}$	11.0 m^4
	$I_{G,out}$	132 m^4
	J_G	23.7 m^4
Main tower	A_T	2.6-4.2 m^2/column
	$I_{T,in}$	13.5-23.2 m^4/column
	$I_{T,out}$	26.0-85.3 m^4/column
	J_T	17.6-37.3 m^4/column

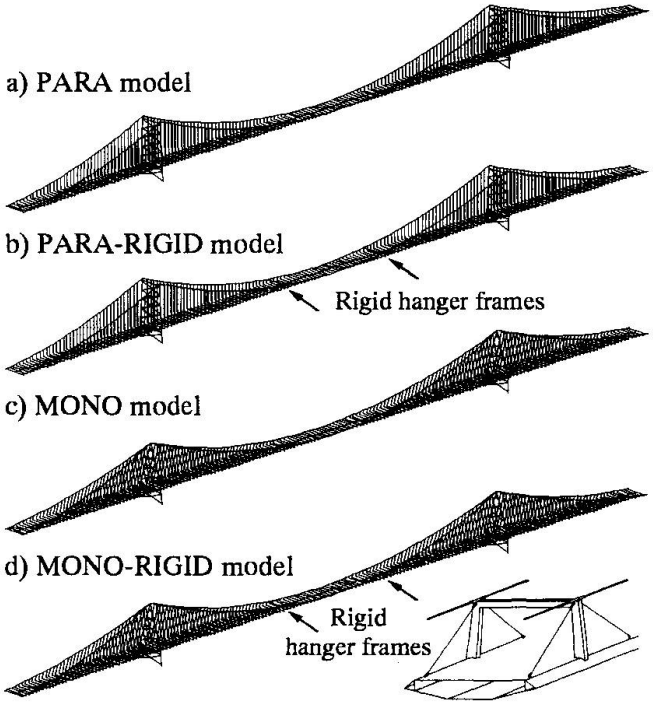

Fig. 4 Analytical models

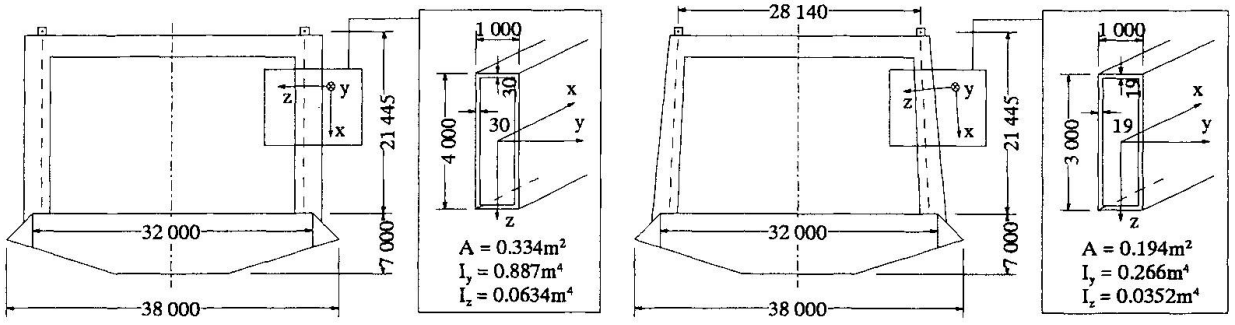

a) PARA-RIGID model b) MONO-RIGID model

Fig. 5 Sectional values of rigid hanger frames

installed at 0.36 L and 0.64 L (L : center span length) of the center span of the former two models (*Fig. 4*). *Figure 5* shows the rigid hanger frames used in this study and their sectional values.

a) 3rd mode (1st symmetric)

b) 11th mode (2nd symmetric)

c) 12th mode (3rd symmetric)

Fig. 6 Symmetric vertical deflection modes (MONO model)

a) Vertical components of 15th, 26th and 31st modes

b) Out-of-plane components of 15th mode

c) Out-of-plane components of 26th mode

d) Out-of-plane components of 31st mode

Fig.7 Symmetric torsional modes (PARA-RIGID model)

4. Natural vibration mode characteristics

Before the coupled flutter analysis, we performed an eigen-analysis for the natural vibration modes of the four models. The results showed that the 1st symmetric vertical deflection mode of both the PARA and MONO models was obtained in the 3rd solution mode. The 1st symmetric vertical mode of the PARA-RIGID and MONO-RIGID models was obtained in the 2nd solution mode instead of the 3rd one, however, the natural frequency was the same as that in the PARA and MONO models. In all the four models, the 2nd and 3rd symmetric vertical modes were obtained in the 11th and 12th solution modes, respectively. The 1st symmetric torsional mode of the PARA model was obtained in the 17th solution mode. In the PARA-RIGID model, it was obtained in the 15th solution mode instead of the 17th one, as well as in the 26th and 31st solution modes while the frequency increased. The 1st symmetric torsional mode of the MONO model was obtained in the 26th solution mode. In the MONO-RIGID model, it was obtained in the same 26th solution mode while the frequency increased, as well as in the 15th, 22nd and 30th solution modes. All these symmetric torsional modes of the PARA-RIGID and MONO-RIGID models had large out-of-plane (in the horizontal direction perpendicular to bridge axis) components. Among them, newly obtained torsional modes in the PARA-RIGID and MONO-RIGID models are the ones that the out-of-plane modes in the PARA and MONO model changed into and the frequencies increased. *Figure 6* shows the symmetric vertical modes of the MONO model, and *Fig. 7* shows the symmetric torsional modes of the PARA-RIGID model.

5. Coupled flutter characteristics

Coupled flutter characteristics were analyzed using a modal analysis technique (Miyata, Yamada and Ota 1989, Iwamoto 1995). Unsteady aerodynamic forces based on the plate-wing theory were used in the analysis. In order to investigate the influence of modes, many cases of analysis with various modal combinations were carried out. *Figs. 8* to *11* show the relationship between the wind velocity U and the logarithmic decrement δ of flutter mode branches. In the *Fig. 9* for the PARA-RIGID model, the 8th, 10th, 17th and 18th solution modes, which were not described in the previous section, represent the swinging log mode of the side span, the out-of-plane mode and the coupled modes of the 4th symmetric vertical deflection and side span out-of-plane components for the latter two modes, respectively.

Figures 8 to *11* show that there is large difference between the results obtained using the 1st through 40th modes and those using the basic two modes: the 1st symmetric vertical and

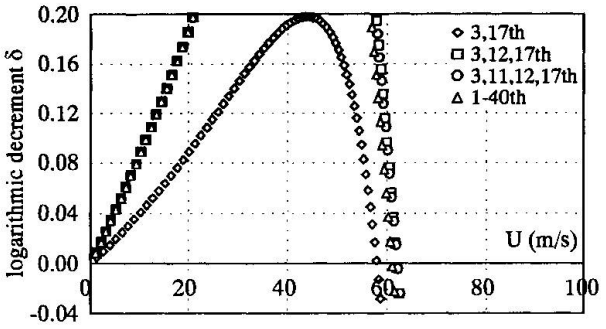

Fig. 8 U-δ curve (PARA model)

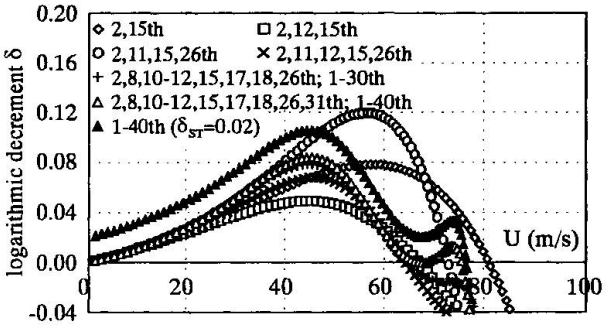

Fig. 9 U-δ curve (PARA-RIGID model)

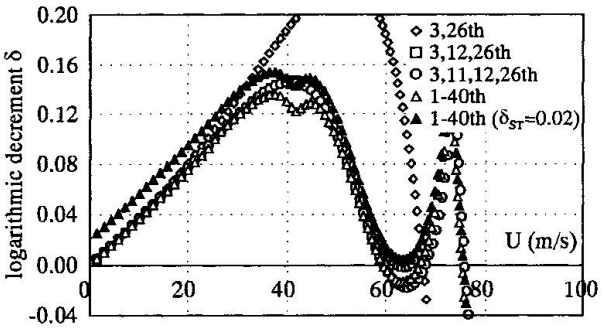

Fig. 10 U-δ curve (MONO model)

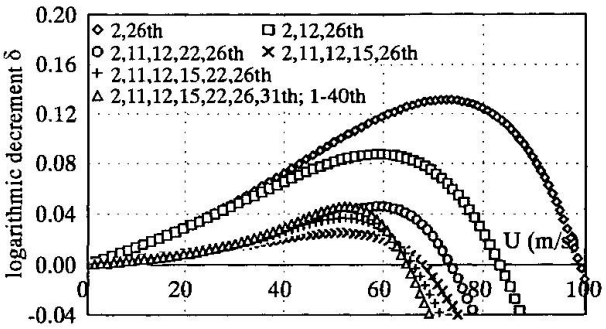

Fig. 11 U-δ curve (MONO-RIGID model)

Table 2 Flutter critical wind velocity [m/s]

Applied modes	Analytical model			
	PARA	PARA-RIGID	MONO	MONO-RIGID
Basic 2 modes (δ_{ST} = 0)	58.4	81.4	67.8	99.2
1-40th modes (δ_{ST} = 0)	61.1	67.1	59.5	65.5
1-40th modes (δ_{ST} = 0.02)	-	76.6	75.7	-
Selberg's equation	55	77	63	89

torsional modes. The flutter critical wind velocity of the former case is considerably lower than that of the latter case, in all the models except the PARA model. The 3rd symmetric vertical mode (the 12th solution mode) has the largest effect on the critical wind velocity, followed by the 2nd symmetric vertical mode (the 11th solution mode). Both modes greatly decreased the critical wind velocity of the other three models than the PARA model. The symmetric torsional modes in the two models with rigid hanger frames also seem to contribute to decreasing the critical wind velocity except the 31st solution mode of the PARA-RIGID model.

The U-δ curves of the PARA-RIGID and MONO models obtained from multi-mode flutter analysis have complex shapes, that is, the logarithmic decrement reaches a negative peak right after the flutter occurring and increases to positive value again. In consideration of these shapes of U-δ curves, coupled flutter analysis was performed again with the structural damping of logarithmic decrement δ_{ST} = 0.02 considered. The results demonstrate that, as shown in the figures, the U-δ curves shift to the upper side and the critical wind velocity increases by approximately 10 to 15 m/s. In addition, flutter analysis with unsteady drag forces based on the quasi-steady theory considered was performed for all four models. Although the δ value tended to increase overall, almost no change was observed in the critical wind velocity.

Table 2 summarizes the estimated values of the critical wind velocity for the four models. In this table, the values obtained from Selberg's equation are also listed as a reference. The final values for the four models are approximately 61, 77, 76 and 65 m/s, respectively. Mono-duo shaped main cable system and rigid hanger frames are found effective as wind-resistant countermeasures. However, it is also found that the flutter characteristics aren't necessarily improved highly even if the two countermeasures are used at the same time. This is a problem to be solved in future investigation.

6. Conclusions

This paper discussed the coupled flutter characteristics of the ultra long-span suspension bridges in which mono-duo shaped main cable system and rigid hanger frames are applied as wind-resistant countermeasures. Based on the analytical results, we reached the following conclusions.

(1) Through the concentrated installation of rigid hanger frames, large degree of coupling of the out-of-plane components was formed in a basic mode in which 1st symmetric torsional components had been previously dominant. In addition, several symmetric torsional modes were obtained by the formation of the coupling of the torsional components in modes in which out-of-plane components had been dominant, leading to the increase in the natural frequencies in all these modes.

(2) In the flutter analysis using the models with the wind-resistant countermeasures, there was large difference between the U-δ curves obtained from the conventional basic two-mode analysis and those from the multi-mode analysis. In addition, there were several dominant modes other than the basic two modes that affected the flutter critical wind velocity, such as the 2nd and 3rd symmetric vertical deflection modes.

(3) When mono-duo shaped main cable system and rigid hanger frames were applied individually, the flutter critical wind velocity considerably increased as compared with the conventional suspension bridge model if reasonable structural damping was taken into consideration. Thus, mono-duo shaped main cable system and rigid hanger frames are effective as wind-resistant countermeasures. However, the joint use of the two countermeasures didn't necessarily improve the flutter characteristics highly. This is a problem to be solved in future investigation.

References

1) K. Maeda, M. Iwamoto and Y. Fujino et al. : Structural characteristics of an ultra long-span mono-duo type suspension bridge taking jointly with supplementary hangers system, *Journal of Structural Engineering*, Vol. 42A, 1996. (in Japanese)

2) K. Maeda, M. Iwamoto and Y. Fujino et al. : Effects of rigid hangers in aerodynamic stability of an ultra long-span mono-duo type suspension bridge, *Journal of Structural Engineering*, Vol. 43A, 1997. (in Japanese)

3) M. A. Astiz and E. Y. Andersen : On wind stability of very long spans in connection with a bridge across the Strait of Gibraltar, *Strait Crossings*, J. Krokerborg (ed.), Balkema Rotterdam, 1990.

4) K. H. Ostenfeld and A. Larsen : Bridge engineering and aerodynamics, *Aerodynamics of Large Bridges*, A. Larsen (ed.), Balkema Rotterdam, 1992.

5) T. Miyata, H. Yamada and H. Ota : Flutter analysis of a truss stiffening suspension bridge by a 3D frame model method, *Proceedings of JSCE*, No. 404/I-11, 1989. (in Japanese)

6) M. Iwamoto : *Prediction of aerodynamic behavior of cable supported bridges*, Ph. D. thesis, University of Tokyo, 1995. (in Japanese)

Field Measurements of a 1210 m Span Suspension Bridge during Erection

Guy L. LAROSE
Technical Mgr
Danish Maritime Institute
Lyngby, Denmark

Rickard JOHNSON
Ph.D. Student
KTH Royal Inst. of Technology
Stockholm , Sweden

Aage DAMSGAARD
Dir.
Danish Maritime Institute
Lyngby, Denmark

Summary

The dynamic behaviour of a 1210 m span suspension bridge was monitored on site from the start of the erection of the main span in April 1997 to the bridge opening in December 1997 in Sweden. Measurements of accelerations, wind speed and direction were recorded continuously. This paper presents the main findings of the first 18 days of the field measurement campaign corresponding to the period of lifting and hinging of all deck segments of the main span. Variations of natural frequencies and structural damping as a function of completion of the main span are given and compared to finite element calculations. Correlation between wind speed, accelerations and aerodynamic damping are also given and compared to analytical and experimental predictions based on a section model study and an aeroelastic model study of the bridge during erection.

1. Introduction

Suspension bridges are at their most vulnerable stage with regards to dynamic wind action during the early phases of erection. The unique opportunity to study this aspect through field measurements arose in the spring of 1997 in Sweden with the construction of the Höga Kusten Bridge. A measurement campaign was initiated by the Danish Maritime Institute (DMI) in collaboration with the Department of Structural Engineering of the Royal Institute of Technology (KTH), Stockholm, and the Scandinavian Bridge Joint Venture (SBJV), the superstructure contractors for the project. This campaign was the final stage of a thorough aerodynamic investigation at DMI of this remarkable structure.

The purpose of the field measurements was to validate predictions of the dynamic behaviour of the bridge based respectively on finite-element analyses and model scale experiments in wind tunnels. At first, the field data aimed at providing estimates of natural frequencies and structural damping as a function of percentage of completion of the bridge deck. Also the campaign aimed at providing a precious evaluation of the dynamics on an asymmetric erection configuration envisaged by SBJV [1]. The wind-tunnel tests on a 12 m long aeroelastic model pointed out that the aerodynamic stability of the bridge could be enhanced if an asymmetric construction scheme, i.e. to erect more deck segments on one side of the mid-span than the other, was adopted [2].

The Höga Kusten Bridge, 500 km north of Stockholm on the east coast of Sweden, has a 1210 m main span flanked with end spans of 310 m and 280 m. The suspension cables are supported by two 180 m high concrete pylons, leading to a 40 m navigation clearance. The steel closed-box girder of the main span is 22 m wide by 4 m deep and is built in segments of 40 m weighing approximately 280 tons each. The bridge has the longest span of the regions of the world where

the ground is snow-covered more than five months a year. The high exposure to strong winds and the possibility of important snow accumulation that could change the aerodynamics of the deck cross-section were taken into account in the design of the superstructure.

This paper presents the main findings of the first 18 days of the campaign corresponding to the erection of the main span [3]. Additional measurements were carried out to evaluate the changes in frequency and structural damping as the welding of the girder progressed, during the deck surfacing and after the removal of the catwalk. These observations are not reported here.

2. Monitoring procedures and instrumentation

The instrumentation was composed of five servo-accelerometers (Schævitz A225-001), one cup-anemometer and one wind-direction sensor. The wind measurement sensors were mounted on a mast fixed to a cross-bridge between the main cables 120 m from mid-span and 20 m above the deck. Wind data collected from a 10 m mast on the South end span was also made available by SBJV during the campaign. Three accelerometers were mounted at mid-span to depict lateral, vertical and torsional vibrations of the deck and were kept stationary while a set of two accelerometers were moved gradually toward one of the pylons as the erection progressed. These two accelerometers were set up to measure vertical and torsional oscillations of the deck and were moved until they reached the ¼ point, 305 m from mid-span.

Data acquisition was performed with a PC placed inside the stiffening girder at mid-span. Continuous and simultaneous recording of the signals from the sensors was made at a sampling frequency of 10 Hz after low pass filtering at 2 Hz. The time histories were all stored in files of 10 minutes on the PC hard disk. Daily visits to the site were made to ensure that all the equipment was functioning, to back-up the data and to take note of the bridge configuration.

3. Bridge configuration

The main span contains 31 girder segments, numbered 10 to 40 by SBJV. Each segment was lifted from a barge with a floating crane, attached to the hangers and simply hinged to the previous segment. The 31 segments were hinged before welding started. To avoid man made vibrations, the data analysis focused on the off-work hours, defining 12 erection stages (see Fig. 1). For the first seven stages, only stage 5 had a symmetric configuration. Stage 3, 5-7 and 12 corresponded well to the configurations studied on an aeroelastic model at DMI.

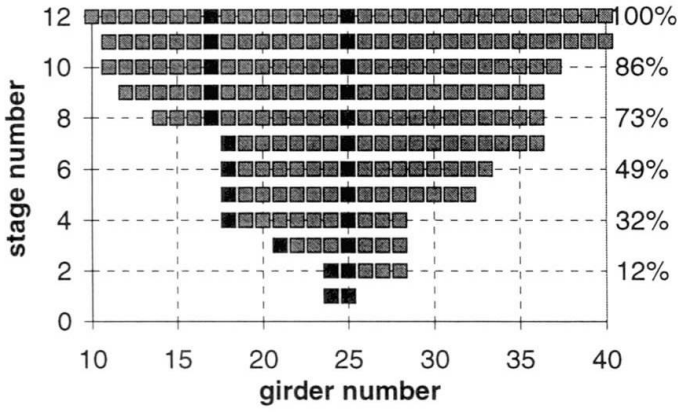

Figure 1 Deck configurations studied. Light grey: hinged segments; dark grey: accelerometers location. The percentage of completion is indicated on the right ordinate.

4. Main findings and discussions

The measurement period was characterised by winds from the WNW-NNW quadrant, more or less perpendicular to the bridge axis. The 10-minute mean wind speed at deck height was typically in the 6 to 14 m/s range with the exception of two occasions where the passage of a depression brought stronger winds from NW, in the 14-16 m/s range during stage 4 and in the 18-22 m/s range during stage 9. The construction was stopped for a full day during the latter wind storm. Fig. 2 shows time histories of the deck accelerations at mid-span recorded during that storm. The bridge response was dominated by random buffeting induced by the turbulent wind. No organised motion associated with vortex-shedding excitation or the like were observed. Also shown in Fig. 3 are the corresponding spectra of the response. In general, the wind excited mainly the lowest natural modes of each degrees of freedom, facilitating the evaluation of the bridge dynamic characteristics.

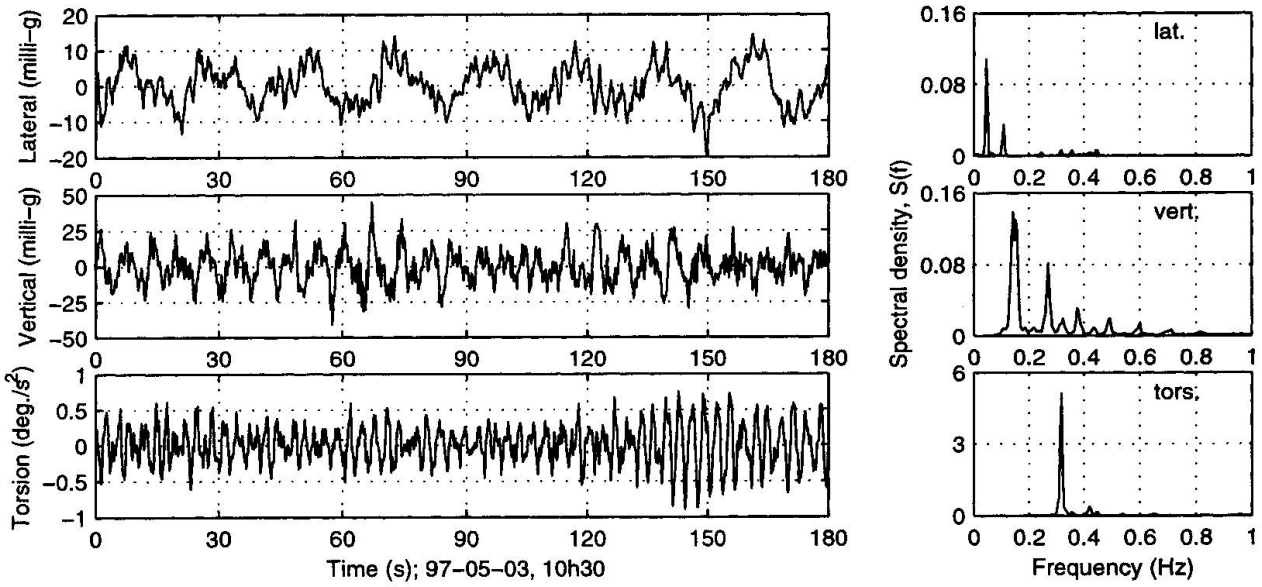

Figure 2 Typical time histories and spectral density of the bridge response at mid-span.

4.1 Natural frequencies and total damping

The data analysis was performed on groups of 3 consecutive 10-min. files selected for stationary conditions (constant wind speed and direction), good root-mean-square (rms) response and off working hours. Two techniques were used for the estimation of frequency and damping from short ambient vibration records, namely the maximum likelihood technique (MLT) and the random decrement technique (RDT). The MLT is a frequency domain approach where the spectra peaks are fitted with a single degree-of-freedom mechanical admittance function assuming a probability distribution for the spectral estimates. The frequency and damping parameters are varied until the joint probability distribution between each point and the curve fitted reaches a maximum. The spectral analysis was performed with 8192-point fast-Fourier transform. Four vertical modes and the lowest symmetric lateral and torsional modes were identified and analysed.

The RDT is based in the time domain and simply consists of removing the wind excitation from the measured response to be left uniquely with the properties of the mechanical system. Sections

of the response that satisfy a certain threshold are averaged and the auto-correlation function of a given mode is built. Both methods give consistent results. Figs. 3 and 4 present respectively the estimates of frequencies and damping as a function of the bridge completion. Fig. 3 also presents the frequencies predicted from finite-element calculations using a commercial finite-element programme. The agreement is very good.

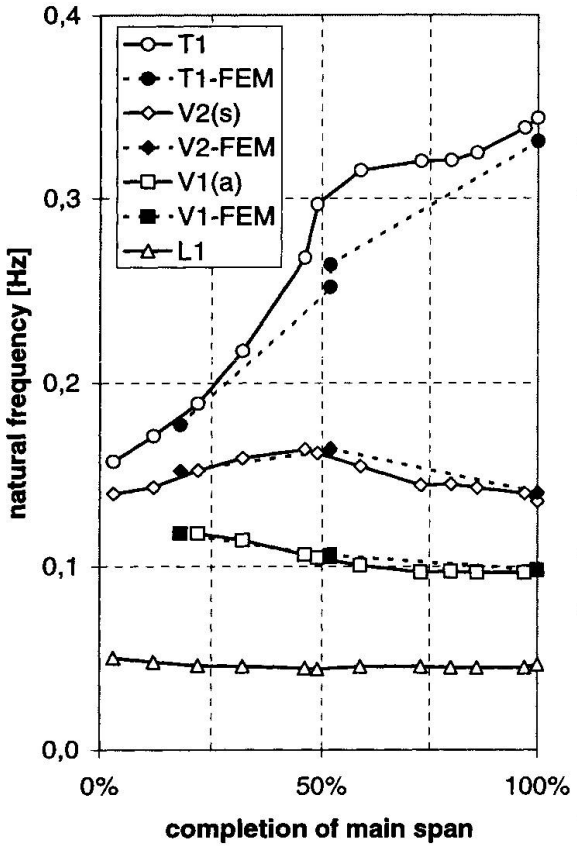

Figure 3 Variations of natural frequency as a function of bridge completion

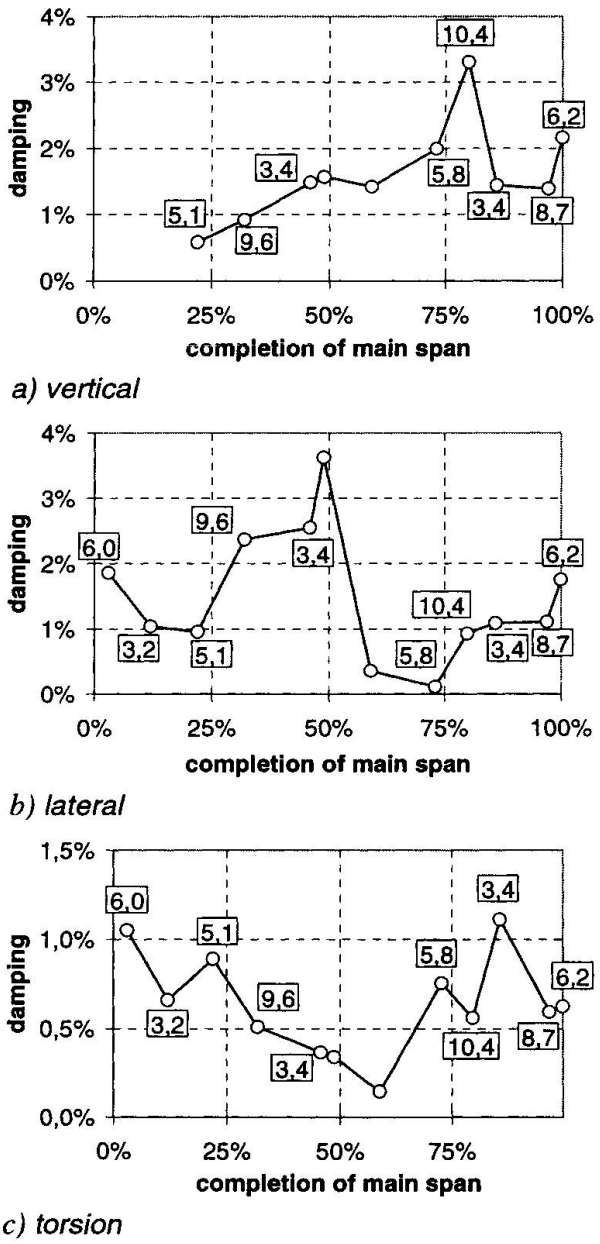

Figure 4 Variations of total damping (ratio of critical) as a function of bridge completion

The wind speed corresponding to the damping estimates are also given in Fig. 4 in the boxes near the data points. By inspection of Fig. 4 it is not possible to conclude if there was a systematic increase or reduction of damping as the erection of the main span progressed. However, it can be observed that the damping in torsion was in most cases 0.5 to 1% of critical which is considered to be low. For the vertical modes, the damping might have slightly increased as the bridge was built and was in most cases between 1% and 2% of critical. It was also observed that generally the damping increased with the amplitude of vibrations. For example, an increase of 15% in amplitude translated to a 20% increased in total damping for the lowest lateral mode for a constant windspeed.

4.3 Correlation wind speed and dyanmic response

Fig. 5 presents the rms acceleration at mid-span as a function of the erection period. With the exception of a number of very narrow peaks, probably caused by impacts of the lifting crane, the period of the largest rms response and therefore also the most severe wind load occurred between May 2nd, 3rd and 4th, that is, erection stage 9 during which the 10-min averaged wind speed reached above 20 m/s.

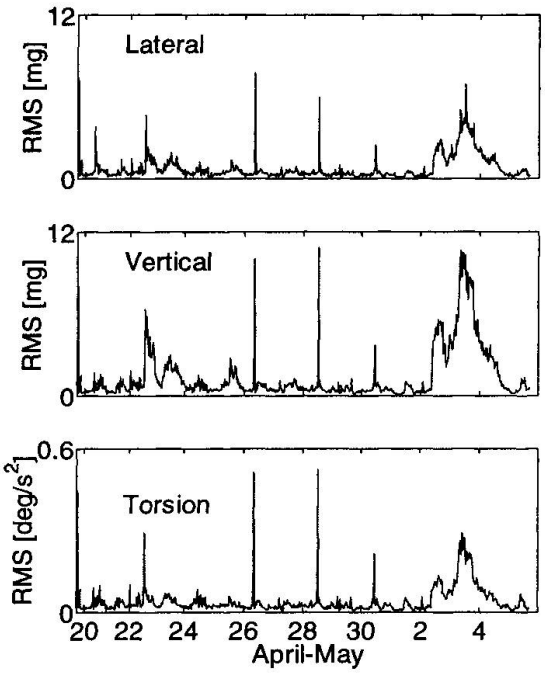

Figure 5 Variations of rms response as a function of date of erection.

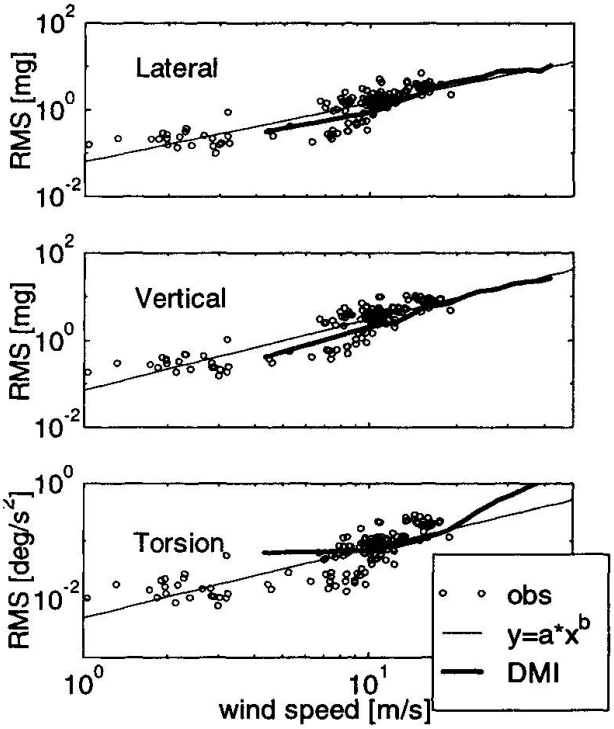

Figure 6 Variations of rms acceleration as a function of windspeed for stage 9.

The correlation between wind speed and magnitude of accelerations is clear. In Fig. 6 the rms response are plotted versus windspeed. Also plotted is a 2nd order least square fit of the observed data. Also shown in Fig. 6 are the results of the wind tunnel tests on a 1:150 scale aeroelastic model (solid line on the graphs) of the bridge for a configuration corresponding to stage 12, i.e. all deck segments are hinged but not linked to the end span. The agreement between model scale and full scale observations is excellent for the vertical and lateral degrees of freedom, the response showing similar magnitude and variation with windspeed.

4.4 Aerodynamic damping

Through analysis of the bridge response during the May 3rd wind storm it was possible to estimate the variations of total damping as a function of wind speed at deck level for winds perpendicular to the bridge axis. The results are shown on Fig. 7 for the fundamental modes of vibrations of the deck for stage 9 (main span 80% completed). It is clear that the total damping increased with windspeed. This increase is attributed to a combination of aerodynamic damping and an increase of structural damping with the amplitude of vibration. To evaluate the importance of the aerodynamic damping, curves showing predictions based on quasi-steady and unsteady aerodynamics are shown in Fig.7.

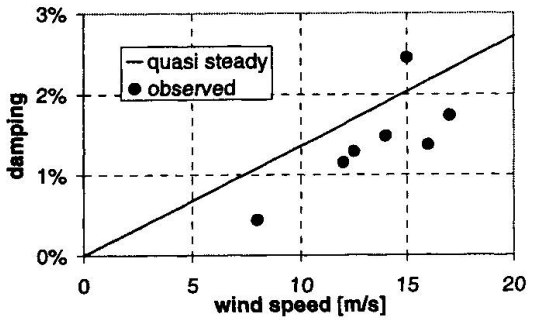

a) lateral

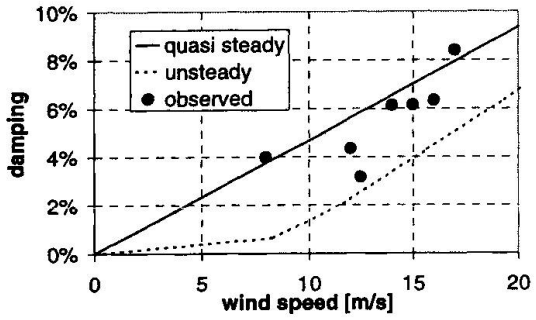

b) vertical

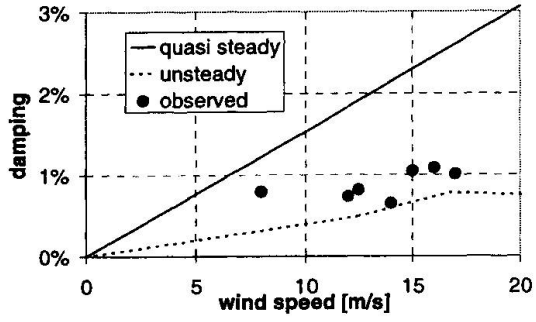

c) torsion

Figure 7 Variations of total damping as a function of windspeed for stage 9.

The quasi-steady aerodynamic damping predictions are based only on the static coefficients of the deck cross-section measured in turbulent flow, while the unsteady predictions are based on the measured aerodynamic derivatives through dynamic section model tests as reported in [4]. For the range of wind speeds of interest, the quasi-steady predictions overestimated the damping excepted for the lateral mode, while the unsteady predictions appeared to follow well the trend observed in full-scale .

5. Conclusions

The field measurements of the dynamic behaviour of a suspension bridge during construction have indicated that the structural damping for small amplitudes of motion can be relatively low, especially for the torsional degree of freedom of the deck. It also indicated that finite-element calculations can provide satisfactory predictions of the dynamic characteristics of the structure as it is being built. Results of wind tunnel tests on a 1:150 scale aeroelastic model compared very well with field observations. The aerodynamic damping estimated from the aerodynamic derivatives of the deck cross-section through section model tests proved to be reliable, while the predictions based on quasi-steady aerodynamics overestimated the aerodynamic damping for the range of windspeed experienced during the field measurements.

References

[1] Madsen, B.S., Höga Kusten Bridge, Sweden, construction of the bridge girder, in *Proc. of New Technologies in Structural Engineering,* LNEC. Lisbon, July 1997, pp. 821-826.

[2] Tanaka H. et al., Aerodynamic stability of a suspension bridge with partially constructed bridge deck, in *Proc. of 15th IABSE Congress*, Copenhagen, June 1996, pp. 113-118.

[3] Johnson R. and Larose G.L., *Field measurements of the dynamic response of the Höga Kusten Bridge during construction*, DMI-KTH Joint Venture Research Report, 03/1998.

[4] Larose G.L. and Livesey F. M., Performance of streamlined bridge decks in relation to the aerodynamics of a flat plate, *J. Wind Eng. & Ind. Aerodyn.*, **69-71** (1997), 851-860.

Normandie Bridge: Wind Measurements and Validation of Previsional Studies

Didier DELAUNAY
Chief Eng.
CSTB
Nantes, France

Gérard GRILLAUD
Head of Division
CSTB
Nantes, France

Jocelyne JACOB
Chief Eng.
SETRA
Bagneux, France

Michel VIRLOGEUX
Consulting Engineer
Bonnelles, France

Summary

At the design stage of the Normandie Bridge, previsional studies were carried out in order to estimate the wind induced dynamic behaviour of the bridge. These studies concerned the turbulent characteristics of the wind field at the site, the aeroelastic stability of the bridge, and the bridge response to the turbulent wind. During two years (1995-1996), in-situ measurements of the wind and of the dynamic response of the bridge have allowed to check the validity of the wind turbulence characteristics used for the design, and to compare the dynamic participation of height vibration modes to the predicted values corresponding to CSTB wind-tunnel measurements carried out on a taut-tube model and to theoretical computations made by SETRA. The results confirm the wind stability of the bridge and the conservative nature of its design.

1. Introduction

When it opened in January 1995, the Normandie Bridge (France), was, with a span of 856m long, the first cable-stayed bridge entering the domain of very long spans, which was reserved up to now for suspension bridges. The design of such bridges being governed by wind effects, various studies were conducted for its wind design [1,2]. These previsional studies have concerned both the estimation of the turbulent wind characteristics on the site [3,4], leading to a "wind model", and the previsions of the dynamic response obtained by a combined approach: theoretical computations using the « quasi-steady » spectral approach, and wind tunnel experiments on a taut-tube model [1,5].

In order to validate the different stages of the wind design, the completed bridge was equipped in 1995 with four anemometers, six accelerometers shared in two sections of the deck, and one accelerometer at mid-height of the South pylon. The field measurements lasted two years, allowing acquisition of data during strong wind periods.

We present here a first analysis of these data. For turbulence characteristics, the comparison of measurements with design data was made for the variances of the 3D fluctuations, their spectral distribution, the lateral turbulent length scales, and the spectral distribution of the lateral correlations (coherence functions). Concerning the dynamic response, fourteen vibration modes of the bridge were identified. Dynamic participation of eight of them was compared to the wind tunnel results, and the aerodynamic damping was evaluated.

2. Instrumentation - Data processing

Four tilted Gill 3-D propeller anemometers were set up along the deck, at a height of 69m (7 m above the deck), with distances between them covering the range 5.4 m - 38.7 m. The propeller distance constant is 2.1 m, i.e. a response length of 0.14 s. for a wind-speed of 15 m/s, which is adequate due to the large turbulence scales at this height, as it was proven by comparison with sonic anemometers. The propeller arms were tilted in order to avoid an under-estimation of the vertical fluctuations. Corrections for the propeller non-cosine response were made.

Inside two deck sections, respectively at mid-span and 100m south the mid-span, vertical accelerations were measured on both sides at a distance of 7.95 m from the deck longitudinal axis, and horizontal accelerations were measured in the direction perpendicular to the deck. On the south pylone, the horizontal accelerations were measured in the direction of the deck axis.

The instantaneous values of the wind components, and of the accelerations were filtered and recorded at a frequency of 10 Hz. Sequences of 4096 points (6mn50s) were stored when the mean wind speed exceeded 12 m/s with a mean direction between 235 and 285 deg. (the direction perpendicular to the deck is 270 deg.). More than 130 hours of data have been recorded during the two measurement years, including runs with mean wind speeds up to 22 m/s.

To reduce the sampling error in the estimation of the power spectral density (p.s.d.) of the acceleration, it is necessary to average a lot of spectral estimates together. In the same time, the determination of the damping coefficients requires a good frequency resolution, and then a long stationnary series of data. To overcome these contradictions, the method of selective ensemble averaging was used [6], which consists in grouping sequences of 1024 points according the mean wind speed and direction (the range width stands between 1 m/s and 2 m/s for the speed and is about 10 deg. for the direction), and in linking them to process series of 4096 or 9192 points by Fast Fourier Transform.

3. Turbulence characteristics

We consider here the horizontal component u in the mean wind direction and the vertical component w. Table 1 gives the turbulence intensities I_u and I_w , the longitudinal turbulence scales L_u^x, L_w^x, obtained by fitting a Von Karman spectrum to the p.s.d. of the fluctuations, and the coefficients of the lateral coherence, defined as the square of the normalized co-spectrum between fluctuations in two points. The wind model values are also given, as well as the wind-tunnel values during testings on the taut-tube model.

		Turbulence Intensity (%)		Longitudinal turbulent scales (m)		Lateral coherence coefficients	
Wind Sector		I_u	I_w	L_u^x	L_w^x	C_u^y	C_w^y
Sea winds	(1)	7.1	4.6	260	22	15.8	13.5
	(2)	9.0	5.0	200	35	11.0	12.0
	(3)	9.5	6.8	100	20	10.0	10.0
Land winds	(1)	12.5	8.8	170	24	41.4	23.2
	(2)	14.6	8.2	100	30	10.0	10.0
	(3)	15.0	11.6	80	20	12.0	10.0

(1) Field measurements (2) wind model (3) wind tunnel values

Table 1 : Turbulence characteristics on the site

In the wind model, the turbulence intensities and turbulent scales are used to estimate $S_i(n)$, the p.s.d. of the wind fluctuations. The standard deviation of the modal acceleration of the structure being proportional to $\sqrt{nS_i(n)}$ where n is the mode frequency, the comparison between measurements and wind model, is made on the values of this term, corrected by the wind oblicity ($\cos\theta$), and in the frequency domain of the 14 first modes (0.15-0.95 Hz) (fig.1). In case of sea winds (270 deg.) the model fits well measurements, but in case of land/sea winds (250 deg.) the model over-estimates of about 20%, the excitation due to the longitudinal component, and under-estimates of about 15% the excitation due to the vertical component.

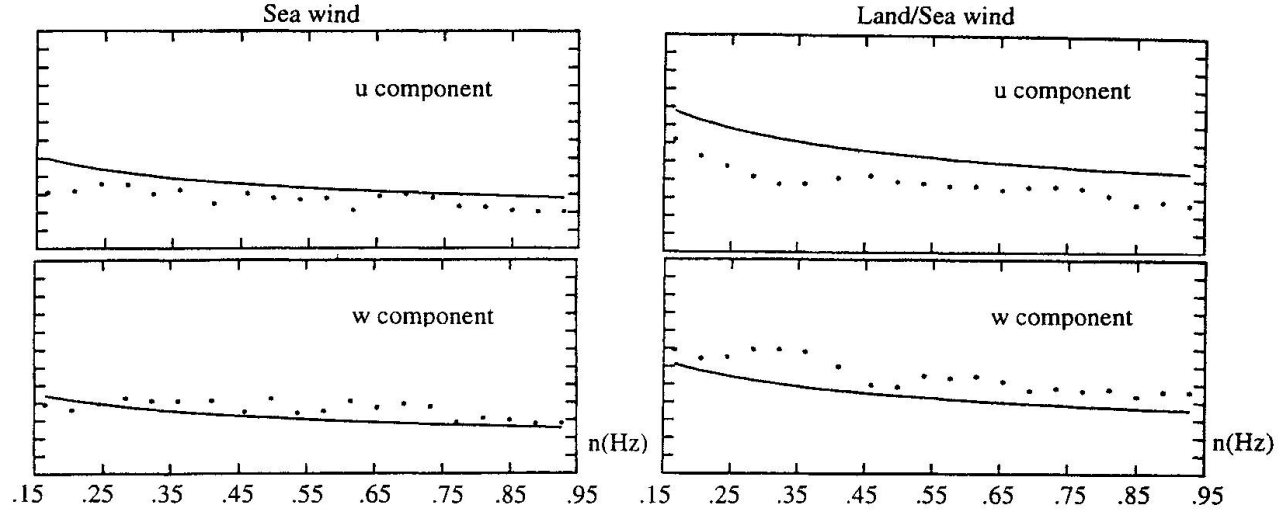

Figure 1 : Dsp of wind fluctuations $\sqrt{nS_i(n)}\cos\theta$

The coherence coefficients deduced from the measurements are higher than in the wind model, but as their values are greatly influenced by low frequency fluctuations, of minor importance for the bridge response, a direct comparison of the coherence functions in the frequency domain 0.15 Hz - 0.95 Hz (fig.2) is more adequate. The model fits well the measurements for the vertical fluctuations, but it overestimates the correlation between longitudinal fluctuations, when the separation between points is greater than 10 m, which is conservative for the structure.

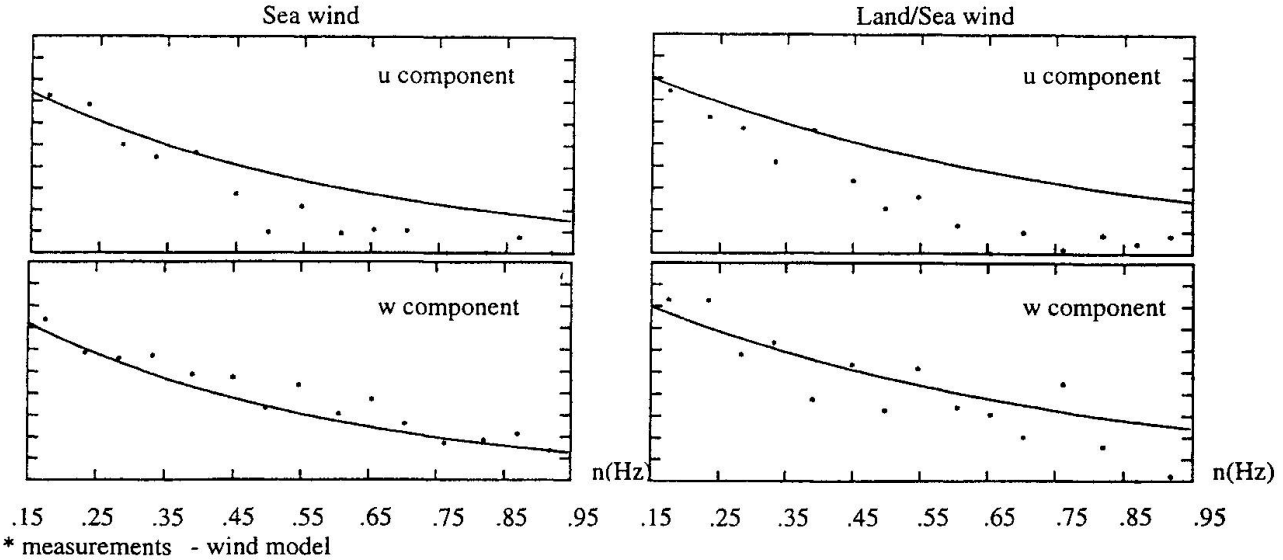

Figure 2 : Lateral root-coherence (Separation 5 m)

4. Dynamic behaviour of the bridge

By comparing the p.s.d. of acceleration at the various measurements points, seven vertical flexion modes, three horizontal oscillation modes and three torsional modes have been identified (table 2). One mode at 0.606 Hz has been observed on the pylon only. These observed modes are compared with the results of computations [1] and with the previous modal identification on the bridge, made by forced vibration testings [7]. The modal frequencies are very close to the previous estimations, except the frequency of the first torsional mode (0.727 Hz) which is higher than the value predicted by computations (0.486 Hz). As the modelisation of the torsional stiffness was not perfect in the computational model, a higher torsional frequency was expected. However, a so large frequency shift is rather surprising ans it adds security to the bridge.

Observed modes during strong winds			Measured natural frequencies (Hz)	Computed natural frequencies (Hz)
Natural frequency (Hz)	Type	Code	Identification 1995 from [7]	SETRA from [7]
0.168	Horizontal sway 1 (symmetric)	BH1	0.171	0.154
0.233	Vertical flexion 1 (symmetric)	FV1	0.232	0.226
0.295	Vertical flexion 2 (anti-symmetric)	FV2	0.293	0.27
0.388	Vertical flexion 3 (symmetric)	FV3	0.388	0.383
0.397	Horizontal sway 2 (anti-symmetric)	BH2	0.399	0.362
0.42	Horizontal sway 2bis (anti-symmetric)	BH2b	0.423	not computed
not observed	Vertical flexion 4 (anti-symmetric)	FV4*	not observed	0.385
0.466	Vertical flexion 4 (anti-symmetric)	FV4	0.464	0.475
0.544	Vertical flexion 5 (symmetric)	FV5	0.543	0.525
0.606	only observed on the pylon	8bis	not observed	not computed
0.618	Torsion (symmetric) + horizontal sway	9	0.622	0.52
0.678	Torsion (symmetric, very weak level)	10	0.677	not computed
0.696	Vertical flexion 6 (anti-symmetric)	FV6	0.694	0.616
0.727	Torsion 1 (symmetric)	T1	0.727	0.486
0.93	Vertical flexion 7 (symmetric)	FV7	0.925	0.714

Table 2 : Observed modes on the site

The modal amplitudes are computed by integration of the p.s.d. of the displacements, in the vicinity of the mode frequency. To take into account a frequency shift between the real bridge and the project, and consequently on the taut-tube model, the modal amplitudes are plotted versus the reduced wind speed Vr=V/nB, (n is the mode frequency and B the deck width) corrected by $\cos\theta$. The modal amplitudes are normalized by $I_u B$ (for horizontal modes) or $I_w B$ (for vertical modes), in order to make the results independant of the upstream turbulence intensity.

Figure 3 shows the results for the first horizontal oscillation mode (BH1) and the first vertical flexion mode (FV1). For the mode BH1, the wind-tunnel measurements gave lower values (of about 30-50%) than the field measurements. This can be easily explained by the effects of drag forces on the stays, not considered on the taut-tube model, but introduced in the design process of the bridge. Considering the five first vertical flexion modes, the measured amplitudes are very close to the values obtained with the taut-tube model. For the first torsional mode, the measurements appear to be slighly lower than the taut-tube model values.

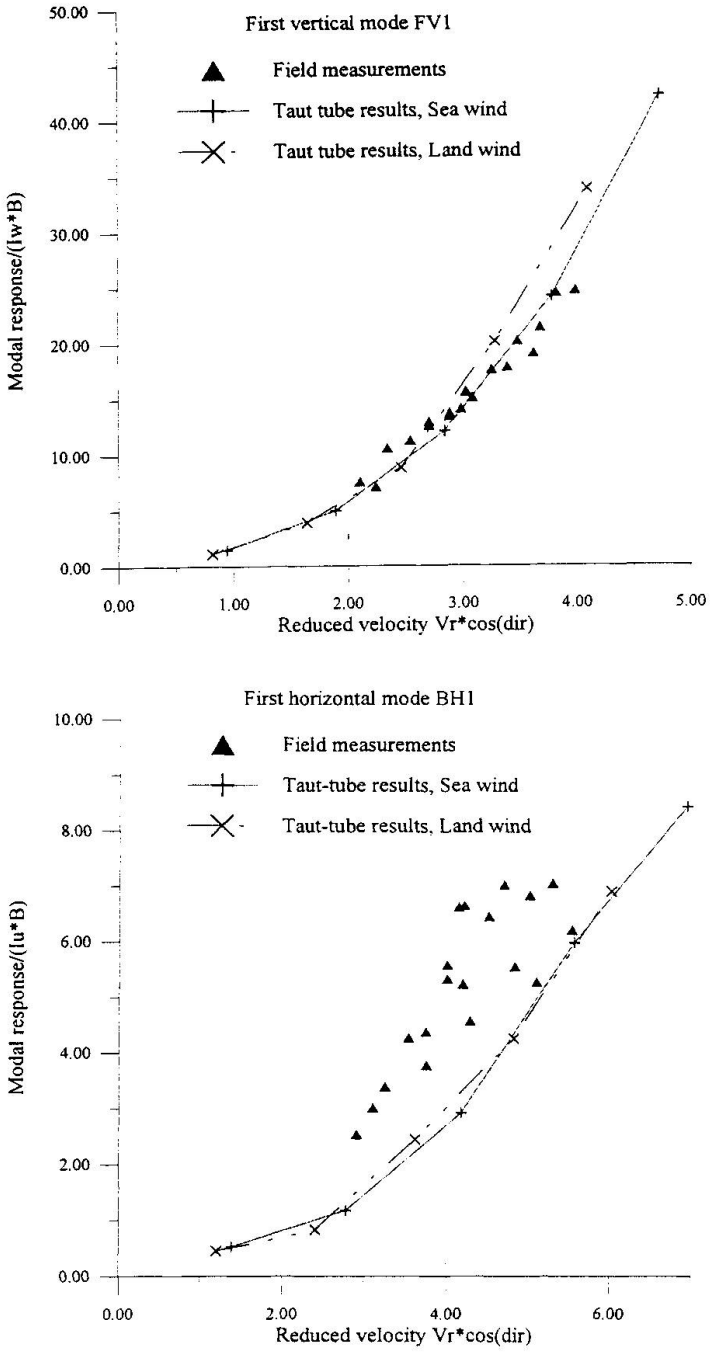

Figure 3 : Normandie Bridge - Comparison field measurements/taut tube model results

The damping ratios are defined relatively to the critical damping, and represent the sum of the structural and the aerodynamic dampings. They are obtained by fitting the theoretical curve of a single degree of freedom linear visco-elastic system, to the resonance peak of each mode. The fitting is made by the maximum likelihood method, which is much more precise than the classical least square method [8].

The damping ratio for the mode BH1 lies between 0.5% and 1.6%, and is generally greater than the structural damping (0.6%) which was measured during the forced-vibration testings. This difference cannot be explained by the aerodynamic damping which is very low for this mode, but probably by the bias due to the little number of spectral lines inside the peak (only seven in the half-power bandwidth when using 8192 points sequences). Concerning the vertical flexion, all the modes give a similar evolution versus the reduced windspeed (fig.4). This evolution was very well predicted by computing an aerodynamic damping using the slope $C'_N = 4.5$ of the curve of the lift coefficient, value which was measured in the wind-tunnel at 1/50 scale [2]. The damping ratio linked to the torsional modes lies between 0.6% and 1%, to be compared to the structural damping of 0.4% obtained from the forced vibration testings. Here, the difference can be explained by the aerodynamic damping, as it was already observed with the taut-tube model tests.

5. Conclusion

The analysis of wind data over a two-year period, including high wind speed sequences, up to 22 m/s for the mean value, have allowed to validate the wind model used for the design of the Normandie Bridge, in terms of the turbulence description. This data base will allow to constitute a new wind model for sea wind, adapted to long-span bridges.

The dynamic behaviour of the bridge has been well defined, by identifying fourteen vibration modes, and by estimating modal amplitudes and damping ratios for eight of them. The results are generally in good agreement with wind-tunnel measurements on the taut-tube model and are from 50% to 100% lower than the values issued of the computational approach which was used in the design of the bridge. This confirms the validity of the previsional studies made in 1991, and the high level of security of the bridge. These results could be completed by new theoretical computations, taking account of the real characteristics of the wind on the site, as well as the new modal characteristics, as they have been measured.

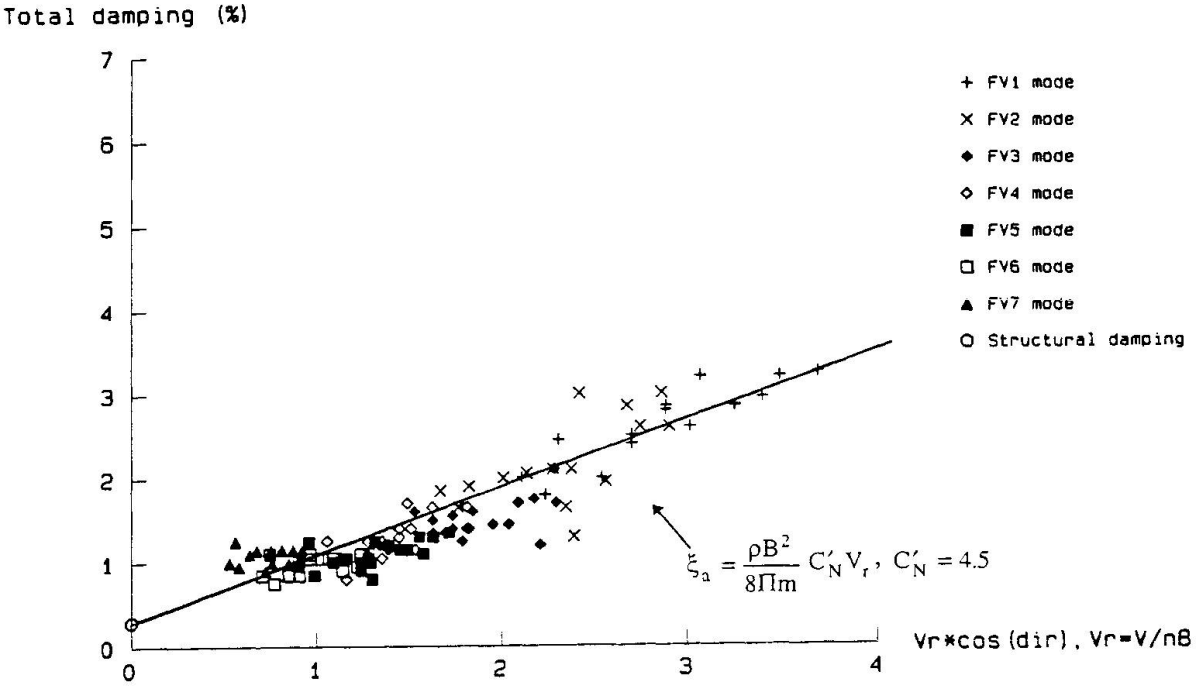

Figure 4 : Normandie Bridge - Field measurements - Damping of the vertical modes

Acknowledgements

These studies of wind action on the Normandie Bridge were initiated by CCI du Havre who acted as sponsors of the studies. The assistance and co-operation of the sponsors are gratefully acknowledged.

References

[1] Virlogeux M., 1992, "Wind design and Analysis for the Normandie Bridge", Aerodynamics of Large Bridges, A Larsen Ed., 1992 Balkema, Rotterdam, ISBN 905410042 7.

[2] Bietry J., Grillaud G., 1994, "Wind studies for the Normandie Bridge", Ponts Suspendus et à Haubans, Conférence AFPC, 12-15 oct. 1994, Deauville, France.

[3] Delaunay D., 1988, Etude expérimentale des caractéristiques de la turbulence atmosphérique au-dessus de la mer (site du Pont de St-Nazaire), CSTB, EN-CLI 88C

[4] Delaunay D., 1990, Etude expérimentale de la turbulence atmosphérique sur le Pont de Normandie, CSTB, EN-CLI 90.12C

[5] Grillaud G., Flamand O., Barré C., 1991, Comportement au vent du Pont de Normandie, étude en soufflerie sur maquette aéroélastique à l'échelle du 1/200è., CSTB, EN-AS 91.5 C

[6] Littler J., 1995, An assessment of some of the different methods for estimating damping from full-scale testing, J.Wind Eng. Ind. Aerodyn., 57, 179-189

[7] Bietry J., Jan P., Epreuves dynamiques du Pont de Normandie , CSTB, EN-D 95.5 C

[8] Agrati S., 1995, Estimation of structural parameters from ambient vibration test, Tesi di laurea, Politecnico di Milano (I), Facolta di Ingegneria, Dipartimento di Meccanica.

The Future Fehmarn Belt Link

Dietrich L. HOMMEL
Chief Eng., Bridges
COWI Consult. Eng. and Planners AS
Copenhagen, Denmark

D.L. Hommel graduated from Technical Univ. of Braunschweig, Germany, in 1966. In 1968 he joined Leonhardt, Andrä und Partner, where he was involved in bridge designs in Germany and abroad during 25 years. Since 1995 he is member of COWI, and is presently the project manager for the Fehmarn Belt Feasibility Study.

Lars HAUGE
Chief Eng,
COWI Consult. Eng. and Planners AS
Copenhagen, Denmark

L. Hauge graduated from the Technical Univ. of Denmark in 1986. Since 1990, he has been employed by COWI, where he works with design of cable supported bridges. He was recently project manager for the detailed design of the cable stayed bridge of the Oeresund Link and is presently design group leader for the bridge for the Fehmarn Belt Link.

Summary

This article describes the Feasibility Study for a future fixed Link across Fehmarn Belt and focuses on the combined roadway and railway bridges solutions. The about 19 km wide and up to 29 m deep Belt is heavily trafficed by ships which are demanding large spans for safe navigation. Furthermore, the Fehmarn Belt is important for the exchange of waters to and from the Baltic Sea and major structures will influence the presently undisturbed flow of water. Environmental guidelines were developed to define an improved structural layout of the underwater part of bridge piers and pylons especially. The presentation will describe the general status of the Feasibility Study, highlight the investigations for the approach bridges and present the two alternative main bridge solutions studied. The study will be concluded in the summer of 1998, and a final decision for this link will not be available before 1999.

1 Introduction

In the treaty between Denmark and Sweden concerning the Øresund Link, Denmark has 1991 agreed to study possibilities for a fixed link across the Fehmarn Belt in the future and together with Germany. The traffic ministries of Denmark and Germany decided to initiate studies which are funded jointly by the two countries and supported by the European Community. This resulted in a Pre-feasibilty Study during 1992/93 - awarded to a Joint Venture between COWI (Denmark) and Lahmeyer International (Germany) - which defined the extent and a number of main structural solutions like tunnels and bridges or combinations thereof for the next study phase. The following Technical Investigations as part of the Feasibility Study was

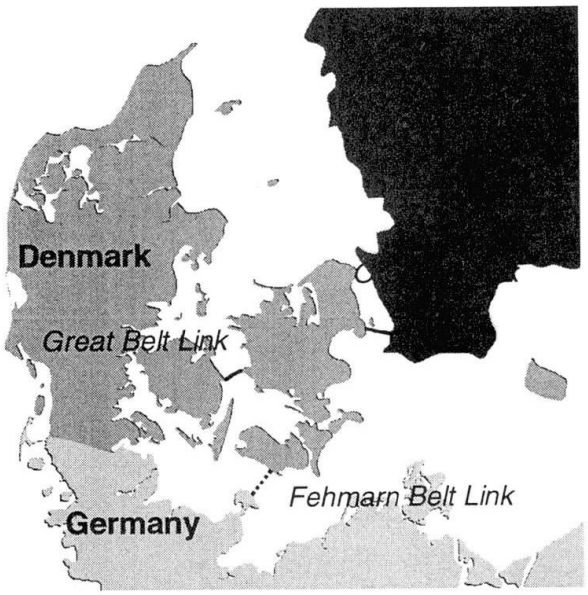

in 1995 contracted to the same group of consultants and limited to the coast-to-coast connection between the islands of Fehmarn and Lolland, as illustrated in Fig. 1.

Parallel to the technical investigations the Client had contracted within the frame of the Feasibility Study a Geological-Geotechnical Investigation and an Environmental Investigation as well to provide relevant information for the three study teams.

Fig. 1 : Location of Fehmarn Belt Link

2 Development of the Technical Investigations

During the first phase of the study 7 solution comprising bored and immersed tunnels and bridges were reviewed, cost estimates developed and compared to each other. In the second phase - which has started in December 1997 - a total of 5 solutions with some modifications are studied in a conceptual design and later evaluated to recommend the most viable one within the three capacity groups under review. This article is limited to a description of the bridge alternatives only.

The bridge solution for the Fehmarn Belt is envisaged to comprise a cable supported bridge spanning the navigation channel and two approach bridges. The bridge will accommodate four lanes of motorway traffic and a dual track railway arranged in two levels.

Two scenarios for the ship traffic have been studied, east bound and west bound ship traffic in the same navigation channel with a 1,700 m clearance and east bound and west bound ship traffic in separate navigation channels with 2 times 700 m navigation clearances separated by approximately 700 m.

A vertical clearance of 65 m is required over the entire width of the navigation channel.

3 Long Span Bridge

Two cable supported bridge concepts have been studied matching the two principal arrangement of the ship traffic, a multi-span cable stayed bridge, with separated navigation channels and a suspension bridge, with one navigation channel.

3.1 Cable-Stayed Bridge

The cable-stayed bridge is outlined with three main spans of 720 m and a total length of 3,144 m.

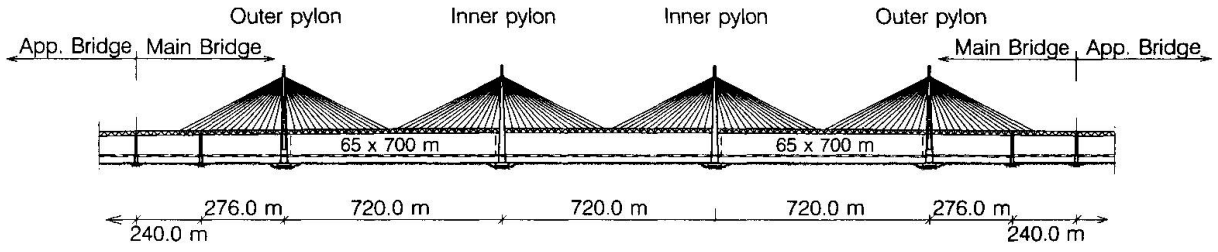

Fig. 2 : Cable-Stayed Bridge

Compared to a conventional single main span cable-stayed bridge, a multi-span bridge requires additional stiffness from either the cable system or from the pylons to minimise deflection from unsymmetrical distributed live load. Three solutions have been considered to provide the additional stiffness :

1. "Crossed cable" solution
2. "Triangulated pylon" solution (rigid pylon)
3. "Semi-rigid pylon" solution (semi-rigid pylon)

The investigations showed that the "semi-rigid pylon" was the optimal solution considering the site specific conditions.

3.1.1 Superstructure

For the cable-stayed bridge, where different conditions prevail for different sections of the girder, a combination of cross section types is appropriate. The investigations showed that the optimal solution has two layouts of the girder, a single composite, with a concrete roadway deck and lower steel deck, and a double composite with a concrete roadway deck and a lower railway deck.

The side spans are outlined with double composite girders to limit the uplift forces in the backspan piers. The 195 m of the girder closest to the pylons are outlined as double composite structures to carry the global compression forces efficiently by the concrete. The remaining parts of the girder are outlined as single composite structures. The girder depth of 15 m, is determined by the approach bridges. The girder is supported by the cable stays every 24 m. The cable stay force is transferred to the cross section in such a way that the vertical component is taken by the vertical strut and the horizontal component by the horizontal edge beam, in which the cable stays are anchored.

3.1.2 Substructure

Foundations

The pylon foundations are assumed to be constructed as prefabricated cellular caissons with an open outer base structure off site in a drydock and towed to the site. The caissons are to be placed on crushed stone beds in an excavation to allow the base structures to be fully

embedded into the sea bed and thus reduce the flow resistance as much as possible. At the sea level, the outer shaft walls are to be strengthened to sustain the ship impact forces.

Pylons
The pylon are proposed as concrete structures constructed by climbing formwork as recently applied on both the Great Belt and the Öresund bridges. The proposed layout requires that the inner towers are semi-rigid, and the outer towers are as flexible as possible. For architectural reasons, the inner and outer pylons have the same shape. The difference in stiffness is obtain by omitting material in the centre of the pylon.

3.2 Suspension Bridge

The suspension bridge is outlined with a main span of 1,752 m and side spans of 600 m.

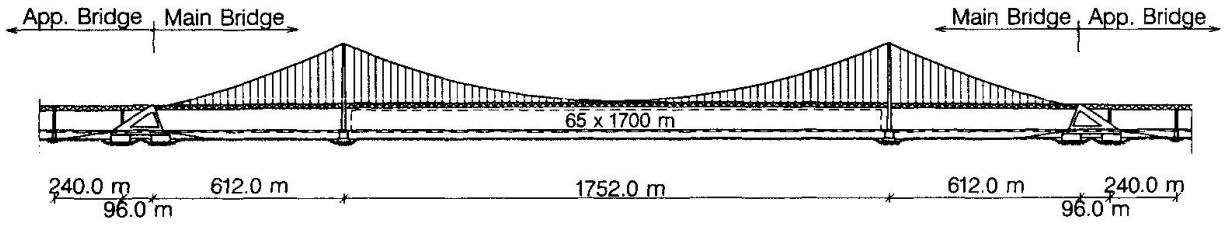

Fig. 3 : Suspension Bridge

The suspension bridge is outlined with a continuous girder between the anchor blocks. A number of advantages is obtained :

- the longitudinal movements are reduced, compared to a traditional system with joints at the pylons,
- the number of vulnerable elements as bearings and joints is minimised,
- the appearance is improved.

A torsional support is arranged at the pylons, and longitudinal supports are arranged at the anchor blocks. The optimal solution was found to be an all steel structure with a sag to span ration of 1/9. During the tender design in 1979 for a suspension bridge for combined road and railway across the Great Belt, extensive analysis were carried out to demonstrate that an all steel solution was adequate. The calculations showed that all requirements could be fulfilled with a light, all steel solution.

3.2.1 Superstructure

The roadway deck is outlined with as an orthotropic steel deck, supported by cross beams every 4 m. At the hanger anchorage a larger cross beam is provided together with a slender tension member, which connects the hanger anchorage and the lower truss joint and thus transfers the hanger force into the truss.

A distance of 28.5 m between the main cables has been selected, which preliminary calculations have demonstrated to be sufficient to ensure the aerodynamic stability of the bridge. Vertical hangers are arranged every 24 m. Twin hangers are foreseen at each position.

3.2.2 Substructure

Pylons
The design and construction principles are identical to the cable-stayed bridge pylons.

Anchor Blocks
The anchor blocks are to be divided into two separated caisson bases to support a high caisson beam. The caisson structure forms the support for a triangular structure which consists of the splay chamber and the front legs as support for the end span of the approach and the main bridge girders. The rear part of the caisson beam and the rear caisson base contain the massive cable anchorage.

The caisson bases and the lower part of the caisson beam are assumed to be produced off site in a drydock and towed to the site. The anchor blocks are protected from ship impact by streamlined artificial islands in the direction of the current flow.

4 Approach bridge

The approach bridges govern the costs of the link and have a determining impact on the water flow in the belt. The span length has been optimised to minimise construction cost. This minimum has proved to be almost constant in a certain range of span lengths. To minimise the environmental impact relatively large spans of 240 m have been selected. For aesthetic reasons all spans are identical. Expansion joints are arranged every five spans, i.e. every 1,200 m to limit the requirements to the railway expansion joint especially.

4.1.1 Superstructure

The girder has been chosen with a composite cross section with an overall depth of 15 m.

The road deck is outlined as a transversely post-tensioned concrete deck. Above the support, where the deck is subjected to large tension forces, a cross section without transverse post-tensioning will most likely have to be arranged, to be able to utilise the longitudinal mild reinforcement. The deck is 24.7 m wide between the outer parapets.

The railway deck is outlined as a closed steel box stiffened by troughs and has dual tracks with emergency walkways on both sides. Application of a lower deck in steel has proven to provide a robust structure, especially with regard to accidental loads such as fire, derailment and ship collision. The lower deck acts as a torsional stiff girder being able to distribute the load beyond the damaged areas. It has further an extra reserve in the overcritical area.

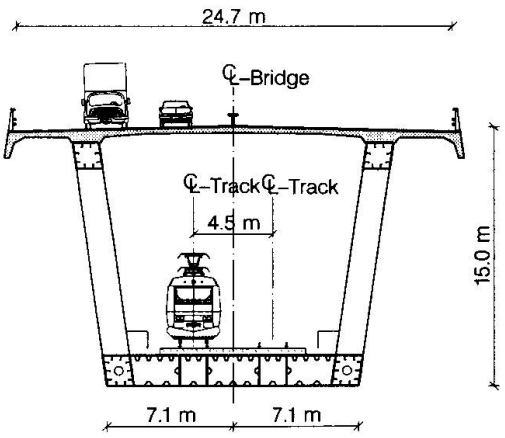

Fig. 4 : Cross section, approach bridge

All interior surfaces are to be corrosion protected by dehumidification. By keeping the relative humidity below 60% no corrosion will occur, and by avoiding to paint the interior surfaces substantial savings can be obtained.

4.1.2 Substructure

The geological profile for the chosen alignment generally shows two different soil conditions for the approach bridges. The profile allows for a direct foundation of the northern piers, whereas a piled foundation might be foreseen for the southern piers to reduce expected large settlements in the tertiary clay formations.

The approach bridge piers are to be divided into three parts, the pier shaft, the caisson shaft and the caisson base.

This division allows for extensive on-shore prefabrication. The caisson's base and shaft are assumed to be produced as one unit and the pier shaft as another unit. The caissons and the pier shafts will be produced in a drydock or a prefabrication yard and transported to the site.

The caisson shaft is to be designed to sustain and transfer ship impact loads to the base structure. Furthermore, the caisson shaft is to be shaped in a way to reduce resistance to the water flow in the Belt. An shape with circular ends has been chosen so far, but an improved elliptical shape is studied at present. The caisson unit can be rotated around a vertical axis with the caisson shaft main axis parallel to the current direction.

The caissons are to be constructed as prefabricated cellular structures with an open outer base structure. At the interface zone between the pier shaft and the caisson shaft a massive in-situ cast structural plinth is assumed.

The caissons are to be placed on a crushed stone bed's constructed in an excavation allowing for the base structure to be fully embedded into the sea bed. Where piles are required, the open cell caisson base is assumed to serve as a template for the construction of 35-45 m long bored Ø3 m piles. The bored piles are foreseen with a 4.5 m conical enlargement at the tip of the piles.

After drilling and casting of the piles the piletops are rigidly connected to the bottom of the caisson base, before the caisson will be ballasted with sandfill. For the piled foundations no crushed stone layer or underbase grouting have been foreseen.

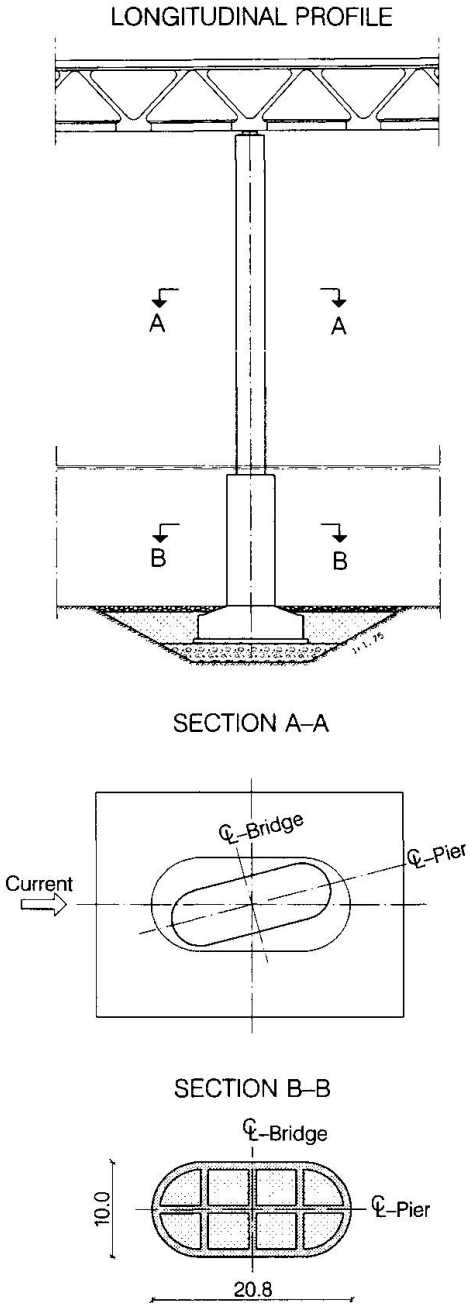

Fig. 5 : Approach bridge pier

Optimisation of Life-Cycle Costs of Concrete Structures

Susanne TROIVE
Civil Eng.
Royal Institute of Technology
Stockholm, Sweden

Hakan SUNDQUIST
Prof.
Royal Institute of Technology
Stockholm, Sweden

Susanne Troive, born 1963, received her civil Eng. degree in 1987 at the Univ. of Lulea, Sweden and finished her licentiate thesis in 1996 at The Royal Inst. of Technology

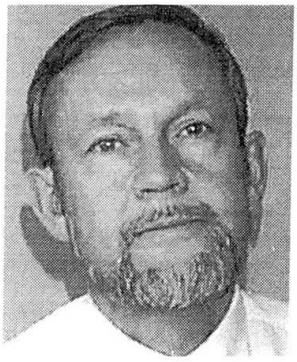

Hakan Sundquist, born 1944, received his civil eng. degree in 1967 and finished his Ph.D. thesis in 1979 at The Royal Inst. of Technology. Since 1992 is he professor in Structural Design and Bridges at The Royal Inst. of Technology

Summary

In the standards and design recommendations, required service life for new bridges is long, often 120 years or longer. It is also specified how the design parameters shall be chosen to reassure that the expected service life is achieved. The authors of this paper do not believe that this approach is economical for countries with a high real rate of interest. Instead, if the life-cycle costs and expected service lives for different designs are calculated, then the optimal design according to minimum annuity cost should be chosen. This approach also simplifies introduction of new materials or new designs. In this paper, an optimisation example is presented, where design parameters for an ordinary reinforced concrete bridge deck is optimised regarding to minimum annuity cost. A high concrete quality, made of Swedish high quality cement, is the most economical in this example. Other concrete mixtures would produce other results.

1. Introduction

Of tradition, research within structural engineering has been separated from economy. The economical consequences of improvements, innovations et cetera have been undertaken. Especially within the field structural measures to lengthen the service life of structures, in combination with the life cycle cost of the structure, very little research is done.

Nowadays it is not difficult to build and maintain bridges with respect to long service lives; but it is expensive. Nowadays, design recommendations often prescribe service lives of about 120 years or longer, and it is also specified how to choose design parameters, as for example concrete quality, concrete cover and maximum crack width, to achieve this long service life, and often with a safety marginal. These design specifications has led to higher investment costs, and if this approach really is economical for the nation has not been examined - the costs for the longer service lives have been of lower interest.

A long service life does not guarantee a good economy. Investigations show, that only about ¼ of replaced bridges are replaced because of structural deficiency /1/. To provide cost effective concrete structures, the design parameters should be chosen with respect to minimum annuity

cost. It is therefore necessary to predict the expected service life for different designs of a concrete structure, already in the design phase. Then the life cycle cost, LCC, for the different alternatives can be calculated and distributed over the service life to an annuity cost.

2. Optimal durability

An insufficient durability leads to costs for repair, rehabilitation or replacement in a too close future. The higher durability of a structure, the higher investment costs, but also, the cost due to insufficient durability decreases. Optimal durability will be found at minimum total cost, Fig. 1. A low durability, that is a short service life, causes a high annuity cost because the annuity factor increases rapidly for short service lives.

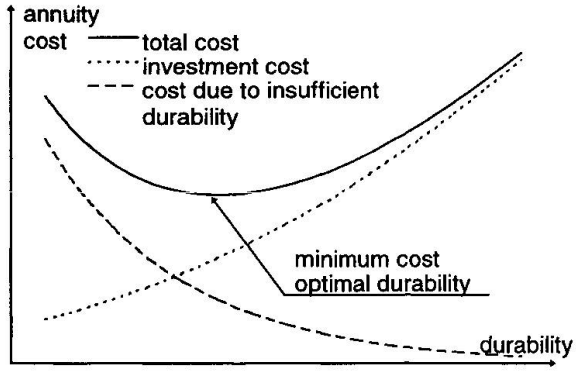

Fig. 1 Optimal durability occurs at minimum total cost, the sum of investment cost and cost due to insufficient durability.

To design structures with low annuity cost, it is necessary to connect the deterioration model to the life cycle cost of the structure. The common factor in the deterioration model and the economical model is time. This enables economical design with interaction formulae. Therefore, it is important to base the design recommendations on functional demands, not specific minimum values for each single parameter. It is also important to bring useful equations for durability calculations into the design process.

3. Optimisation example

3.1 Description of the problem

In this paper, an example of how design parameters can be chosen for optimal durability is presented, some other examples will be presented in /2/. The structural design of an ordinary reinforced concrete bridge deck is optimised regarding to minimum annuity cost. Deterioration of the bridge is caused by reinforcement corrosion due to chloride diffusion. The chloride environment is aggressive, and it is supposed to correspond to de-icing salted environment. There are no beams or other bearings, the deck is carried only by itself. Span length varies between 5 and 20 m. The bridge carries an external load of 30 kN/m^2 but also its own weight and the weight of the pavement. Minimum tolerable concrete cover is chosen to 20 mm.

The ordinary form of an optimisation problem is:

- Given: constant parameters
- Find: design variables
- Optimise (minimise): objective function
- Satisfy: design constraints

The objective function to be minimised, is the annuity cost. The design parameters are: total height of the section, concrete cover, water to cement ratio and reinforcement area. Four constraints are given; minimum load bearing capacity in ultimate limit state, balanced section

control, maximum crack width (0.4 mm) and maximum mid span deflection in the middle of the span (span length/400).

The optimisation results in a spectra of design parameters that, depending on span length and rate of interest, yield the optimal design. The partial coefficient method is used for capacity and deflection calculations. In structural design of bridges also other demands, like shear forces and accidental loads, are important. However, the optimisation problem, presented in this paper, only regards durability, loads in ultimate limit state, and deformation caused by the traffic. In an extended calculation, also other demands may be included.

The used optimisation method is the Method of Moving Asymptotes, MMA, which is a convex approximation method for structural optimisation /3/. MMA is an iterative method. In each iteration, a convex sub problem which approximates the original problem, is generated and solved. An important role in the generation of these sub problems is played by a set of parameters which influence the "curvature" of the approximations and also act as "asymptotes" for the sub problem. By moving these asymptotes between each iteration, the convergence of the overall process can be stabilised.

3.2 Annuity cost

For investments with equal service lives, optimal design can be chosen based on minimum life cycle cost, *LCC*. If service lives differ, a comparison between annuity costs is more suited. The annuity cost can be calculated by eq. 1 where *LCC* is the life cycle cost, discounted to present value, F_A is the annuity factor, B_n is the sum of all costs and benefits in year n, r is the real discount rate, real interest rate calculated for costing purposes, and N is the service life.

$$A = LCC \cdot F_A = \sum_{n=0}^{N} \frac{B_n}{(1+r)^n} \cdot \frac{r}{1-(1+r)^{-n}} \qquad (1)$$

In economical calculations, the discount rate is very important. A high discount rate favours shorter service lives. The discount rate can be chosen in different ways, where the interest rate an alternative investment can bring, or bank rate for a loan, are the most common. For cost-benefit analyses a discount rate can be calculated out from the financial situation for the society today compared to tomorrow. The discount rate may also be politically decided, as for example in Sweden, 4 % is recommended for cost benefit analyses within the transport sector. The discount rate in the following example considers real interest rate calculated for costing purposes, and varies between 2 % and 12 %.

3.3 Service life calculations

During the last decades, concrete durability has been a highly prioritised research area. Technical service life of a structure is usually divided into initiation time and propagation time /4/. The initiation time used to be calculated with Fick's 2nd law of diffusion. However, later research has showed that both diffusion coefficient and chloride surface concentration are time dependent, and the classical solution of Fick's 2nd law has to be modified, se for example /5/. In de-icing salted environment, chloride surface concentration increases in winter period and decreases during the summer. At a distance of 20 to 30 mm from the surface, the relative humidity is almost constant during the year and from this distance and deeper, the chloride profile often looks similar to profiles in marine environment.

Still, there is not enough knowledge of concrete deterioration, to present equations that can be used by structural designers, in purpose to predict expected service life of concrete structures in different environments, already in the design phase. Therefore, in this paper, expected service life in de-icing salted chloride aggressive environment is calculated out from eq. 2, which is an approximation of the classical solution of Fick's 2nd law of diffusion by /6/. The relation between diffusion coefficient and water binder ratio obtained by /7/ is used.

$$t = \frac{x_{cr}^2}{12 \cdot D_{eff} \cdot \left(1 - \sqrt{C_{cr} / C_s}\right)^2} \qquad (2)$$

In eq. 2, is t the initiation time for reinforcement corrosion, x_{cr} is the distance between the concrete surface and the reinforcement, D_{eff} is the effective diffusion coefficient, C_{cr} is the chloride threshold value, and C_s is the chloride concentration at the concrete surface, extrapolated from the chloride profile inside the concrete.

An example of measured chloride concentrations versus water binder ratio, in concrete made of ordinary Portland cement and with water reducer, is shown in Fig.2 /8/. The concentrations have been obtained from 15 to 40 years old outdoor structures. The relations between chloride concentrations and water binder ratio is likely to be exponential.

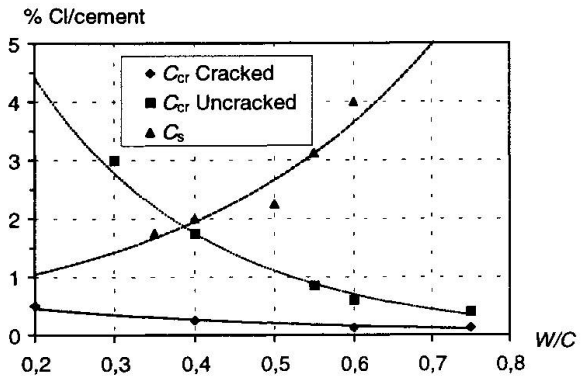

Fig. 2 Measured chloride threshold values and maximum surface chloride concentrations by water binder ratio. Redrawn from /8/.

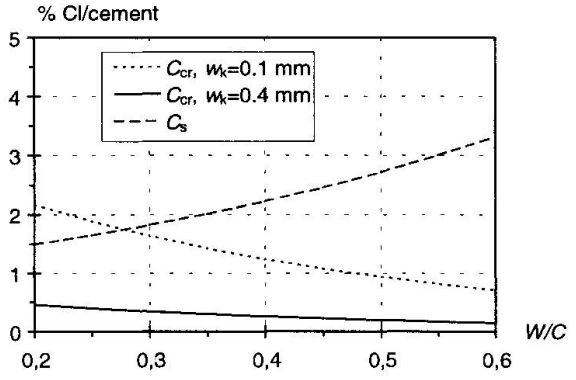

Fig. 3 Chloride concentrations used in the calculations. Chloride aggressive environment.

Other investigations show that the chloride threshold value is smaller than in Fig. 2, c.f. /9/. Therefore, in this paper, the chloride threshold value is supposed to be exponentially related to water binder ratio and linearly dependent on crack width as shown in Fig. 3. The chloride surface concentration is supposed to be exponentially dependent on water binder ratio, Fig. 3, and refers to de-icing salted environment is in this example.

3.4 Results

Optimisation of the problem results in a spectra of optimal design parameters that together yield the most economical design. It is important to remember that every single parameter is a part of the total design and can not be treated separately; it is the combination of the design parameters that is important. The parameters are chosen so that the total design is optimised.

The optimisation method MMA was easy to use, and optimal value was found already after 5-10 iterations. Optimal water to cement ratio became in all these examples as small as tolerable, here chosen to 0.35. Total height was independent on discount rates because of the deflection constraint; 255 mm for span length 5 m, 510 mm for 10 m, 764 mm for 15 m, and 1019 mm for span length 20 m.

I Fig. 4 to 7, results from optimisations for different discount rates and span lengths are presented. The objective function, Fig. 4, is the sum of concrete cost and reinforcement cost, including construction cost, and it is almost linear because of the long service lives achieved. Most important for the results were the discount rate and the interactions between chloride concentrations and water to cement ratio.

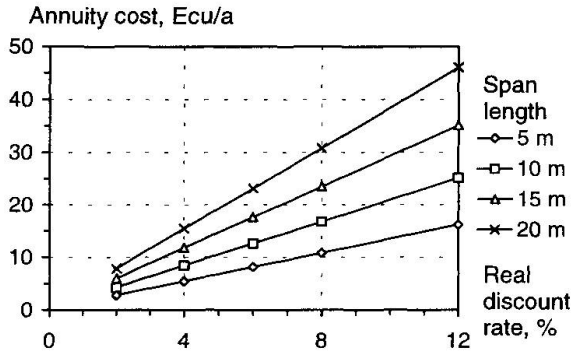

Fig. 4 Objective function, annuity cost.

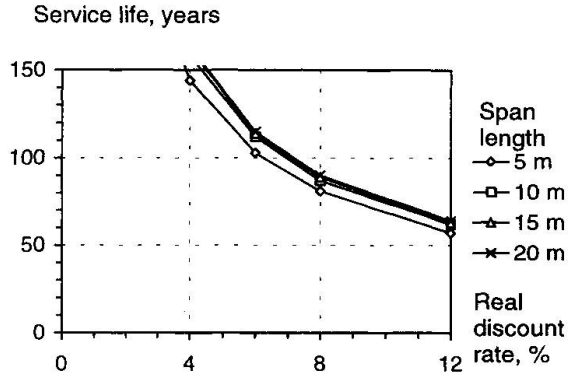

Fig. 5 Optimal service life.

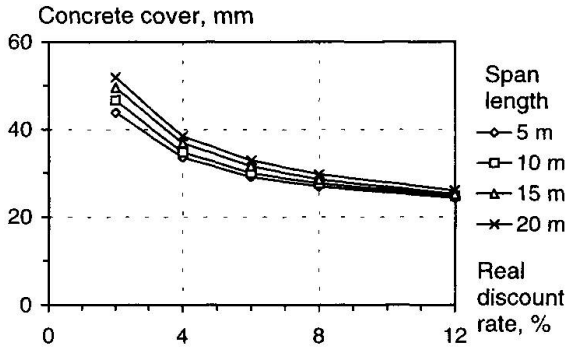

Fig. 6 Optimal concrete cover.

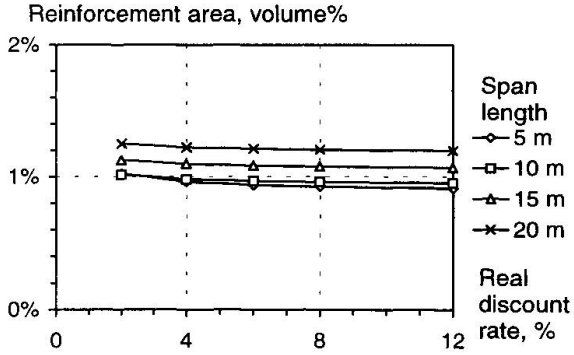

Fig. 7 Optimal reinforcement area in % of concrete volume.

In Fig. 5, optimal service life, related to discount rate and for various span lengths, is shown. The service lives for the optimised structures are long, about 60 years at discount rate 12 %, 80 years at discount rate 8 %, 110 years at discount rate 6 % and still longer at lower discount rates. This is mainly caused by the used relations between chloride threshold values respective chloride concentrations and water to cement ratio. Typical Swedish bridge concrete made of Swedish high quality cement withstands deterioration due to chloride ingress quite well. The cost for better concrete quality is rather low and the benefit exceeds the cost.

At small discount rates, concrete cover is about 50 mm in optimal design, but optimal concrete cover decreases with increasing discount rate, Fig. 6. Optimal concrete cover increases with increasing span length. The reinforcement amount is rather high, cf. Fig. 7, crack widths are limited, and with the assumed crack width approach, a high chloride threshold value can then be used.

In all optimisations, constraint number one, load bearing capacity in ultimate limit state, and constraint number four, maximum mid span deflection, was dimensioning. Constraint number two and three, balanced section control respectively maximum crack width, were not dimensioning in any case.

4. Conclusions

In this paper, the calculations show that economical optimisation of concrete structures in the design phase is possible. However, the result of an optimisation calculation is strongly dependent on input. The calculations are only intending to be examples of how to optimise structures with respect to economy, durability and structural design. Different concrete mixtures, environments and other conditions would of course produce other results. These examples are made for bridge concrete made of Swedish high quality cement with water reducer and air content adhesives. More research is needed to find better relations between concrete recipes respectively structural design and service life of concrete structures. However, the inputs to the calculations in this report are intended to be as close to reality as possible.

The example shows, that high concrete quality, normal concrete covers and small crack widths are economical if a higher threshold value then can be used. Optimum service life is long. However, the calculated service life is the mean service life, not calculated with safety marginal. In the calculations, the benefit of the bridge expects to be unchanged during the service life. Functional deficiency may decrease the benefit.

To build cost effective structures, the structural designer has to choose optimal design with respect to long term economy. If the expected service life for different durability alternatives can be calculated, and the maintenance and repair cost can be estimated, then the design corresponding to minimum annuity cost can be chosen. In this way, different designs can be economically compared, and introduction of new designs, new materials, or new construction methods will become easier.

5. References

1. Iizuka, Hiroshi (1988), *A statistical study on lifetime of bridges*, Structural Engineering / Earthquake Engineering, Vol. 5, No. 1, p51-60, April 1988, Japan Society of Civil Engineers, 1988.
2. Troive, Susanne (1998), *Optimisation of design parameters for minimum LCC of bridge decks, Royal Institute of Technology, Stockholm.* Not yet published research report
3. Svanberg, Krister (1987), *The method of moving asymptotes - a new method for structural optimisation*, International Journal for Numerical Methods in Engineering 24, p359-373, 1987.
4. Tuutti, Kyösti (1982), *Corrosion of steel in concrete*, CBI research, fo 4•82, Stockholm 1982.
5. Poulsen, Erwin, (1996), *Estimation of Chloride ingress into Concrete and Prediction of Service Lifetime with reference to Marine RC Structures*, Durability of Concrete in Saline Environment, Cementa AB, Lund 1996, pp 113-126.
6. Sarja, A. and Vesikari, E. (1996), *Durability design of Concrete structures*, Report of RILEM Technical Committee 130-CSL, E & FN SPON, London, 1996
7. Poulsen, Erwin, (1993), *Estimation of diffusivity for different concrete qualities* (in Danish), Marina betongkonstruktioners livslängd, Dansk Betoninstitut A/S, Aalborg Portland and Cementa A/S, Stockholm, 1993.
8. Pettersson, Karin (1997), *Service life of concrete structures - in a chloride environment*, CBI-report 1:97, Stockholm 1997.
9. Sandberg, Pettersson, Arup and Tuutti (1996), *Cost-effective design of high performance concrete structures exposed to saline environment*, Concrete in the Service of Mankind, 24-28 June 1996, Dundee, Scotland.

Earthquake Damage of Prestressed Concrete Viaduct Structures

Wael ZATAR
Graduate Student
Saitama Univ.
Urawa, Japan

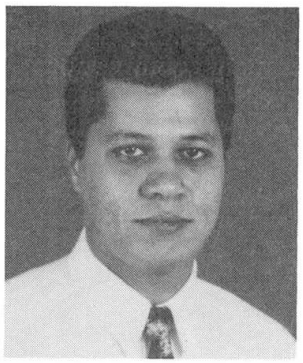

Wael Zatar, born in 1968, received his Bsc in 1990 and Msc in 1994 from Cairo Univ., Egypt. Doctoral student in Saitama Univ. Member of JCI and JSCE.

Hiroshi MUTSUYOSHI
Prof. Dr
Saitama Univ.
Urawa, Japan

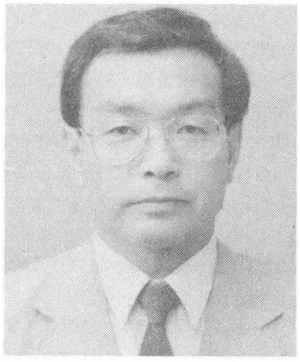

Hiroshi Mutsuyoshi, born in 1953, received his Msc degree in 1978 and doctoral degree in 1984 from the Univ. of Tokyo. Currently Prof. at Saitma Univ., Head of FSO. Member of IABSE, ACI, JCI and JSCE.

Summary

In order to clarify the inelastic response behavior of prestressed concrete (hereafter PC) viaduct structures under severe earthquake excitations, experimental and analytical studies were conducted. Small-scaled models were designed so as to represent actual viaduct structures. Specimens representing PC girders were made and tested experimentally. The experimental program consisted of reversed cyclic loading tests and substructured pseudo-dynamic test in which the PC girder was tested experimentally while the RC piers of the viaduct model were simulated analytically. Response analyses were also conducted and a comparison between the experimental and analytical results was performed. It was clarified that not only the RC piers but also the PC girders are subjected to inelastic deformations and may undergo extensive damage due to earthquake excitation.

1. Introduction

Viaduct structures and elevated bridges are becoming more common for highways and railways. A common type of both the viaduct structures and elevated bridges generally consists of RC piers and PC girders. Various loading tests have been carried out to study the inelastic response behavior of the elevated bridges when subjected to ground motions. Since the girders of these bridges are generally hinged to the piers, only the piers are subjected to earthquake forces. On the other hand, because of the monolithic moment-resisting connection between the superstructure and the piers in the viaduct structures, less response can be observed in the piers bottom ends and another plastic hinges at the tip of the piers can be formed allowing for some energy absorption at these locations [1]. Additionally, not only the piers but also the girders might have some damage. Yet not enough tests have been performed to study either the inelastic response behavior of such PC girders or the complete viaduct structures in which some members may undergo extensive inelastic deformation and thus significantly affect the total response behavior and their integrity. The objective of this study is to obtain the inelastic response behavior of such PC viaduct structures under severe earthquake. In the current study, experimental and analytical studies were conducted. Specimens representing PC girders were tested under statically reversed cyclic loading to obtain the hysteretic load-displacement behavior for three specimens while one specimen was tested using a substructured pseudo-dynamic test in which a modified excitation of the Hyogo-Ken Nanbu 1995 earthquake was used. Takeda's tri-linear model was used for the RC elements. One component model was employed for the inelastic member model during the analytical study.

2. Outlines of tests

2.1. Test specimens

Four partially PC members representing the PC girders of the viaduct structures were tested (Fig. 1). All details of the specimens are shown in Fig. 2. The specimens have the same dimensions but the significant differences were the amount and arrangement of the prestressing tendons and the reinforcing bars. Specimens (A-1), (A-2) and (A-3) were tested under statically reversed cyclic loading while specimen (B-1) was tested by a substructured pseudo-dynamic test. The upper parts of the specimens that represent bonded PC girders were placed monolithically with lower parts that represent reinforced concrete piers of the viaduct models as can be shown in Fig. 2. The design philosophy implicitly requires that shear failure be prevented or delayed so that the member under consideration may fail in flexure. The details of specimens are shown in Table 1. The compressive strength of concrete is about 400 kgf/cm^2. Yielding stresses of the reinforcing bars are 3600 kgf/cm^2 and 3400 kgf/cm^2 for D13 and D6 respectively while the yielding stresses of the prestreesing tendons are 10500 kgf/cm^2 and 12200 kgf/cm^2 for tendons D17 and D11 respectively. The specimens were fixed on a testing floor. The load was applied to the specimen at a height of 150 cm from the bottom end of the PC girder (Fig. 2).

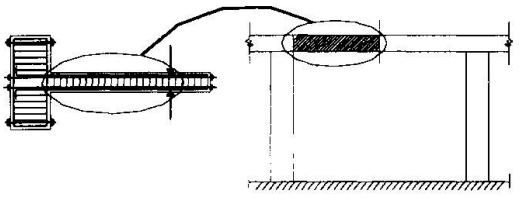

Fig. 1: Experimental test specimens

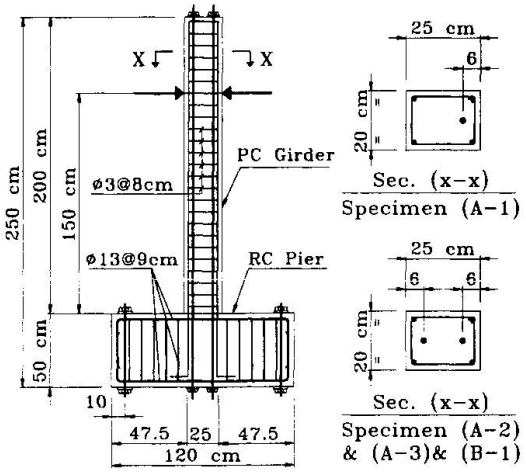

Fig. 2: Test specimens

Table 1: Details of test specimens

Specimen No.	Prestressed		Reinforcement	
	R.S. *	L.S. **	R.S. *	L.S. **
A-1	ø17	--	2D6	2D6
A-2	ø11	ø17	2D13	2D6
A-3	ø17	ø17	2D6	2D6
B-1	ø11	ø11	2D13	2D13

* R.S. : Right side of specimen at the test setup
** L.S. : left side of specimen at the test setup

2.2. Statically reversed cyclic loading tests.

Statically reversed cyclic loading tests were carried out for specimen (A-1), (A-2) and (A-3). The objective of conducting these tests is to clarify the load-displacement characteristics of the PC girders. The specimens were tested using the setup shown in Fig. 3. The repetition of each cycle was 10 times. The applied displacements imposed to the specimens through the actuator were multiples of the prestressing tendons yielding displacements. The yielding displacements considered in the current study are the measured displacements corresponding to attaining the yielding loads.

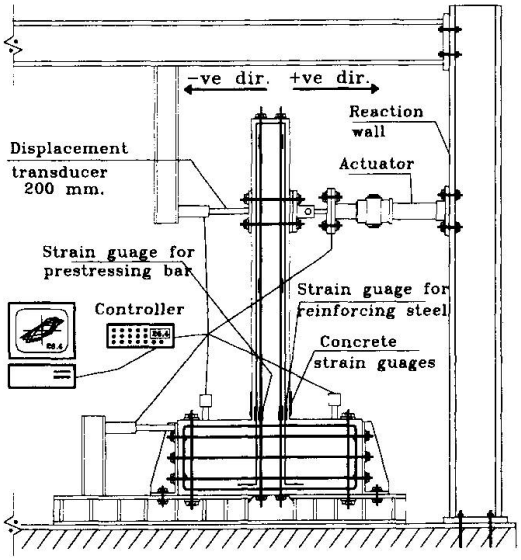

Fig. 3: Experimental Loading setup

2.3. Substructured pseudo-dynamic test

2.3.1. Structural model

Substructured pseudo-dynamic test is a computer-controlled experimental technique in which direct numerical time integration is used to solve the equation of motion. By incorporating substructuring concept, it is possible to test only the critical member effects on seismic response of the whole structure. In the current study, the considered viaduct model shown in Fig. 1 has a 1/10 scale of the

real one. The PC girder of the viaduct structure is considered as the experimental substructure. It was assumed that the viaduct girder is symmetric with respect to the center. Consquently, the PC girder has two identical cantilever members satisfying compatibility and equilibrium conditions at the center as can be seen in Fig. 1. The used model numbering scheme, dimensions and degrees of freedom are shown in Fig. 4.

2.3.2. Experimental procedures

For testing the experimental member in specimen (B-1) of the viaduct model shown in Fig. 1, a substructured pseudo-dynamic testing technique was employed in which the load was applied quasi-statically during the test and the dynamic effects were simulated numerically [2]. Analytical inelastic mechanical model and its restoring force-displacement model were used for all members in the structure except the PC girder [3] whose restoring force was measured directly from the test [4]. Takeda's tri-linear model [5] was used for the RC members. Such a realistic conceptual model recognizes the continually degrading stiffness due to bond slip, shear cracks and energy absorption characteristics during earthquake excitation. The earthquake used for the test was the modified Hyogo-Ken Nanbu 1995 earthquake (NS direction). The time scale was amplified as half the original one while the maximum ground acceleration was 818 gal [6]. Fig. 5 shows the used input ground acceleration. Since the constitutive operator splitting (OS) method was found to be the most effective one in terms of both stability and accuracy [7], it was implemented in this study for integration of equation of motion numerically. The integration time interval was taken as 0.0005 second while the earthquake time interval was taken as 0.005 second.

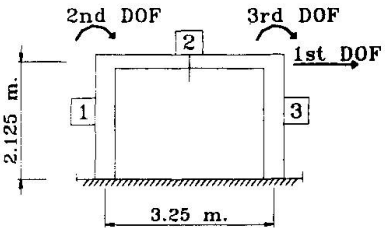

Fig. 4: Model used in the sub-structured pseudo-dynamic test

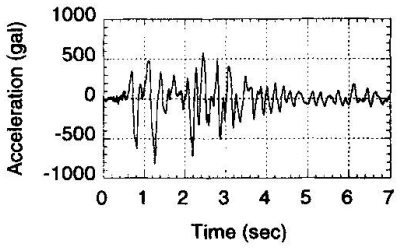

Fig. 5: Input ground acc. for the substructured pseudo dynamic test

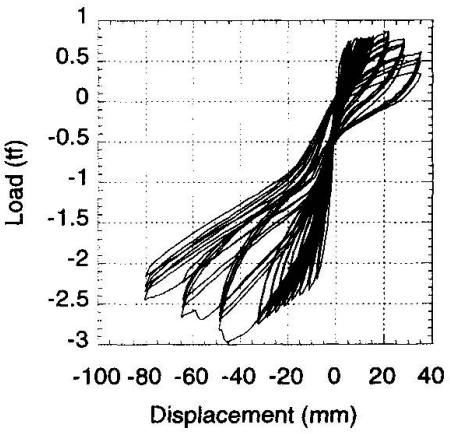

Fig. 6: Load-displacement curve for specimen (A-1)

3. Test results

3.1. Statically reversed cyclic loading tests

The hysteresis loops for all specimens indicated stiffness degradation, Bauschinger effect for both the unloading and reloading and also showed pinching of hysteretic load-deformation curves. Cover spalling and buckling of longitudinal steel bars were also noticed. The inelastic response behavior of the PC girders changed, during the tests, resulting in a decrease in the load carrying capacity. Therefore, adequate ductility without decrease of the load carrying capacity should be maintained to satisfy the requirements of seismic resistant structures.
Fig. 6 shows the load-displacement curve for the specimen (A-1). For the left side of the load- displacement curve, the maximum displacement was about 3 times the yielding displacement of the prestressing tendon. On the right side of the load-displacement curve, the reached displacement was about 13 times the yielding displacement of the reinforcing bars. The hysteresis loops show that the

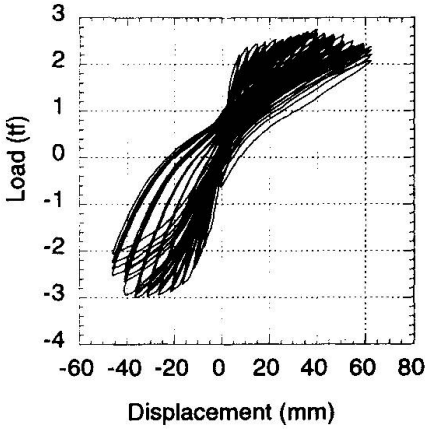

Fig. 7: Load-displacement curve for specimen (A-2)

deformational capacity is different in the two directions because of the unsymmetric arrangement of the prestressing tendons. Fig. 7 shows the load-displacement curve for the specimen (A-2). The displacement reached about 4 times the yielding displacement of the prestressing tendon in the left side of the curve, while it reached about 8.5 times the yielding displacement of the reinforcing bars in the right side. It can be seen, from Fig. 7, that the skeleton curve in the right side can be approximated by a skeleton curve for prestressed concrete while the skeleton curve for the left side can be approximated by a tri-linear model for reinforced concrete. The last observation can be attributed to the relative ratio of prestressing tendons to reinforcing bars in the specimen. Also because of the unsymmetry of the cross section, the ultimate load was different in the two directions. Fig. 8 shows the load- displacement curve for the specimen (A-3), the test was performed till the displacement reached about 2.5 times the yielding displacement of the prestressing tendon. The skeleton curve for both directions of loading can be approximated by a skeleton curve for prestressed concrete because the resistance of the cross section was mainly dependent on the prestressing tendons rather than the reinforcing bars.

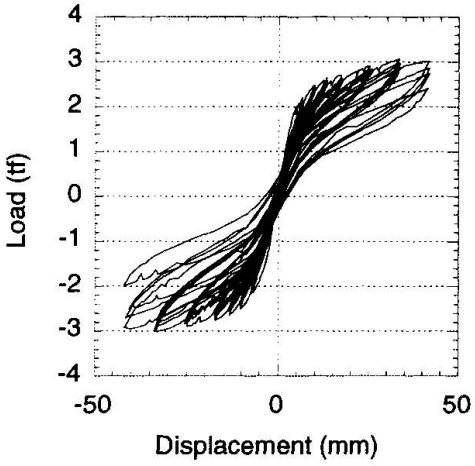

Fig. 8: Load-displacement curve for specimen (A-3)

3.2. Substructured pseudo-dynamic test

The model used for the substructured pseudo-dynamic (PSD) test is shown in Fig. 4. The resulting hysteresis loops for the left end of the PC girder is shown in Fig. 9-A. Both the Bauschinger effect and pinching of the hysterestic loops are clear in the figure. The figure also shows that a considerable damage occurred to the PC girder during the earthquake excitation. From other test results, it was noticed that not much energy was dissipated in the plastic hinge formed at the top of the RC pier. Fig. 9-B shows the moment-rotation curve at the bottom end of the pier. It can be noticed from the curve that a considerable damage occurred during the earthquake excitation. A comparison between the hysteresis curves shown in Fig. 9-A and 9-B shows that not only the RC piers but also the PC girders may undergo extensive damage during earthquake excitation. The time history of the response acceleration in Fig. 10 shows that the maximum obtained accleration was about 12.2 m/sec^2. The time and direction of this maximum acceleration are consistent with the time and direction of the maximum input ground acceleration. The time history of the response displacement in Fig. 12 shows that the maximum displacement reached about 8.5 cm.

4. Analytical results

The last viaduct model was studied analytically. One component model proposed by Giberson [8] was employed for the inelastic member model. The inelastic moment-rotation relationships of the springs were calculated by means of ordinary flexural theory. Furthermore, the rotation due to bond-slip of the reinforcing bars and the prestressing tendons from the connecting joints was taken into consideration using Ohta's method [9]. Takeda's tri-linear model was used for the RC piers. A value of 2% modal damping was assumed for all modes until one member has a rotation angle equals to the yielding rotation angle. The damping was then considered equals to zero because only the hysteretic damping was dominant after the yielding displacement is reached.

Fig. 9-C and 9-D show that the analytical results agreed well with the experimental ones in terms of energy absorption, damage extent and ductility factor. The analytical acceleration and displacement time histories in Fig. 11 and 13 also showed good agreement with the experimental ones in terms of the maximum values, corresponding time and the over all time histories.

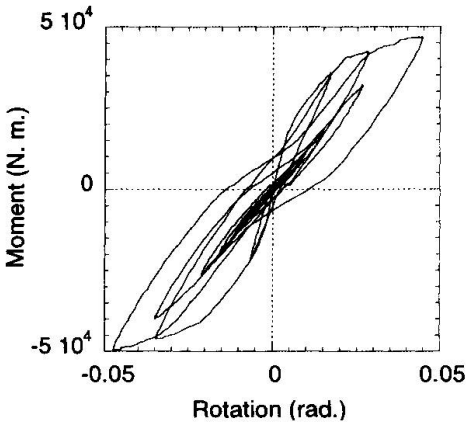

Fig. (9-A): Left end of PC girder (Experimentally)

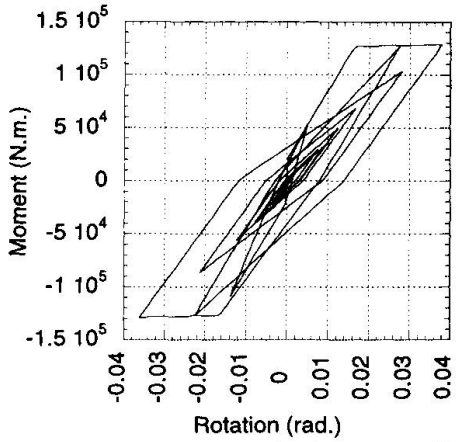

Fig. (9-B): Bottom end of RC pier during the substructured pseudo-dynamic test.

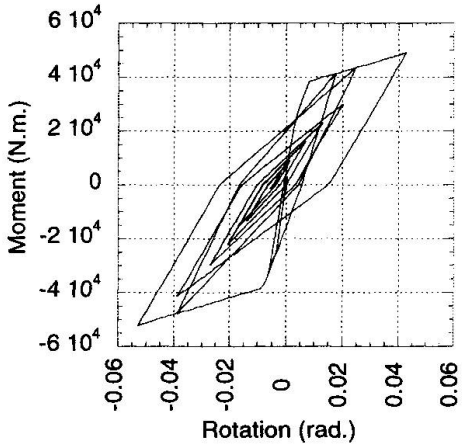

Fig. (9-C): Left end of PC girder (Analytically)

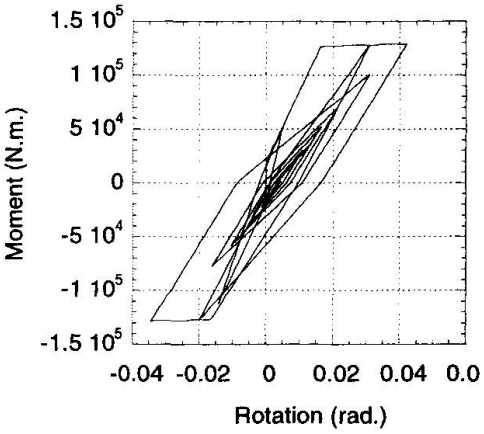

Fig. (9-D): Bottom end of RC pier (Analytically)

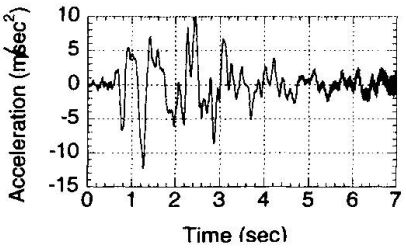

Fig. 10: Acceleration-time history of the substructured PSD test (Experimentally)

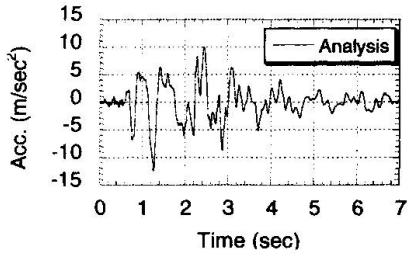

Fig. 11: Acceleration-time history of the substructured PSD test (Analytically)

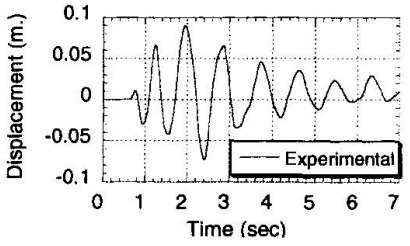

Fig. 12: Displacement-time history of the substructured PSD test (Experimentally)

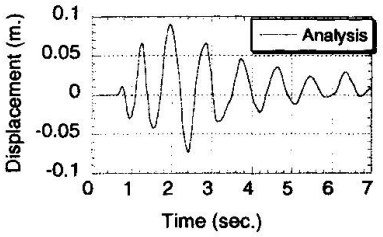

Fig. 13: Displacement-time history of the substructured PSD test (Analytically)

5. Conclusions

In order to clarify the inelastic response behavior of partially prestressed concrete girders of a viaduct structure under severe earthquake, small-scaled specimens representing half of a girder bay of a viaduct structure were tested under statically reversed cyclic loading tests and by a substructured pseudo-dynamic method. Analytical investigation for the same viaduct model was also carried out. From the results, it can be concluded that:

1. Not only the RC piers but also the PC girders are subjected to inelastic deformation that may cause a considerable damage during real earthquake excitations. As a consequence, adequate care should be given to the PC girders design to satisfy the requirements of a seismic resistant structure.
2. The inelastic response behavior of the PC girder of a viaduct structure can be remarkably changed. Consequently, the load carrying capacity decreases. Therefore, adequate ductility without decrease of the load carrying capacity should be maintained in order to ensure a seismic resistant viaduct girder.
3. A good agreement between both the experimental and analytical results was obtained in the resulting time histories, hysteresis curves and dissipated energy during earthquake excitation.
4. Further analytical response analyses have to be carried out in order to accurately identify the significant parameters of the PC girder that influence the overall response behavior.

Acknowledgment

The authors would like to acknowledge the financial support of the grant-in-aid for scientific research of the Ministry of Education, Science and Culture in Japan.

References

1. Priestley, M. J. N., Seible, F. and Calvi, G. M. "Seismic Design and Retrofit of Bridges," John Wiley & Sons Inc. 1996.
2. Yamada, Y., Iemura, H., and Tanzo, W., "Substructured Hybrid Loading of Structural Members Under Combined Axial, Shear, and Bending Loads" 8th Symposium of Earthquake Mechanics in Japan, 1990, pp.1503-1508.
3. Mutsuyoshi, H., Machida, A., Sadasue, K., and Oba, S., "Earthquake Response Behavior of First-Level Girder in R/C Frame Structure Based on Pseudo-Dynamic Test Method," Transactions of JCI, Vol. 14, 1992, pp.289-296.
4. Mutsuyoshi, H., Tanzo, W., and Machida, A., "Influence of Member Ductility on The Total Seismic Response of RC Piers Using Substructured Pseudo-Dynamic Tests," Transactions of JCI, Vol. 15, 1993, pp.353-360.
5. Takeda, T., Sozen, M. A., and Nielsen, N. N., "Reinforced Concrete Response to Simulated Earthquake," Journal of the Structural Division, ASCE, Vol. 96, No. ST2, paper 7759, Dec., 1970, pp.2557-2573.
6. Preliminary Report on The Great Hansion Earthquake, January 17, 1995. Japan Society of Civil Engineers, 1995.
7. Nakashima, Ishida and Ando, "Numerical Integeration Methods for Substructure Pseudo-Dynamic Test Method," Transactions of The AIJ, Structural Engineering Series, No. 417, 1990, pp.107-117. (In Japanese)
8. Giberson, M.F., "Two Nonlinear Beams With Definitions of Ductility," Proc. of ASCE, Vol. 95, No. ST2, 1969.
9. Ohta, M., "A Study on Earthquake Resistant Design for Reinforced Concrete Bridge Piers of Single Column Type," Report of The Public Works Research Institute, Ministry of Construction, Vol. 153, 1980.

Vertical Component of Earthquake Motion and Inelastic Response of RC Piers

Hassan KHAIRY
Dr Candidate
Saitama Univ.
Saitama, Japan

Atsuhiko MACHIDA
Prof. Dr
Saitama Univ.
Saitama, Japan

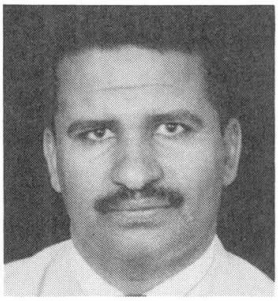

Hassan Khairy, born 1960, received his Civil Engineering Bsc in 1984 and Msc in 1989 from Assiut Univ., Egypt. Doctoral student in Saitama Univ. Member of JCI and JSCE.

Atsuhiko Machida, born 1940, received his D.Eng. degree in 1976, Univ. of Tokyo. He was awarded JSCE prize (Yoshida prize) four times. His research includes seismic resistance design of RC structures.

Summary

In this study, inelastic response analysis was carried out to analyze the effect of vertical component of motion on inelastic response of RC bridge piers. RC piers with different properties and dimensions were studied under two cases of earthquake waves. In the first case, piers were subject to horizontal motion only whereas in the second case piers were subject to horizontal and vertical components. Comparing the results of the two cases indicated that effect of vertical component should be included in the analysis and design of piers to resist strong motions such as the Great Hanshin earthquake. Vertical component had influence on both of axial and lateral load capacities and caused change of failure mode of many cases. In general, vertical motion increases the level of damage, generates fluctuating axial forces and leads to non-ductile behavior of piers consequently bigger quantity of shear reinforcement is needed to maintain ductility level.

1. Introduction

In seismic design of RC structures, designers usually do not consider that the effect of vertical motion is important because horizontal motion usually has the most significant role on the behavior of bridge piers. However, in many earthquakes of the last twenty years, the vertical component was high relative to the horizontal one. The Great Hanshin earthquake on January 17, 1995, was characterized by its high horizontal peak acceleration (**0.8 g** in some sites) and its high vertical or up-down motion which reached about **0.6 g** in some sites. More details about Hanshin Earthquake were given in reference (1). The question is: what is the influence of the vertical component on the severe collapse of RC bridge piers that occurred during such earthquake? To answer this question, we utilized nonlinear 3D FEM to carry out inelastic response for RC piers under two cases of loading; in the first case- denoted by **HZ** motion only- the piers were subject to horizontal wave of **0.8g** peak acceleration which was recorded at Nishinomya City during the Great Hanshin earthquake whereas in the second case- denoted by **HZ & VL** motion- piers were subject to horizontal motion of case 1 in addition to vertical motion of **0.6g** peak acceleration. For each studied case, the pier was subject to constant compressive stress during the motion.

2. Modeling

In 3D model, concrete was modeled as 8-node isoparametric 3D element and 2 node 3D truss element for modeling both of longitudinal and transverse reinforcement. The super structure was represented by concentrated mass at top of the pier and mass of pier was lumped at the joints. Nonlinear Newmark approach (2,3) was used to solve the nonlinear equation of motion. A finite element software named MARC was utilized in the analysis. Fig. 1(a, b) shows the simplified 3D finite element model and parameters of the study respectively. Von Mises criterion with normality flow rule was adopted to consider nonlinearity of steel reinforcement. Nonlinearity of

concrete was adopted through constitutive equations which were considered in two stages. For uncracked concrete, we used a model based on theory of plasticity (4) to model concrete in compression as in Fig. 2. We modified the model to consider the effect of transverse reinforcement on increasing both of ultimate strength and corresponding strain due to confinement. The modification was based on a model proposed by Mander et al (5,6) as in Fig. 3.

For cracked concrete, we used constitutive equations based on smeared crack model as in Fig. 4 (a, b). More details were illustrated in previous works by the authors, e.g. (7,8). In this study, shear reinforcement ratio was defined as $A_{sh}/(e.h)$ in which A_{sh} is the area of stirrup branches in the direction considered, e and h are spacing of stirrup and depth of the pier respectively. Stress level was defined as $P/(A_c.f_c')$ in which P is the axial load, f_c' is the concrete strength and A_c is the area of concrete section. Percentage of main reinforcement was defined as $A_s/(d.b)$ where A_s is the area of main steel in tension side, d and b are effective depth and width of pier respectively.

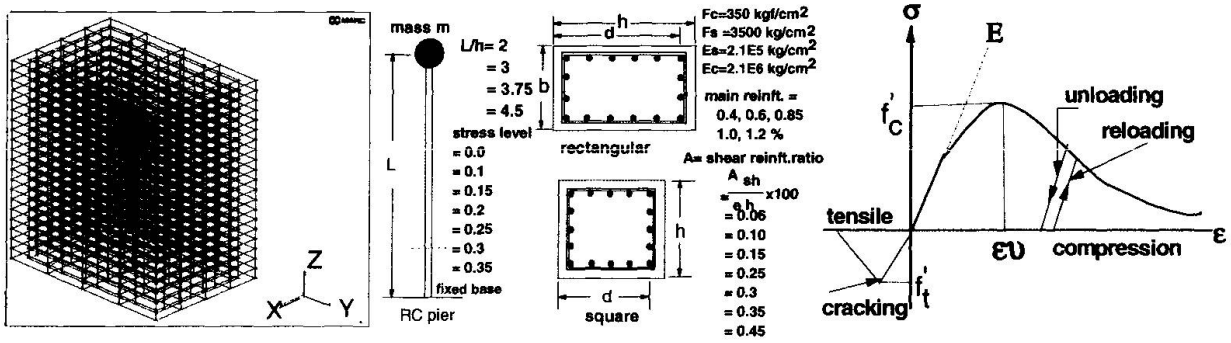

Fig. 1 A) 3D model b) Parameters of the study *Fig. 2 Modeling of concrete in compression*

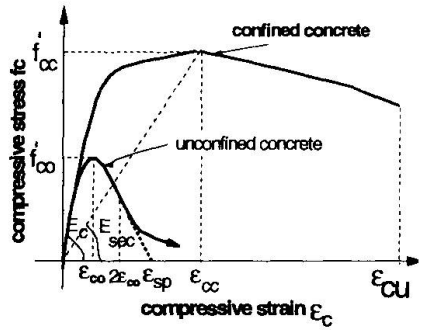

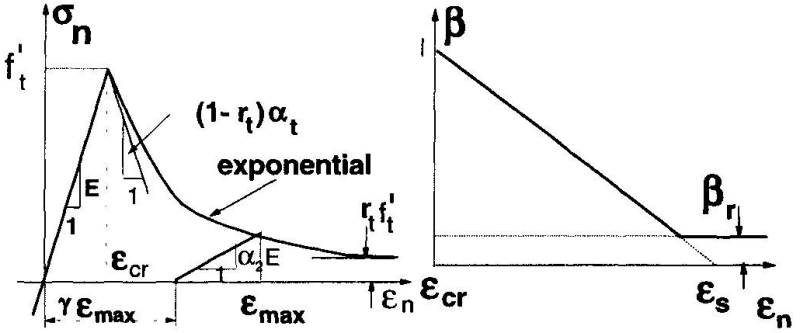

Fig. 3 Park model *Fig. 4 a) Tension stiffening b) Retention factor*

3. Results and Discussion

3. 1 Effect of Vertical Motion on Inelastic Response

Fig. 5 (a & b) illustrates the effect of vertical motion on acceleration response of RC pier of 0.3 % shear reinforcement. Including vertical component caused significant increase in the level of response. The rate of increase of peak acceleration was 80 % for the given case. Fig. 6 illustrates effect of shear reinforcement and vertical motion on the peak acceleration of the same pier. By increasing the ratio of shear reinforcement, the effect of vertical motion on changing the level of the response decreased. This implied that effect of shear reinforcement on behavior of piers was more significant in case of VL & HZ motions than that in case of HZ motion only. For example, by increasing the ratio of shear reinforcement from 0.06 % to 0.3 %, peak acceleration was reduced by 3.8 and 7.0 % respectively for the cases of HZ motion only and HZ & VL motions .

Fig. 7 illustrates the effect of vertical motion on axial load response of RC pier. Vertical motion induced fluctuating axial forces in the piers which lead to unstability of the structure and increase in ductility demand (9). Also, due to changing of the sign of axial force, ultimate strength of concrete was reduced. Generally, compressive axial load causes increase whereas tensile load causes decrease of lateral load capacity. If the induced axial force is tensile, the stiffness of the

pier decreases and hence its ultimate shear capacity decreases. The tensile forces cause yielding of main reinforcement and diagonal shear failure. On the other hand, if the induced axial force is compressive, then ultimate load carrying capacity of the pier increases, however ductility of piers decreases significantly due to crushing of concrete at the ends of the diagonal cracks.

In previous studies (7,8,9,10), we determined the optimum shear reinforcement ratios at which failure mode changes from diagonal shear to flexural mode and this was done by considering plastic strain as damage index for concrete. We showed that the optimum shear reinforcement ratio depends on axial stress level, ***L/h*** ratio and percentage of main reinforcement. Also, the required ratio of shear reinforcement increases significantly as the axial compressive stress level increases. In the current study, we analyzed the rate of increase of the axial compressive load due to vertical motion with different peak acceleration. Fig. 8 illustrates the relation of g_v/g_h and $P_{hz\&vl}/P_{hz}$ for different ***L/h*** where g_v and g_h are peak acceleration of vertical and horizontal motions respectively and $P_{hz\&VL}$ and P_{hz} are the maximum induced compression load in cases of HZ & VL motions and HZ motion only respectively. For example if the pier is supposed to be subjected to vertical motion having peak acceleration of 0.5 times the horizontal peak acceleration, then the pier should be designed to carry 1.2 times the actual axial load.

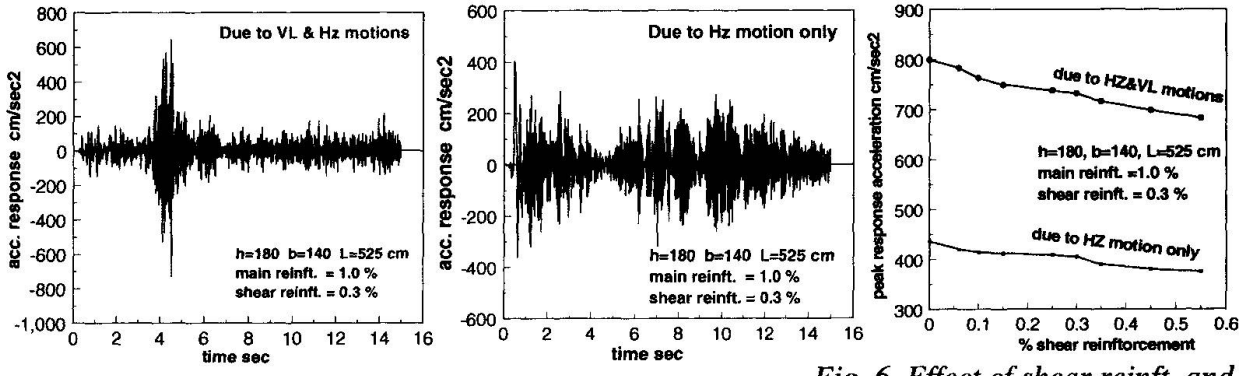

Fig. 5 (a, b) Effect of V. motion on HZ acceleration response

Fig. 6 Effect of shear reinft. and V. motion on peak acceleration

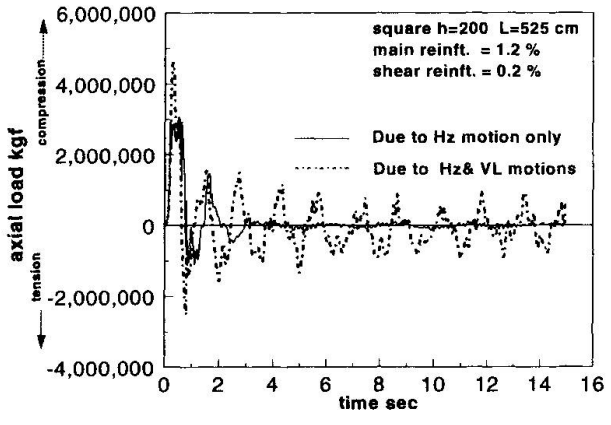

Fig. 7 Effect of vertical motion on axial load response of RC pier

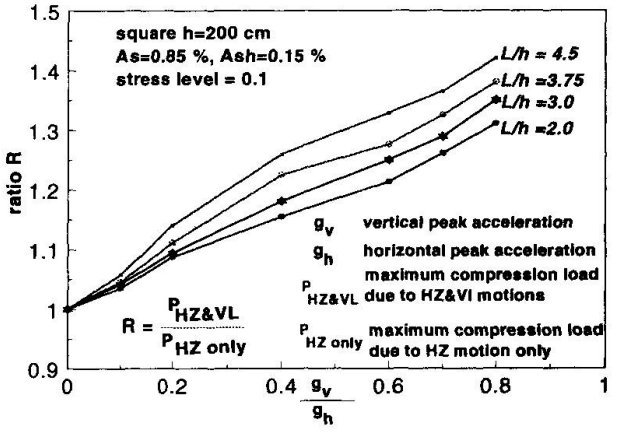

Fig. 8 Effect of vertical motion on maximum axial compression load on the pier

3.2 Vertical Motion and Ductility Level of RC Piers

Displacement ductility of piers factor was calculated from inelastic responses from the relation:

$$D.F = \frac{\Delta_u}{\Delta_y} \qquad (1)$$

Δ_u is the horizontal displacement at the top when lateral load capacity of the pier drops to 80 % of the maximum carrying load (6,8,10,12,13,14). At this level the pier was assumed to collapse due to plastic deformations. Δ_y is the lateral displacement at the top corresponding to first

yielding of main reinforcement. Fig. 9 (a, b) illustrates the relation between shear reinforcement and ductility factor of piers having different axial stress level for the two cases of HZ motion only and HZ & VL motions. Ductility level decreased significantly due to vertical motion and maximum percentages of reduction were 20, 18, 18, 16, 15 % for stress levels 0.1, 0.15, 0.2, 0.25 and 0.3 respectively. So, bigger quantity of shear reinforcement is needed to maintain ductility level if the piers are expected to subject to HZ & VL motions than that in case of HZ motion only. Also, it is clear that the role of shear reinforcement in increasing ductility level was more significant in case of HZ & VL motions especially for higher axial stress levels.

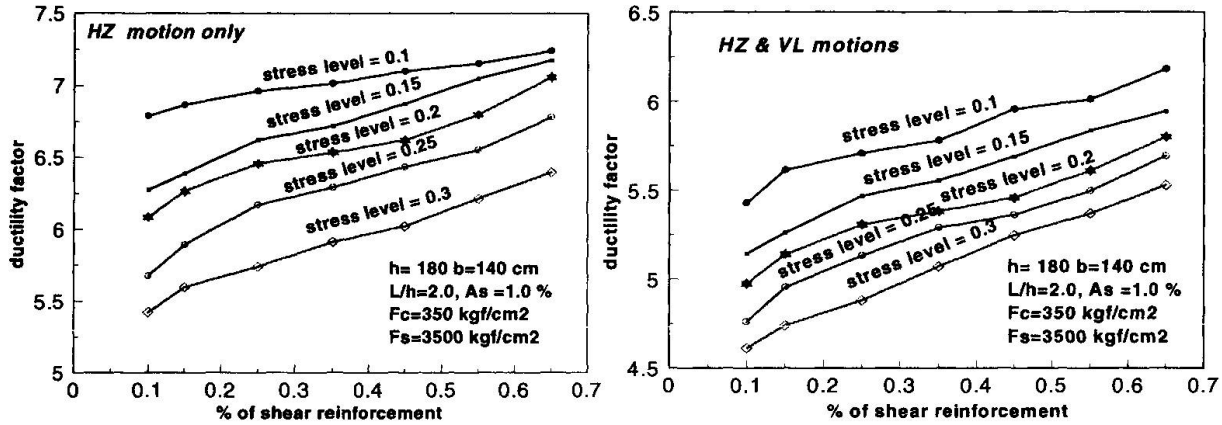

Fig. 9 (a, b) Ductility of piers with different ratios of shear reinforcement and stress level
Case A: *Due to HZ motion only* ***Case B:*** *due to HZ & VL motions*

3.3 Vertical Motion and Failure Mode

We determined final failure mode of piers (8) based on comprehensive analysis of base shear response, stresses and strains. Fig. 10 (a, b) illustrates the effect of vertical motion on the base shear response of piers with two ratios of shear reinforcement, 0.06 and 0.3 %. Vertical motion caused increase in the base shear and the rate of increase was high for higher shear reinforcement. For the given examples, the ratio of maximum shear in case of HZ & VL motion to that of HZ motion only was **1.5** and **1.65** indicating 50 % and 65 % increase in shear response. However, this maximum value dropped to zero after short time of applying the motion in case of HZ & Vl motions whereas in case of HZ motion only, the loss in the load was not so big.

Fig. 11 illustrates the effect of vertical motion on lateral strain response at base of RC pier. Including vertical motion resulted in significant increase in the lateral strain and the rates of increase of both of the maximum tensile and compressive values were 421 and 335 % respectively. The higher tensile lateral strains accelerated the occurrence of diagonal failure. In previous study (8), we showed that for diagonal shear failure, lateral plastic strain is tensile and it is compression if final failure mode is flexural. Also, we noticed that diagonal failure occurred when lateral tensile plastic strain was higher than or equal to 0.004. Applying these considerations on the given example, we see that diagonal failure occurred in case of HZ & VL motions however flexural failure occurred in case of HZ motion only.

Fig. 12 illustrates the effect of vertical motion on axial strain response for RC pier. Both of the tensile and compressive strains increased significantly due to vertical motion. Maximum values increased by 86.6% and 216 % for tensile and compressive strain respectively.

Fig. 13 (a, b) illustrates lateral stress strain relations at base of RC pier for HZ motion only and HZ & VL motions respectively. In the second case, stresses were several times larger than that of the first case. Tensile stresses and strains were high in the second case resulting in diagonal shear failure however flexural failure occurred in case of HZ motion only Also, number of cycles which can be resisted safely was very small in the case of applying the vertical motion. However in other cases, diagonal collapse occurs for the two cases of loading however the severity of diagonal collapse is higher in case of HZ & Vl motions than that of HZ motions.

From these points, the authors concluded that due to vertical motion, piers lost their shear base responses at early stages associated with higher lateral and axial strains. Also the ductility level of the piers decreased significantly. These reasons resulted in severe diagonal shear collapse. This was one of the reasons of such severe collapse of the bridge piers during the Great Hanshin earthquake. The other reasons included the insufficient shear reinforcement ratio and the characteristics of the Great Hanshin motion. These points were studied in other works by the authors, and those who are interested can refer to references (8,15).

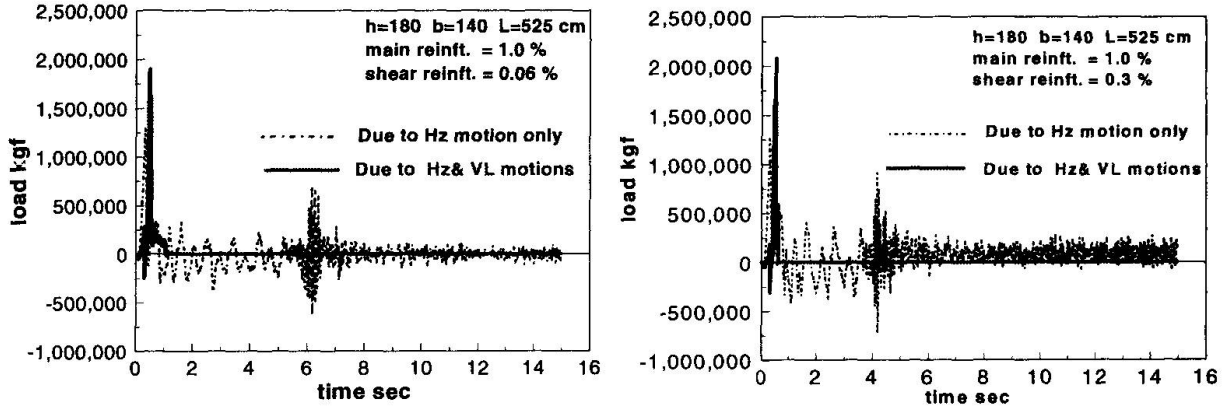

Fig. 10 (a, b) Effect of vertical motion on load capacity for ratios of shear reinft. 0.06 and 0.3 %

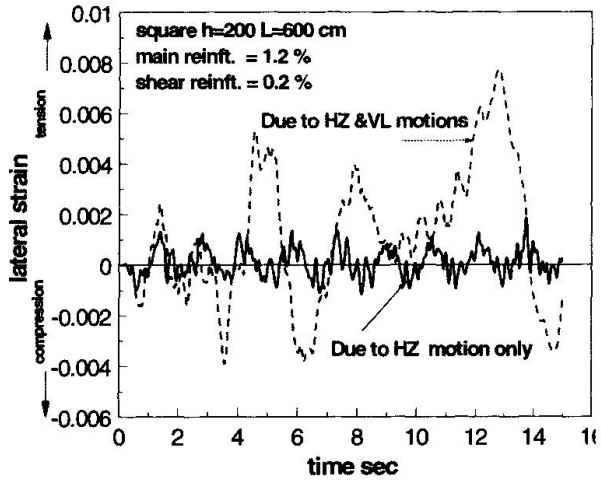

Fig. 11 Effect of vertical motion on lateral strain response of RC pier

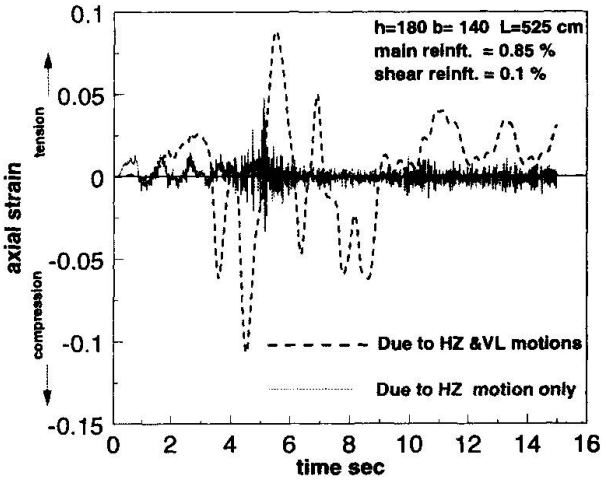

Fig. 12 Effect of vertical motion on axial strain response of RC pier

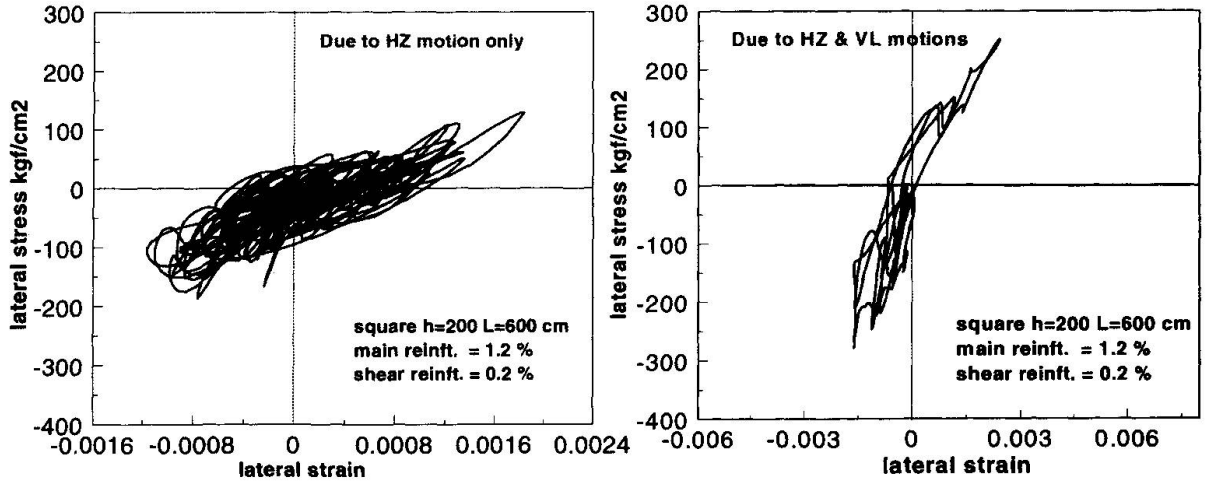

Fig. 13 (a, b) Effect of vertical motion on lateral stress strain for RC pier
Case A *HZ motion only* ***Case B*** *HZ & VL* motions.

4. Conclusions

- Vertical component has remarkable influence on the inelastic response of RC piers and should be included in the seismic design of such structural elements.

- Due to vertical motion, ductility level of piers decreases and the induced plastic strain increases. The induced fluctuating axial forces and plastic strains result in collapse of piers at early stages of applying the motion. The base shear response of piers increases associated with severe drop leading to shear failure. Vertical motion causes change of final failure collapse of some of the studied piers from flexural to severe diagonal shear failure. However in other cases, diagonal collapse occurs for the two cases of loading however the severity of diagonal collapse is higher in case of HZ & Vl motions than that of HZ motions.

- Vertical motion was relatively high during the Great Hanshin Earthquake in Japan, 1995 and this was one of the reasons of the severe collapse of bridge piers occurred during the motion.

Acknowledgment

Financial support by grant-in-aid by the Ministry of Education, ***Monbusho***, for the first author is gratefully appreciated.

References

1. Preliminary Report Of *JSCE* On: The Great Hanshin Earthquake in January 17, 1995.
2. *MARC Research Corporation*, " MARC Manual_," Vol. A-F, 1995.
3. *Bathe K.* " Finite Element Procedures." Printice Hall, Engelwood Clifs, U.S.A, 1996.
4. *Zhishen Wu and Takada-aki.* " A Hardening/ Softening Model of Concrete Subjected to Compressive Loading,". Journal of Structural Engineering Vol. 36B,1990
5. *Mander, J.B., Priestely, M. N., and Park, R.*, " Theoretical stress-strain Model for confined concrete. J. Structural Engineering." ASCE Vol. 114, No. 8, 1988
6. Park *and Paulay*. "Bridge design and research seminar." Vol. 1, Transit New Zealand 1990.
7. *Khairy Hassan, A., and Machida, A.*, "Nonlinear 3D Finite Element Approach for Ductility Requirements of RC Bridge Piers Subject to Strong Earthquake Motions". 5th International Conference, Al Azhar University, Egypt, Vol. 3, December 1997, pp. 12 - 24
8. *Khairy Hassan A. and Machida, A.* " Effect of Transverse Reinforcement on Ductility and Failure Mode of RC Bridge Piers Subject to Earthquake Motion. Nonlinear 3D Finite Element. EASEC-6 International conference, Taipei, Taiwan, Jan. 1998. Also, now under processing for publication in Journal of "Concrete Research and Technology".
9. *Ala Saadedeghvaziri, M. and Foutch, D.A.*. "Dynamic behavior of R/C highway bridges under the combined effect of vertical and horizontal earthquake motions." Earthquake Engineering and Structural Dynamics, Vol. 20, 1991.
10. *Khairy Hassan, A. and Machida, A.*, "Role of Transverse Reinforcement on Ductility and Failure Mode of RC Bridge Piers Subject to Earthquake Motion." Proceedings of Japan Concrete Institute, Vol. 19, No. 2, 423-428, 1997. Also it will be published in JCI transactions.
11. *Khairy Hassan, A., and Machida*, A.,. "Effect of Axial Stress on Ductility and Confinement of RC Bridge Piers Subject to Earthquake. A 3D FEM approach. Proceedings of JSCE, 1997
12. *Machida, A. and Mutsuyoshi, H.*, "Evaluation of Ultimate Deflection of Reinforced Concrete Members,." Proceeding of ninth WCEE, Vol. VI, August 1988, PP. 359-364.
13- *Elnashai, A.S. and McClure, D.C.* "Effect of modeling assumptions and input motion characteristics on seismic design parameters of RC bridge piers. Earthquake Engineering and Structural Dynamics, Vol. 25, May 1996
14. *Higai, T., Junichiro, N., and Yuki, O.*, "Ductility of RC Piers at Post-Yield Shear Failure Under Repeated Reversed Load," The Second East Asia-Pacific Conference on Structural Engineering & Construction. Chiang MAI., January, 1989, pp. 20-25
15) *Machida, A., and Khairy Hassan, A.*, " Influence of Input Motion Characteristics on Inelastic Behavior of RC Piers of Bridges. A Three Dimensional Finite Element Approach. EASEC-6 International conference, Taipei, Taiwan, January 1998. Also, now under processing for publication in Journal of "Concrete Research and Technology".

Reconstruction of the Benten Viaduct after the 1995 Earthquake

Mitsuhiro HAYASHIDA
Eng.
Hanshin Expressway Public Corp.
Osaka, Japan

Hidenao HAYASHI
Advisory Officer
Hanshin Expressway Public Corp.
Osaka, Japan

Shiro KAWAKITA
Chief Eng.
Hanshin Expressway Public Corp.
Osaka, Japan

SUMMARY

"Benten Viaduct" is a reconstructed bridge of Hanshin Expressway Kobe Route, which was suffered from the Hanshin/Awaji Earthquake seriously. This section had been consisted of 8 bridges before the earthquake and revived as an innovative structure, 19-span continuous rigid frame bridge with seismic isolators installed underneath the steel piers. This paper reports the outline of the seismic isolation design and techniques on the field for this innovative bridge structure, comparing the result of analysis with that of vibration experiment applied onto the actual bridge structure.

1. INTRODUCTION

The Hanshin/Awaji Earthquake occurred on January 17, 1995, caused tremendous damage on the Hanshin Expressway Kobe Route, especially at Benten section (referred in Figure 1). The reconstructed bridge, "Benten Viaduct", was determined to be the 19-span continuous rigid frame with steel deck along with the installation of seismic isolator. The general view of structure is shown in Figure 2.

Before the earthquake one of piers stood on the middle of separating zone and the other on the pedestrian lane, and they were of single RC pier. These piers were connected with the superstructure by means of steel bearings that were placed on top of the each pier. When the earthquake struck them, most of the columns were collapsed due to shear force causing bridge fail and girder buckling. Because they were located on National Highway Route 2 which is also a lifeline route of Kobe city, as much as 24 spans of girders and columns of this section were removed immediately. The remove work was completed within seventeen days.

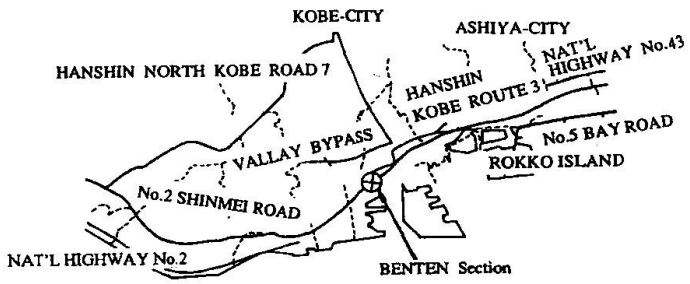

Fig. 1 Location

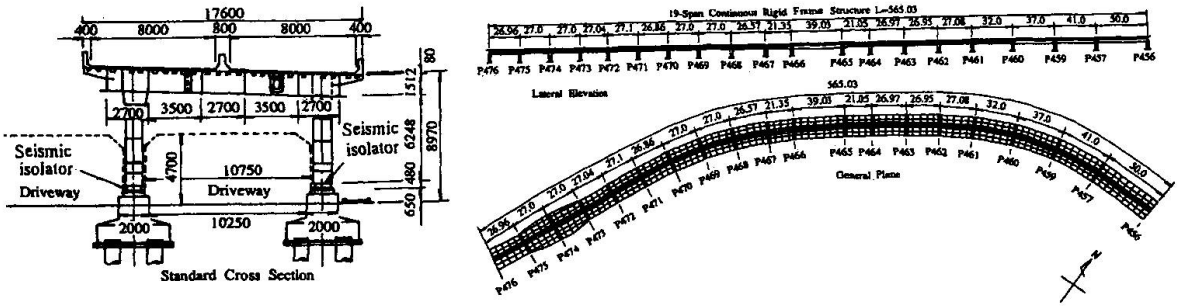

Fig. 2 General View of Benten Viaduct

2. DESIGN

2.1 STRATEGY

For restoring the bridges in Benten section, we set the following three basic strategy.

1) The pile foundation could be utilized as they were since it was found that there had been no damage on it.
2) Steel deck and seismic isolation bearings could be used in order to decrease seismic force acting on the foundation.
3) In order to prevent bridges falling down each bridge pier and the beam of superstructure would be tied rigidly as much longer as could.

According to the strategy above, it was decided to adopt a continuous rigid frame. It was supposed that the additional piling reinforcement was needed for rigid connection or for hinge connection and finally it was concluded to adopt the structure of installing seismic isolation bearing on the foundation (referred in Table 1). Since the Benten Viaduct is warped to the seaside and the overhang length of cross beams differs slightly, analysis was made on the entire structural model of the two types shown on Figure 3.

		Rigid Connection			Hinge Connection			Seismic Isolation Bearing		
					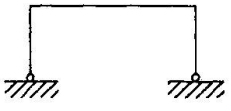			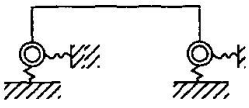		
Column	Stress Resultant	V	H	M	V	H	M	V	H	M
	Dead Load	227.4	120.4	277.3	227.4	76.9	0.0	227.4	29.3	60.7
	Temperature	227.4	140.1	386.0	227.4	79.6	0.0	227.4	30.6	58.7
	Earthquake	241.2	177.2	531.1	267.9	133.8	0.0	260.1	100.6	10.9
Reaction Force on Pile		280≧184(tf/pile)			210≧184(tf/pile)			175≦184(tf/pile)		

Table 1 Comparison of Structure

Both east and west end of Benten Viaduct, 2 spans continuous steel box girder bridges were arranged as a absorber bridge. It was to prevent the adjacent simple girder bridges from a remarkable difference of vibration characteristics.

2.2 OUTLINE OF DESIGN

In static analysis model (a) in the Figure 3 was used. The superstructure consisted of main girders, beams, and piers which was supported by the two way horizontal spring as well as perpendicular and rotational ones. The characteristic of isolator is expressed in natural period (T) and the ratio of yield point load (Qd/Wu)[2]. In order to give an appreciate initial coefficient of bearing reaction for the static analysis model, the period and the ratio of yield point load were decided by applying a representative bridge pier that would satisfy the following three design objects.

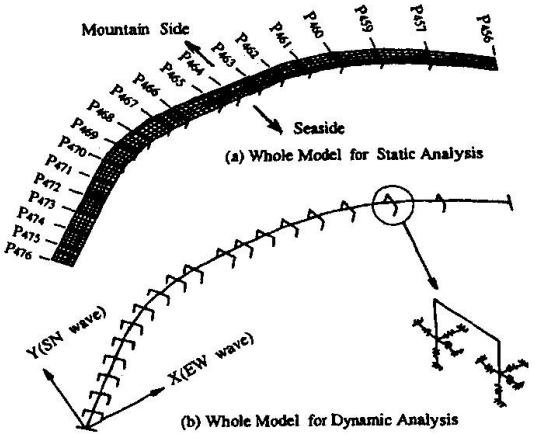

Fig. 3 Entire Models for Analysis

1) In the designed vibration from the horizontal bearing capacity piers will not excessively be plastic during the earthquake. (Khe<0.68)
2) In seismic coefficient method, a designed vibration can at least be decreased by the damping effect. (Dumping constant by the seismic coefficient at the vibration h>10%)
3) Seismic isolator will not be deformed extremely. (Horizontal bearing capacity during earthquake was investigated referring to the superstructure that deflects<250%)

A combination of T=1.4 sec Qd/Wu=12.6% has been adopted to satisfy the above condition.

From the static analysis, deflections were calculated for each bearing and for the girders at both ends. Girder's deflection reached ±84mm maximum depending on the various temperature range. Expansion joints was designed based on this movements.

In dynamic analysis model, the main girders and deck plates were assembled together to a piece of beam so that they would make an entire simple model. The seismic wave taken at the JR Takatori Station was applied [3] for the input of seismic vibration. Earthquake force of EW wave was put into chord direction of warped bridge and SN wave to the lateral direction simultaneously.

The time histories were exemplified in the Figure 4 for the response in the horizontal deflection of the seismic isolator and the bending moment at the beam joint at P470. Maximum deflections were 428mm in the longitudinal direction of bridge and 568mm in the transverse direction, which were observed after 6 seconds from the beginning of earthquake.

The results of natural vibration analysis on the entire model is shown on Figure 5 and all up to 5th modes shows inherent mode of horizontal direction. From the result of natural vibration analysis applied on a plane model, the mode for horizontal move at the bearing position is so remarkable that the similar tendency may be seen in a three dimensional model.

Again the stresses of intersection at the beam and the pier were investigated as members that receive axial compressive force and bi-axial bending moment by applying maximum response values.

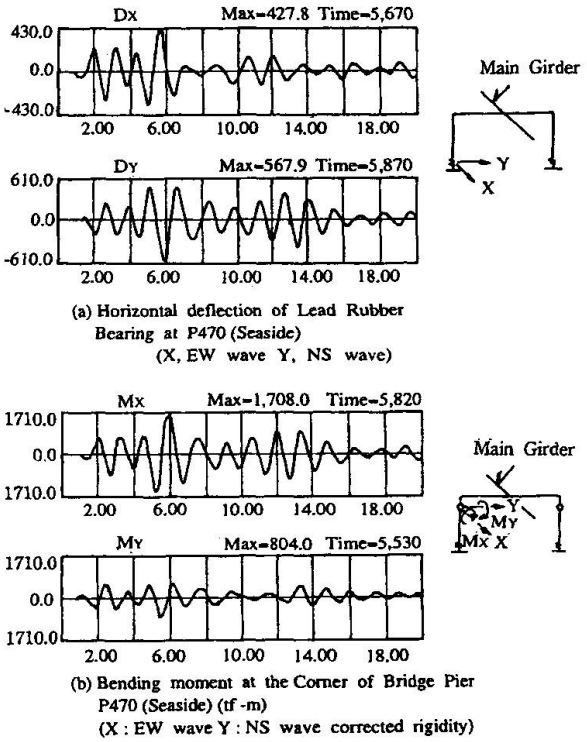

(a) Horizontal deflection of Lead Rubber Bearing at P470 (Seaside)
(X, EW wave Y, NS wave)

(b) Bending moment at the Corner of Bridge Pier P470 (Seaside) (tf -m)
(X : EW wave Y : NS wave corrected rigidity)

Fig. 4 An Example of Response Analysis On Time History

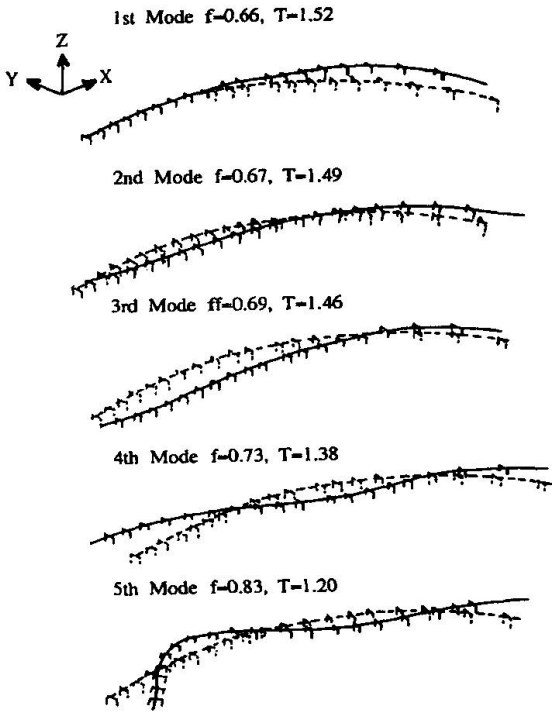

Fig. 5 Results of Natural Vibration Analysis

2.3 SEISMIC ISOLATOR

Seismic isolation bearing was designed referring to the "Manual of Isolation Design for Highway Bridge." There are two types of seismic isolator, LRB (Lead Rubber Bearing) and HDR (High Dumping Rubber). LRB is a laminated-rubber bearing concluding lead plugs inside to give bi-linear deformation characteristic, while HDR is made of laminated super elastic gum.

Benten Viaduct has so much dimension of statically indeterminate that LRB was supposed to be more effective than HDR, because it is softer on various temperature range and harder under strong earthquake force. Each LRB bearings was designed in the same height nevertheless the difference of their design load in order to make the deformation characteristics regular. The appearance of seismic isolation bearing is shown in Photograph 1.

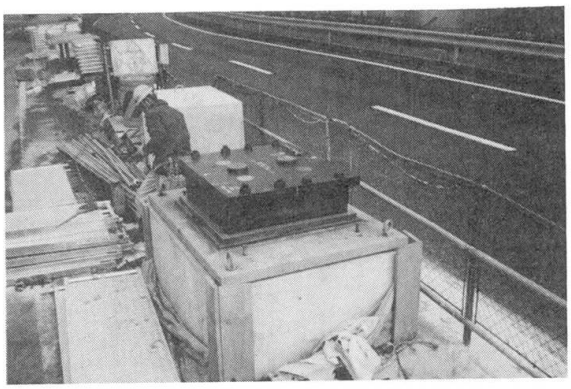

Photo. 1 Seismic Isolation Bearing

Through the static and dynamic analysis, seismic characteristics were corrected like below;

T (natural period of whole superstructure) =1.45 sec
h (dumping constant of isolator when horizontal displacement=100mm) =22 %
shear deflection of isolator (when Kh=0.23) = 50% (design capacity=150%)
shear deflection of isolator (when Kh=0.68) = 196% (design capacity=250%)
shear deflection of isolator (dynamic analysis) = 357% (design capacity=400%)

Also the response analysis on time history is confirmed in the rotating deflection of seismic isolator and axial force of pier, which led to carry the test confirming the effectiveness of bearing by using the response value for the 1/3 scale model bearing.

2.4 EARTHQUAKE RESTRAINER

Benten Viaduct is a long continuous rigid frame bridge which is expected never to fail again. The bridge also has a dumping function against the vibration of earthquake. Besides multiple earthquake restrainers were recommended by the specification [4] by the Ministry of Construction in 1995.

Earthquake restrainers were installed at both ends of the structure where the girders are supported by seismic isolators on ordinary rigid frame steel piers. They were designed to work for longitudinal direction when the displacement became more than the limit given by Ductility Design Method. The steel members of the restrainers were designed by Allowable Stress Design Method using a horizontal force as much as bearing capacity.

Also, for transverse direction, bearing restrainers were installed on the isolators. They were set 5 mm's away from the surface of the upper plate of bearing, and designed with the earthquake force used in Allowable Stress Design Method. This means that, the seismic isolator is usually restricted its displacement not to break the expansion joint on the road and will perform its seismic ability only during a strong earthquake.

3. CONSTRUCTION WORK

3.1 SUBSTRUCTURE WORK

Before the reconstruction project, bearing capacity (qd) of existing pile foundation was researched by means of corn penetrating test. Bearing capacity of 300 to 600 tf/m^2 was confirmed in most part, however, there still found some foundations which had only 150 tf/m^2 of qd. Therefore, these foundations had to be reinforced with adding piles, and the number of them were fourteen, which was 30% of the foundations among Benten section.

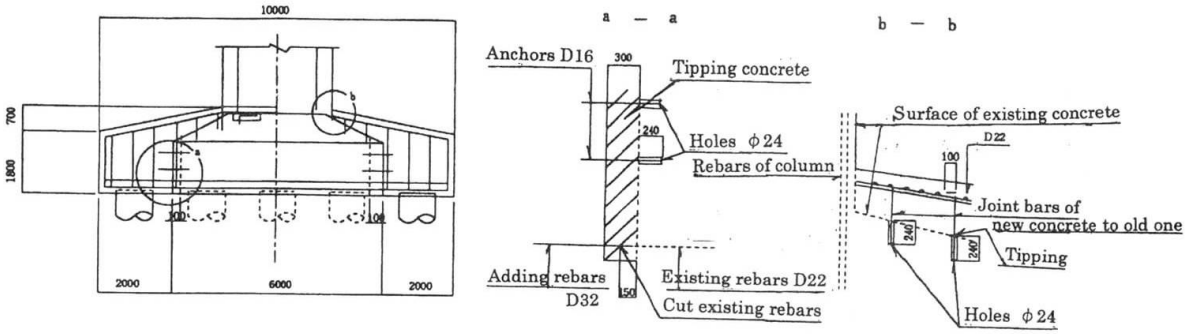

Fig 6 Reinforcement of Pile and Footing

As mentioned above, National Highway Route 2 was the only lifeline route to link the east and west part of Kobe., and the work site was located along the National Highway Route 2. Therefore, there were many controlling field dimensions which obliged the piling works to be took place ni stopping only two lanes ght and day out of six lanes. The location was so close from the downtown and/or residence area that many attentions were paid to save a vibration or noise from the piling work. The earth drill method and pile jacking with oil hydraulics were adopted regularly.

Also, the reinforced bars were jointed to the existing ones by means of enclosed arc welding. Details of reinforcement of footing are shown in figure 6.

3.2 SUPERSTRUCTURE WORK

The length of Benten Viaduct is as much as 686m, which causes ±28mm's expansions at both ends from the difference of temperature of ±10 degrees centigrade. To keep an adequate accuracy of erection, columns and cross beams were built up first. After that, plate girders with steel deck were erected measuring and correcting the errors at each pier points. The accuracy of erection was finally found to be less than 5 mm at the isolators point.

Camber for the dead load was solved statically with partial rigid frame model. It was found that a horizontal deformation of 3.2 to 4.7 mm would be caused by the influence of dead load. Since the actual stiffness of each member was supposed to be stronger than the designed one, the influence of camber on the isolators due to the dead load was ignored.

The steel piers were unstable on the soft seismic isolation bearings until they formed a three-dimension rigid frame. In the field work, a stabilizer system were invented as shown in photograph 2. This system was introduced to stabilize the columns before the erection of girder and deck, and it could save the accuracy of piers and bearings also. The stabilizer was designed to have a temporary horizontal bearing capacity against 0.15G.

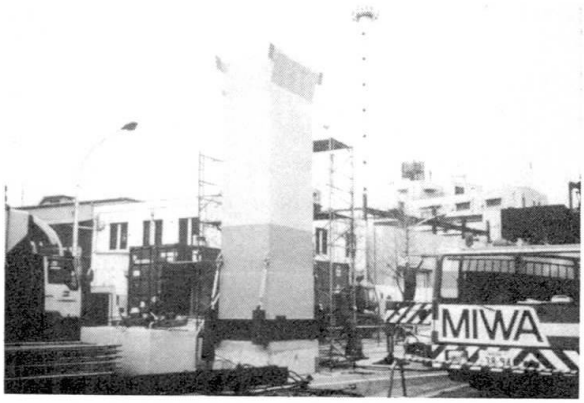

Photo. 2 Stabilizer System

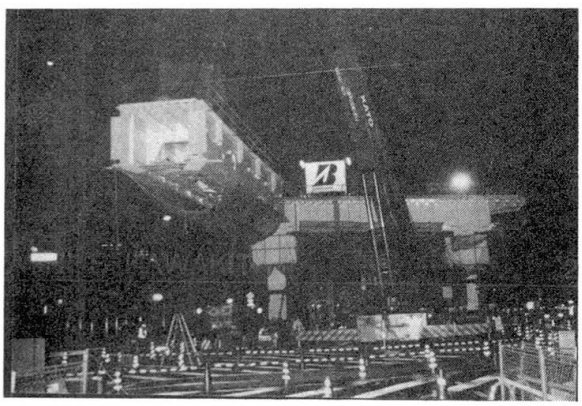

Photo. 3 Erection of Girder and Deck

3.3 ENVIRONMENTAL WORK

Various environmental works were also taken on the Benten Viaduct. For the effect of seismic isolators installed on the foot of piers, it was clarified by confirming test that the traffic vibration on the deck were not conveyed to the ground [5].

The low-noise pavement was introduced on the deck. The effects and durability have been investigated continuously.

Benten Viaduct also has aesthetic cover plates beneath the girder because Kobe municipal government had a plan to develop Benten section into a recreational area.

And more, advanced noise absorbers were adopted like other restored part of Kobe Route. It was installed on top of noise barriers to get the same effect as making noise barriers 1.5 to 2.0 higher.

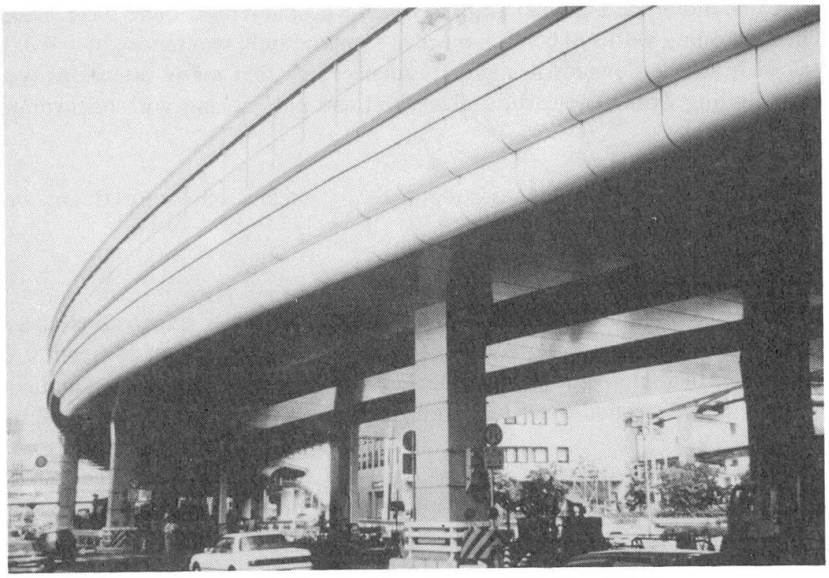

Photo. 4 Complete Structure of Benten Viaduct

4. CONCLUSIONS

Authors reported the outline of design as well as techniques taken on Benten Viaduct. Besides, a series of vibration test was carried out on the actual bridge and reported in another paper [5].

After those trial the viaduct could be completed and reopened on July 17, 1996. There were many new challenges in the designing method for this innovative structure and feasible actions for environment. Authors hope that it can be referred to another trial which will create a new style of bridge.

5. REFERENCES

[1] Japan Institute of Construction Engineering : Report on the Anti-seismic Design for Highway Bridge with Seismic Isolator
[2] HAYASHI, NARITA, MAEDA : Determination Method of Characteristic Values and Estimating the Plastic Deformation of seismic-Isolation Bridges, 3rd Colloquium on Vibration Control of Structures PART B, 1993
[3] Railway Technical Research institute, NAKAMURA : Seismic Vibration Report on The Hanshin Awaji Earthquake, 1995 and Its Analysis, JRVI,I Earthquake Report No.23c, 1995
[4] The Ministry of Construction : Guide Specifications for Reconstruction and Repair of Highway Bridges Which Suffered Damage due to the Hyogo-ken Nanbu Earthquake, to New Highway Bridges and Seismic Strengthening
[5] HAYASHI, KAWAKITA, NAKAHIGASHI, SANADA : Design of the 19-span continuous rigid frame bridge with seismic isolator, New Technologies in Structural Engineering, Lisbon, 1997

Heaving Branch Coupled Flutter for Long Span Bridge

Masaru MATSUMOTO
Prof.
Kyoto Univ.
Kyoto, Japan

Kazuo GOTO
Graduate Student
Kyoto Univ.
Kyoto, Japan

Tadahiro YABUTANI
Graduate Student
Kyoto Univ.
Kyoto, Japan

Kazuhiro ABE
Graduate Student
Kyoto Univ.
Kyoto, Japan

Summary

Flutter stabilization is the major subject to safely design a super long span bridge. Unsteady aerodynamic force, in other word, 8 aerodynamic derivatives, (H_i^*, A_i^*, i=1~4) defined by R. H. Scanlan are significantly important for flutter occurrence. Especially, aerodynamic derivative, A_2^*, showing negative and small value, torsional flutter doesn't occur and coupled flutter stabilize. A_2^* of the rectangular cylinder with vertical plate installed at the mid-chord point of rectangular cylinder with the slenderness ratio, B/D=20, showing negative and the smallest, this section doesn't have highest flutter onset velocity. Furthermore, heaving branch flutter occurs. This paper aims to clarify this mechanism of the heaving branch flutter and the relation between torsional brunch flutter and heaving brunch flutter.

1. Background of this study

The rectangular cylinder with vertical plate and the stable fundamental geometrical shape are shown in Fig.1[1]. Through wind tunnel test under the heaving/torsional 1DOF forced vibration, unsteady pressure around these sections is measured from pressure taps. 8 aerodynamic derivatives are shown in eq.1[2].

$$L = \frac{1}{2}\rho(2b)U^2\left\{kH_1^*\frac{\dot{\eta}}{U} + kH_2^*\frac{b\dot{\phi}}{U} + k^2H_3^*\phi + k^2H_4^*\frac{\eta}{b}\right\} \quad (1)$$

$$M = \frac{1}{2}\rho(2b^2)U^2\left\{kA_1^*\frac{\dot{\eta}}{U} + kA_2^*\frac{b\dot{\phi}}{U} + k^2A_3^*\phi + k^2A_4^*\frac{\eta}{b}\right\}$$

where, L,M:lift and pitching moment per unit length, η, ϕ :heaving and torsional displacement,U:wind velocity, ρ :air density, b:half chord length (=B/2) k:reduced frequency (=b ω/U), ω :circular frequency

These aerodynamic derivatives are calculated through the integration around sections. A_2^* which is the damping term in torsional 1DOF vibration is shown in Fig.2[3]. This derivative is important factor of torsional flutter and coupled flutter. As shown in Fig.2, A_2^* of rectangular cylinder with V.P. is negative and the smallest, therefore this section has the great advantage for torsional flutter and coupled flutter. Furthermore, aerodynamic unsteady force are expressed as shown in eq.1, flutter analysis is conducted. This result is shown in Fig.3[3].

This result indicates that flutter characteristics of rectangular cylinder with V.P. is inferior to that of flat diamond shape box section and flutter of rectangular cylinder with V.P. is heaving branch flutter.

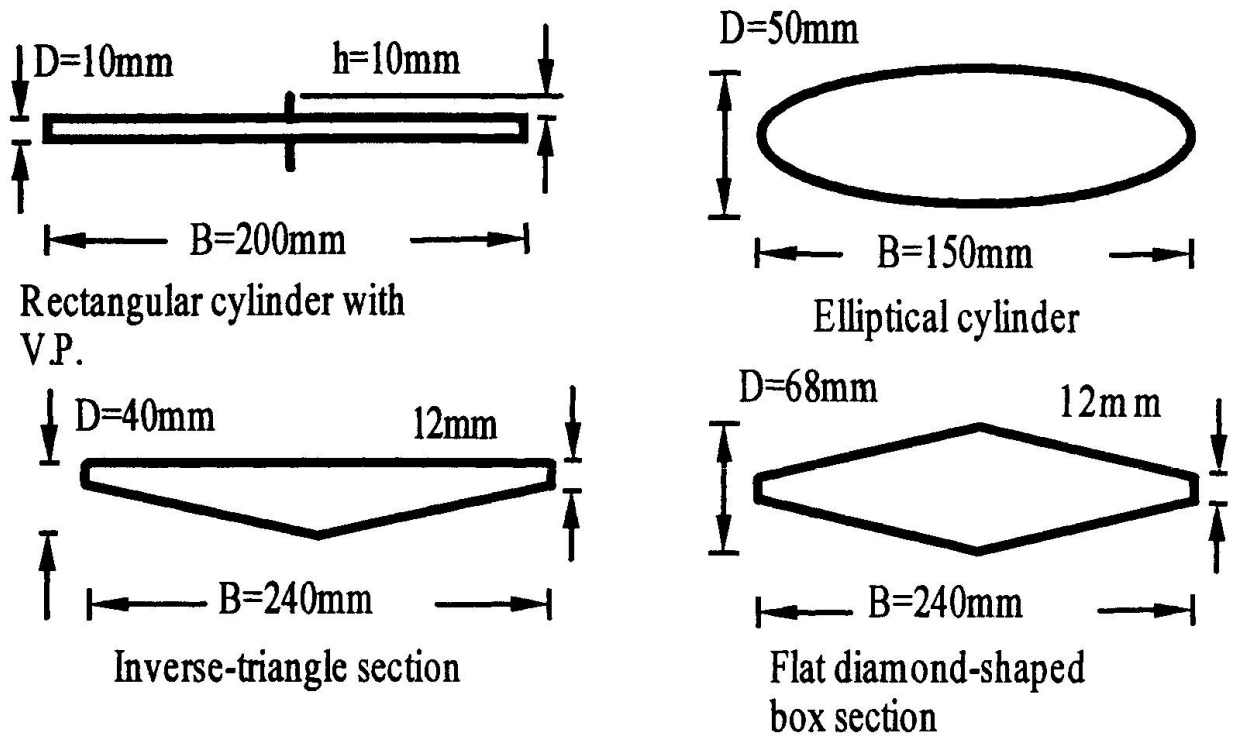

Fig.1. Some deck sections

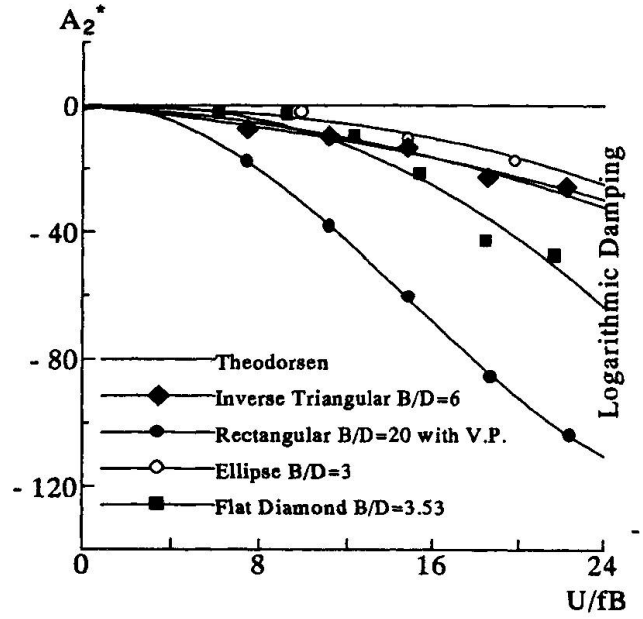

Fig.2 Aerodynamic Derivative A_2^*

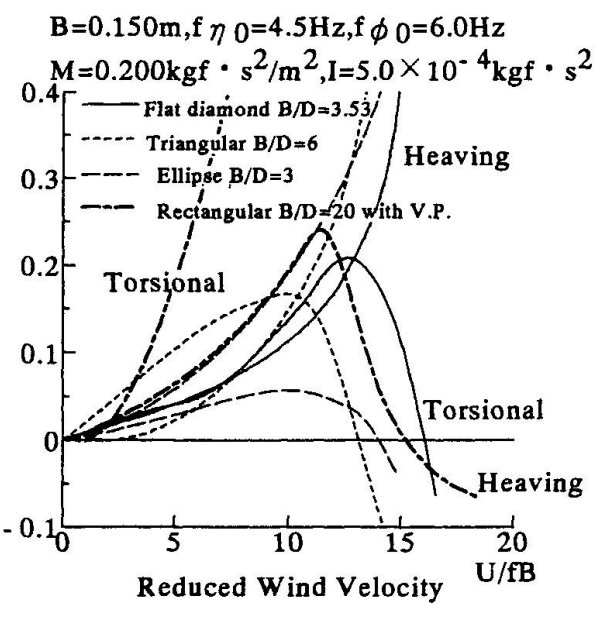

Fig.3 V- δ diagram (Complex eigenvalue analysis)

2. Heaving-Branch Flutter Mechanism

Fig.4 shows flutter characteristics of the rectangular cylinder with V.P. obtained by complex eigenvalue analysis. As shown in Fig.4, the natural frequency of heaving motion being smaller than the natural frequency of torsional one, heaving branch flutter occurs instead of torsional one. In the Velocity-Frequency diagram, it should be noted that two frequency curves, namely heaving and torsional frequencies, cross each other at certain reduced velocity, as for torsional branch flutter, these two frequency curves never cross each other. Around this velocity, the heaving branch flutter occurs. The facts suggest that some relations exist between flutter instability and this frequency crossing.

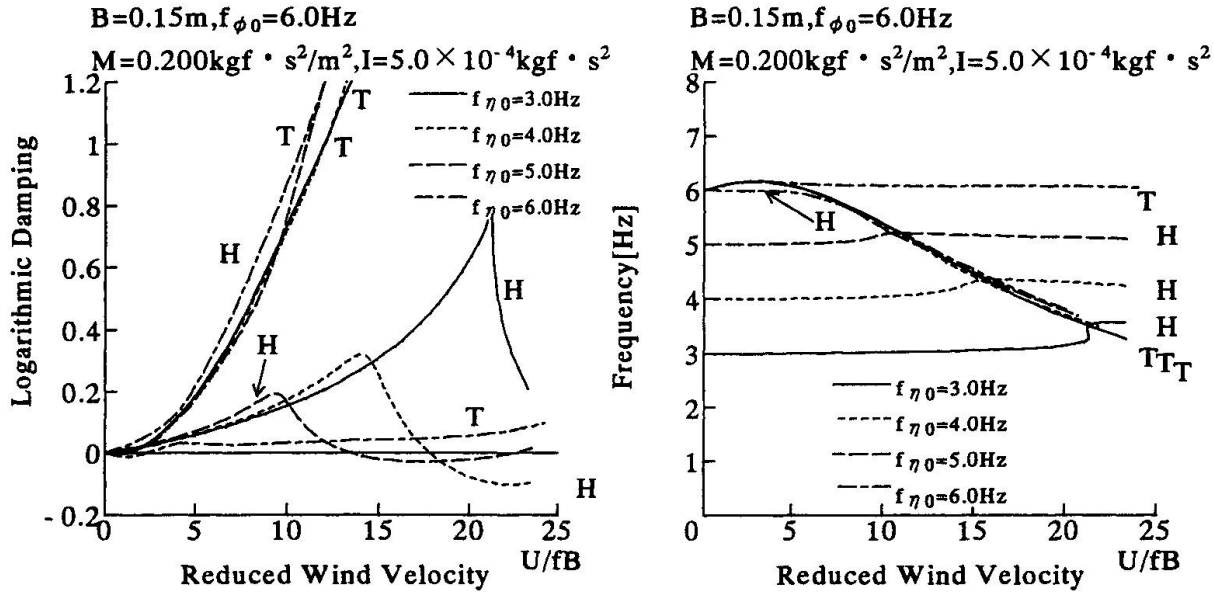

Fig.4 Flutter characteristics of the rectangular cylinder with V.P.

Based on "The step-by-step analysis" which can clarify the each role of aerodynamic derivatives on the flutter instability, the aerodynamic damping for heaving branch is given by following formula[3]:

$$\delta_\eta = -\pi\left(\frac{\rho b^2}{m}\right)H_1^* - \pi\left(\frac{\rho b^2}{m}\right)\frac{(\rho b^4/I)(\omega_\eta/\omega_\phi)^2}{\sqrt{\{1-(\omega_\eta/\omega_\phi)^2\}^2+4\zeta_\phi^2(\omega_\eta/\omega_\phi)^2}}\times \tag{2}$$

$$(|A_1^*|H_2^*\cos\theta_1+|A_4^*|H_2^*\cos\theta_2-|A_1^*|H_3^*\sin\theta_1-|A_4^*|H_3^*\sin\theta_2)$$

where, δ_η is logarithmic decrement for heaving branch and ω_ϕ is torsional frequency.
This analysis is shown in Fig.5. Fig.5 indicates that the aerodynamic damping decreases according to the decrease of the component ◆ (-①②| A_1^*| $H_3^*\sin\theta_1$) with reduced velocity. Therefore, this component plays a significant role of flutter excitation. Around the flutter onset velocity, | A_1^*| H_3^* keeps negative value, and also $\sin\theta_1$ changes from negative to positive (see Fig.6), then, this component ◆ (-①②| A_1^*| $H_3^*\sin\theta_1$) turns from negative to positive.

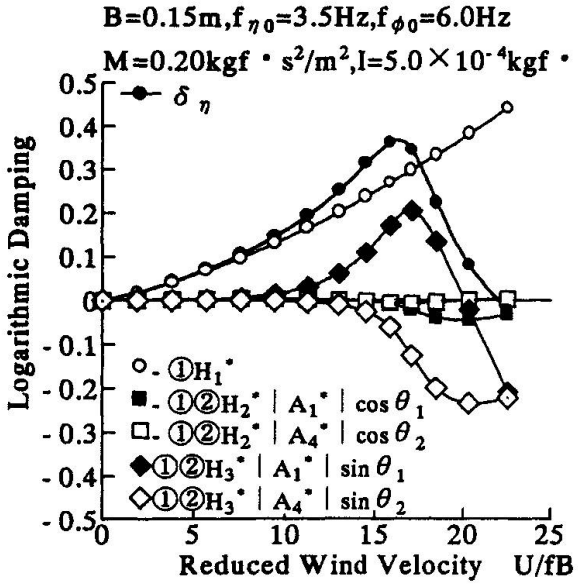

Fig.5 V-δ diagram (Step-by-step analysis)

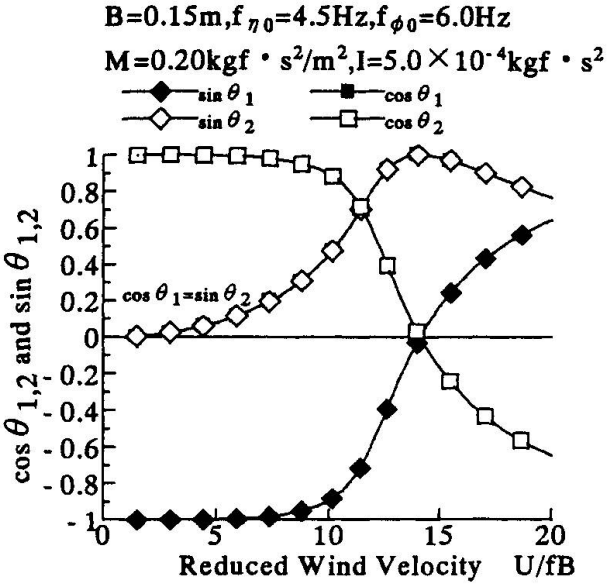

Fig.6 V-sin θ$_1$ diagram

The phase lag of torsional motion to heaving motion, θ$_1$, is expressed by folllowing equations:

$$\theta_1 = \theta - \frac{\pi}{2},\ \sin\theta_1 = -\cos\theta,\ \theta = \tan^{-1}\frac{2\xi_\phi\omega_\eta\omega_\phi}{\omega_\phi^2 - \omega_\eta^2} \tag{3}$$

θ moving from first quadrant to second one, the sign of sin θ$_1$ changes (see Fig.7). The Velocity-Frequency diagram obtained by the step-by-step analysis is shown in Fig.8. As shown in Fig.8, the torsional frequency decreases with reduced velocity, on the other hand, the heaving frequency keeps almost constant value, and then, the crossing point between these two frequencies exists. Because of this crossing, the sign of θ changes as shown in eq.3. As the result that, the component ◆ (-①②| A$_1$*| H$_3$*sin θ$_1$) decreases and the total aerodynamic damping of heaving branch becomes negative value, which means the heaving branch becomes aerodynamically unstable. Thus, it is concluded that the heaving branch flutter becomes unstable because of the crossing of frequency curves.

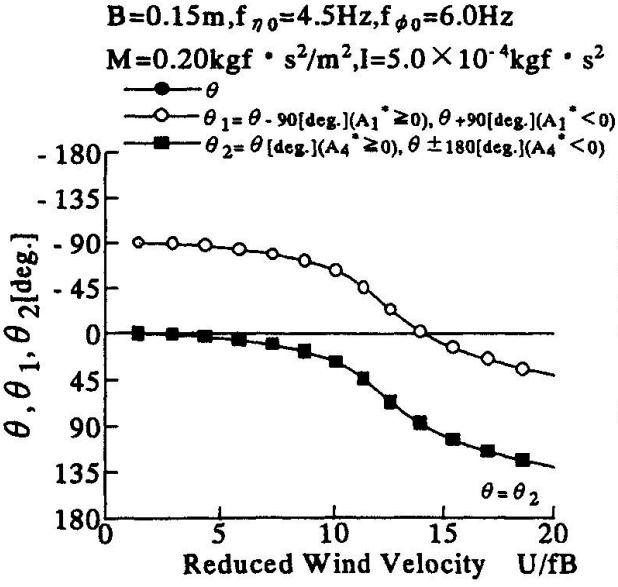

Fig.7 V-θ diagram

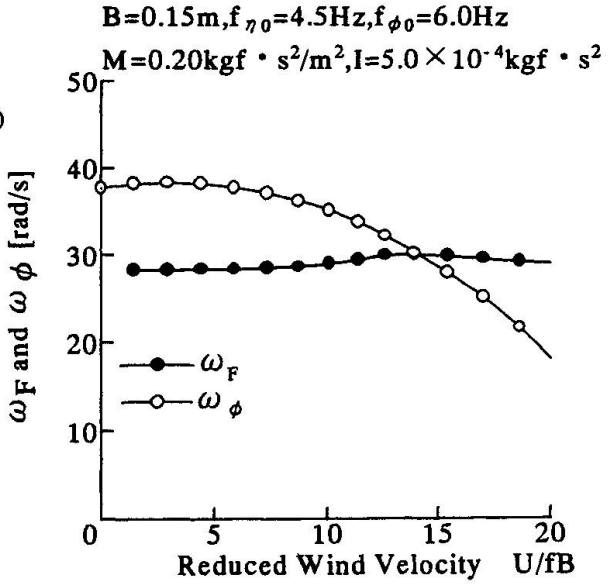

Fig.8 V-ω diagram

For Fig.4, it becomes clear that the flutter onset velocity of heaving branch is controlled by the reduced velocity of the crossing point. Therefore the lower natural frequency of heaving motion leads the higher flutter onset velocity of heaving branch.
The reason why heaving branch becomes unstable earlier than torsional one can be explained as follows. In general, the smaller aerodynamic derivative A_2^* makes the higher flutter onset velocity for torsional branch. A_2^* of the rectangular cylinder with V.P. being the smallest in Fig.2, this section is most stable for conventional coupled flutter. In this section, however, the heaving branch flutter occurs instead of torsional one. It is likely that this section is stable for torsional branch, in return, the heaving branch becomes unstable. To clarify the effect of A_2^*, this derivative being three times as large as the value of the thin airfoil theory by T.Theodorsen, the coupled flutter is controlled by the heaving branch (see Fig.9,10). Therefore, one of the conditions for the heaving branch flutter is considered that A_2^* has large negative value.

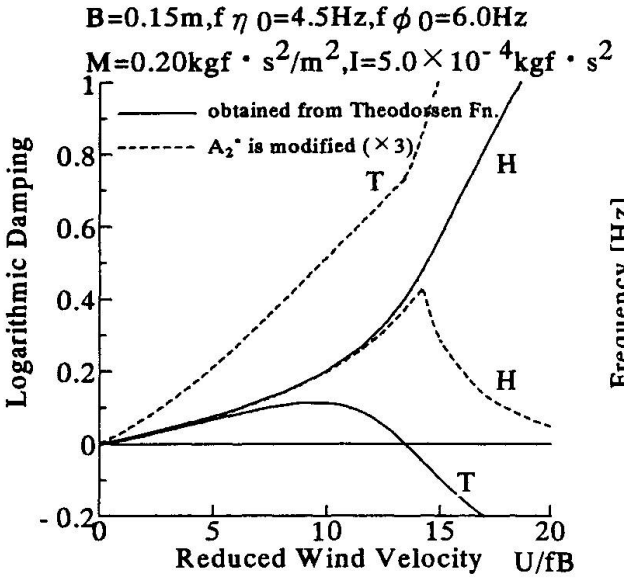

Fig.9 V-δ diagram (Complex eigenvalue analysis)

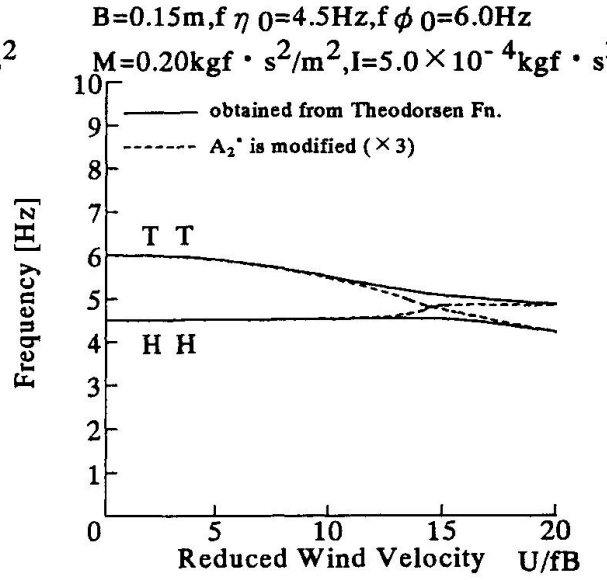

Fig.10 V-f diagram

3. Conclusion

The conclusions obtained in this study are summarized as follows:

(1) It is revealed that some relations between the flutter instability for heaving branch and the characteristic of frequency exist in case of the rectangular cylinder with V.P..
(2) It is possible that A_2^* having large negative value, the heaving branch flutter occurs lower velocity than the torsional one.

Reference

[1] M.Matsumoto, Hamasaki: Flutter stabilization of super long bridges, the 5th East Asia-Pacific Conference on Structural Engineering and Construction (WASECV), (Australia), pp1141-1146, 1995
[2] R.H. Scanlan and J.J Tomko, "Airfoil and bridge deck flutter derivatives", Journal of ASCE,EM6, 1971

[3] M.Matsumoto,Y.Kobayashi, Y.NIihara, H.Shirato and H.Hamasaki: Flutter mechanism and its stabilization of bluff bodies, Proc. of the 9th ICWE(Wind Engineering),New Delhi. 1995

Long Term Performance of Anti-Corrosion Method Using Titanium Clad Steel

Shunichi NAKAMURA
Dr Eng.
Tokai Univ.
Hiratuka, Japan

Koji HOMMA
Dr Eng.
Nippon Steel Corp., Steel Struct. Dev. Center
Futtsu, Chiba, Japan

Summary

A new anti-corrosion method using titanium clad steel plates has been developed and applied to the splash and tidal zones of steel piers. Titanium clad steel plates consist of 1 mm thick titanium plates and 4 mm thick steel plates and are welded to the steel piers. Steel pipes with diameter of 60cm using this anti-corrosion method have been tested and monitored in the actual marine environment for the last five years. The monitoring results show that no corrosion has been found on the titanium clad plates and prove that the new method has sufficient long term durability.

1. Structural forms of the new anti-corrosion method

It has been thought that titanium has excellent anti-corrosion resistance, but it is too expensive to be used for the actual structure. However, we have developed relatively inexpensive titanium clad steel plates, invented a new anti-corrosion method for the splash and tidal zones of steel piers using this material. Titanium clad steel plates consist of 1mm thick titanium plates and 4mm thick steel plates and are welded to the surface of steel piers by TIG welding. Various experiments have been carried out to investigate basic strength and behaviors of this new method, such as mechanical strength of clad plates, electro-chemical effects of electrolytic corrosion, weldability and paintability on clad plates. These tests have all shown satisfactory results. This new method has also shown economical competitiveness compared with other anti-corrosion methods for the severe marine environment, and has therefore been adopted for the steel piers on the Trans-Tokyo Bay Bridge(see fig.1, fig.2 and fig.3), one of the national projects in Japan. We have watched these actual steel piers since they were constructed three years ago, and at the same time we put the test pipes, on which this new anti-corrosion method were applied, into the sea water and monitored for the last five years to investigate the long term durability of this new system.

2. A test on long term durability of the new method

Steel pipes with diameter of 60 cm using this anti-corrosion method have been tested in the actual marine environment for the last five years (see fig.4). The behavior of these prototype specimens have been monitored by observing the thickness change, the electrolytic potential, the electric current from a sacrificial aluminum anode and the surface condition. The steel pipe specimens are covered with the titanium clad steel plates between 1 m above high water level and 1 m below low water level (The length is 4 m). Other than the titanium clad part, the steel pipes in the atmosphere are protected by a heavy duty coating system using fluorocarbon resin and the steel pipes in the sea water are protected by cathodic protection using aluminum anodes.

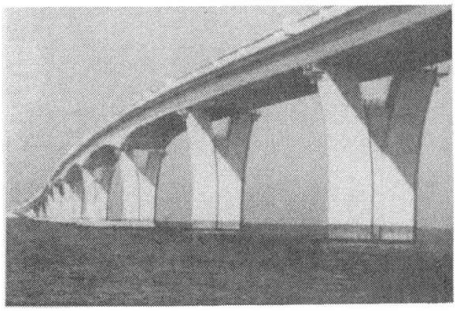

Fig. 1 Trans-Tokyo Bay Bridge

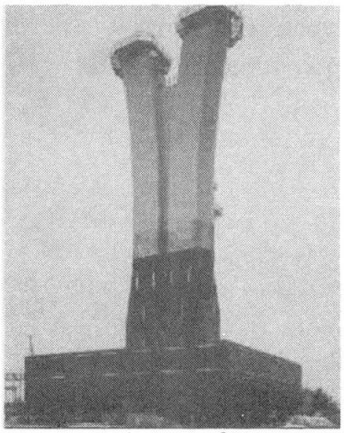

Fig. 2 Steel pier of Trans-Tokyo Bay Bridge

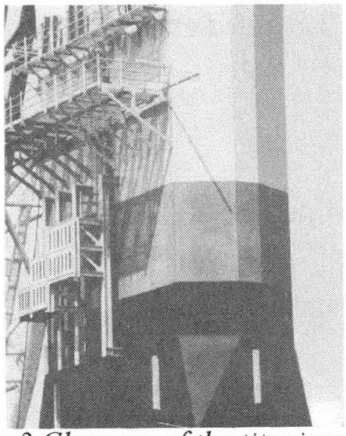

Fig.3 Close-up of the titanium clad part

Fig.5 shows the cross section of titanium clad part after the exposure period. No thickness reduction was observed not only in the titanium clad steel plates, but also in the steel pile adjacent to the titanium clad steel plates(see fig.6). The countermeasures against electrolytic corrosion were the heavy duty coating in the upper boundary in the atmosphere and the cathodic protection using an aluminum anode in the lower boundary in the sea water. Fig.7 shows the change of electric current from an aluminum anode. It was observed that the electric current was settled and the cathodic protection of steel pipe with titanium clad worked successfully.

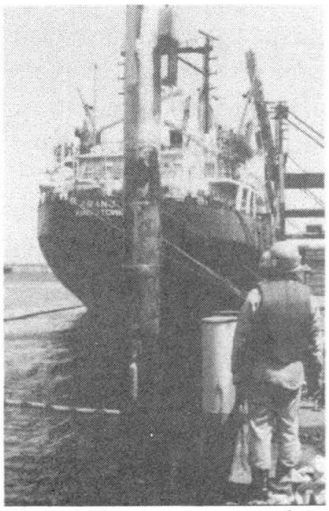

Fig. 4 Exposure test of specimens (when lifted)

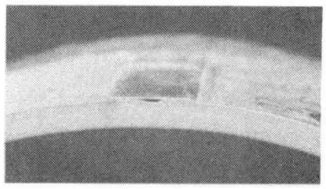

Fig.5 Cross section of specimen

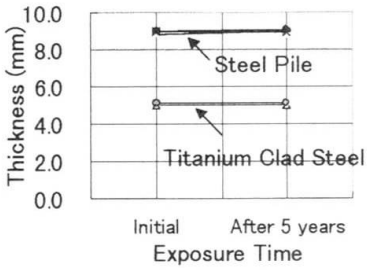

Fig.6 Change of thickness during 5 years

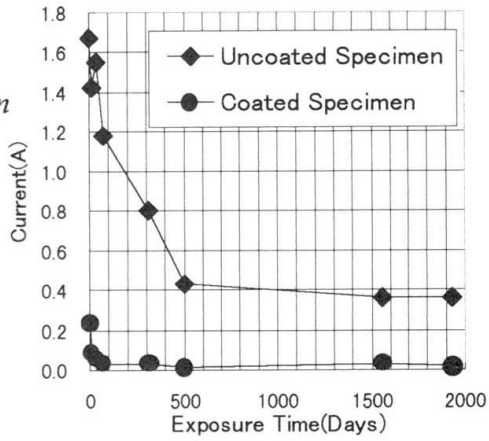

Fig.7 Change of current from a sacrificial aluminum anode

The monitoring results show that the titanium clad steel is perfectly healthy, and electrolytic corrosion does not occur in both upper and lower boundary areas between the steel pipe and the titanium clad part. Therefore, it was confirmed that the titanium clad showed an excellent anti-corrosion property and that the countermeasures against electrolytic corrosion were effective through the actual exposure test.

Effects of the Hyogo-Ken-Nanbu Earthquake on the Akashi Kaikyo Bridge

Atsushi GOTO
Eng., Third Design Div.
Honshu-Shikoku Bridge Authority
Kobe, Japan

Atsushi Goto born in 1964. He graduated from Civil Eng. Dept of Gifu National College of Technology in 1984.

Toshimi MORITANI
Mgr, Third Design Div.
Honshu-Shikoku Bridge Authority
Kobe, Japan

Toshimi Moritani born in 1950. He graduated from Civil Eng. Dept of Gifu Univ. in 1973.

Toshihiro KURIHARA
Dep. Mgr, Third Design Div.
Honshu-Shikoku Bridge Authority
Kobe, Japan

Toshihiro Kurihara born in 1953. He graduated from civil Eng. Dept of Oita National College of Technology in 1974.

Summary

The Hyogo-ken-Nanbu Earthquake of 17 January 1995 (magnitude 7.2) caused devastation in the city of Kobe and surrounding areas. After the earthquake, the Akashi Kaikyo Bridge(approximately 4km long suspension bridge with a center span of 1990m) located a few kilometers away from the epicenter, which was at that time under construction, was inspected but apart from the change in span length that occurred as a result of fluctuation of the sea bed, no damage was found in the bridge structure. Records obtained from velocity meters installed on the towers indicated that the acceleration response at the top level of the towers was approximately 1,100 gals at transverse to the bridge axial direction. Further, measurements of settlement in the foundation ground showed that the ground under tower 2P subsided by about 20 mm.

This information was used to check the post-earthquake soundness of the bridge structure. Unfortunately, earthquake records from which to estimate the actual input earthquake motion were unavailable. Thus, the input motion was estimated from records taken in areas surrounding the bridge and from the velocity meter readings. A response analysis method incorporating the latest findings, such as the dependence of the ground on strains, was used to analyze the bridge. This procedure demonstrated the post-earthquake soundness of the bridge and also revealed information about the bridge's earthquake resistance after completion.

1. Occurrence of the Earthquake

Ever since work commenced in 1986, the bridge has been scheduled for completion by the end of fiscal 1998. At the time of the earthquake, the substructures and towers had been completed, the strands of the main cables had all been installed, and cable squeezing work to round the cable cross section was underway, ready for erection of the stiffening girders.

2. Earthquake Records at the Bridge

No significant records were obtained from seismographs installed near the bridge for design and construction purposes. However, velocities were recorded by meters installed at the top and at the mid-points of the towers; they had been fitted to facilitate the measurement of wind-induced vibrations.

These records indicated that the maximum instantaneous velocity at the tower tops exceeded 100 kines. In terms of acceleration, this represents a maximum acceleration of about 1,100 gals.

3. Results of Inspections and Surveys after the Earthquake

No damage was found in the bridge structure members, such as the anchorages, tower foundations, towers or cables. However, because of fluctuation of the sea bed where the foundation was installed, the center span length increased by approx. 80cm, and the span length on the Awaji Island side increased by approx.30cm. Moreover, ground subsidence of approx.20mm was confirmed in the 2P foundation ground.

4. Effects of Displacement of Foundation and Measures

Based on the results of inspections and surveys mentioned above, investigations were carried out on additional stresses that arise as a result of the displacement of the foundation, and the corresponding measures to be adopted. Results demonstrated that the additional stresses in the cables, main tower foundations, and tower-top saddles were within allowable limits. To cope with the change in bridge shape caused by the relative displacement of the foundations, including the changes in span, stiffening girder lengths were increased — 80 cm was added to two panels in the central span and 34 cm to an anchorage end panel in the Awaji side span.

5. Earthquake Response Analysis

In designing the bridge, the design input earthquake motion was taken to be that resulting from a marine earthquake of magnitude about 8.6. To complement this, the stochastically evaluated motion of a magnitude 6.0 or greater earthquake within a radius of 300 km of the bridge was also considered. However, the motion caused by this strong local earthquake exceeded these input motions assumed in the design of the bridge.

Subsequently, earthquake response analysis was carried out to elucidate bridge behavior during the earthquake, evaluate the post-earthquake soundness of the bridge, and obtain data on the earthquake-resistance of the completed bridge. This analysis entailed consideration of the following scenarios: the foundation system alone; the bridge system while under construction; and the bridge system after completion.

Since records yielding direct estimates of the input earthquake motion are unavailable, the inputs used in the analysis were estimated from records collected in the vicinity of the bridge as well as from the velocity meter readings.

In analyzing the foundation system, it was necessary to take into account the magnitude of the input earthquake motion, the dependence of the ground on strain, and nonlinearities arising through separation of the foundations from the ground. To accomplish this, the modified R-O model was used to obtain the dependence of the ground on strain and a nonlinear spring was used between the foundations and the ground to take separation into account. For the analysis of the completed bridge system, the spring between foundations and the ground was evaluated and the effects of TMDs in the towers were also studied.

The results of this analysis demonstrated the soundness of the bridge in its under-construction state when the earthquake struck, while also providing data about the bridge's earthquake resistance once it is complete.

Configuration Analysis of a Self-Anchored Suspension Bridge

Sung-Pil CHANG
Prof.
Seoul National Univ.
Seoul, Korea

Ho-Kyung KIM
Assist. Prof.
Mokpo National Univ.
Mokpo, Korea

Myeong-Jae LEE
Senior. Research Eng.
Samsung Corp.
Seoul, Korea

Summary

A mono-duo self-anchored suspension bridge is in construction for the crossing of the highway and the railway line between Seoul and the new airport. Contrary to a typical suspension bridge, large axial force is introduced in the stiffening truss of a self-anchored suspension bridge under the dead load state. An algorithm is developed to consider the initial forces of frame members in establishing the initial equilibrium state of a self-anchored bridge. This algorithm utilizes an auto-iterative technique. Based upon an application, it is found that the initial-force-included configuration analysis is necessary for a self-anchored suspension bridge for the proper control of the construction.

1. Initial Configuration of a Self-anchored Suspension Bridge

Contrary to a typical suspension bridge, large axial force is introduced in the stiffening truss of a self-anchored suspension bridge due to the dead load. Consequently the cable anchorages and the tower tops of a self-anchored suspension bridge go through displacement along the bridge axis in the nonlinear equilibrium state analysis under dead load (see fig 1). For this reason, it is difficult to form the aiming configuration of a self-anchored suspension bridge with only the conventional method for an earth-anchored suspension bridge. In order to control the changes of the boundary conditions of the main cable, it is necessary to consider initial axial forces in calculating the unbalanced force caused by the bridge self-weight.

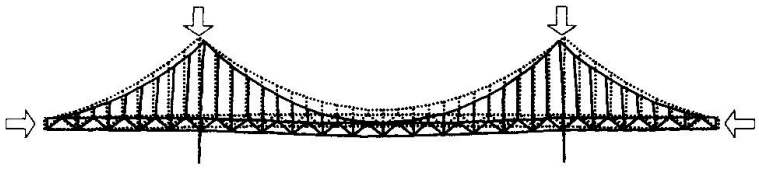

Fig. 1 Dead load deformation due to large axial force

2. Auto-iterative Nonlinear Configuration Analysis

As a prerequisite to the final configuration analysis, strict configuration analysis has been carried out only for the cable net system including the main cables and hangers. The three dimensional elastic catenary cable element has been used in the mathematical modeling of the bridge. The exact configuration of the main cable can be defined by suggested auto-iterative trial-and-error method based on the given design parameters.

An auto-iterative algorithm is developed to consider the initial forces of the frame members in establishing the initial configuration of a self-anchored bridge. This algorithm is based on the geometric nonlinear analysis using Modified Newton-Raphson method and an iterative trial-and-error algorithm is added for the convergence of the final configuration of the total bridge.

3. Application and Effectiveness

The nonlinear configuration analysis has been performed for a self-anchored suspension bridge in Korea which is in construction. It consists of 3 spans of 125m-300m-125m. It has A-shaped towers and a mono-duo cable system sagged horizontally as well as vertically (see fig 2). The mathematical modeling of the bridge is shown in fig 3.
Table 1 shows the importance of the initial-force-included configuration analysis. It can be easily found that the suggested algorithm reduces the difference considerably between the design (target) and the final (result of configuration analysis) configuration.
The determined mathematical model can be used effectively not only for the nonlinear live load analysis or dynamic analysis but also for the nonlinear backward-step construction stage analysis for the prediction of the unstrained member length or the camber control.

Table 1 Result of the configuration analysis

	Description		Design (a)	Conventional Method (b)	Presented Method (c)	Relative Error (%)*
Displ. (cm)	End Link	Δx	0	5.253	0	0
	Top of Tower	Δx	0	8.295	0	0
		Δz	0	6.748	0	0
	Main Cable Anchorage	Δx	0	5.512	0	0
		Δz	0	-0.451	0	0
	Sag of Main Cable	fz	60	60.207	60	0
		fy	13.576	13.573	13.579	-
Tension (ton)	Main Cable (Horizontal)	max.	4842	4453	4840	0.5
		min.		4459	4840	0.5
	Hanger (mid-span)	max.	322.3	293.2	326.8	15.5
		min.	307.6	273.0	307.6	0
	Hanger (side-span)	max.	323.7	295.7	328.0	15.4
		min.	308.8	272.3	308.1	1.9

*) Relative Error = $|\{(c)-(a)\}/\{(b)-(a)\}| \times 100\%$

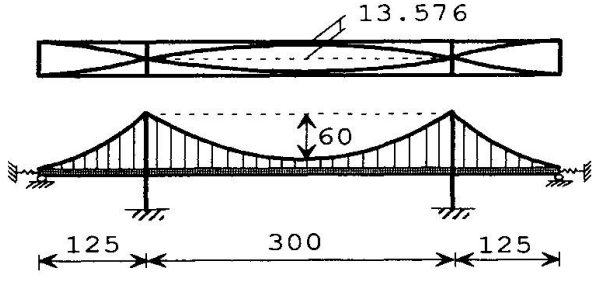

Fig. 2 A Self-Anchored Suspension Bridge

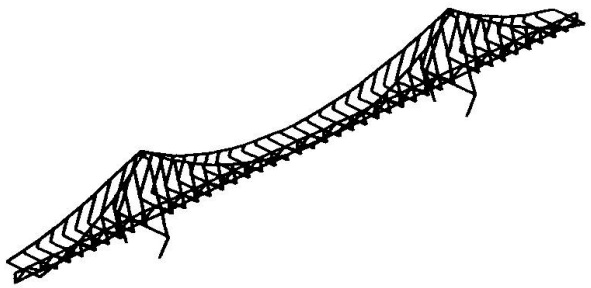

Fig. 3 Mathematical Model

Seismic Behaviour of Long-Span Cable-Stayed Bridges

Li-Chu FAN
Prof.
Tongji Univ.
Shanghai, China

Li-chu Fan, born 1933, received his bridge engineering degree form Tonji Univ. in 1955. Deputy director of academic committee, State Key Laboratory for Disaster Reduction in Civil Engineering.

Shi-de HU
Prof.
Tongji Univ.
Shangahi, China

Shi-de Hu, born 1942, graduated from Tonhji Univ. in 1965. She is the Chief of the Bridge Eng. Division.

Summary

Seismic studies of three of long-span cable-stayed bridges crossing Huangpu River in Shanghai were performed by our research group of State Key Laboratroy for Disaster Reduction in Civil Engineering. The effect of transverse restraint of auxiliary piers on seismic response of Xupu Bridge structure is investigated and discussed. The disaster lessons of Higashi Kobe Bridge during the Kobe earthquake is also discussed.

1. Bridge Description

Nanpu Bridge: Composite cable-stayed bridge, Spans:76.5+94.5+423+94.5+76.5m.
Yangpu Bridge: Composite cable-stayed bridge, Spans:99+144+602+144+99m.
Xupu Bridge: Hybrid* cable-stayed bridge, Spans:2@40+3@39+45+590+45+3@39+2@40m..
* The girder is a mixed structures composed of steel in the center span, no bearings are used in the main span, only sliding bearings are provided at extreme pier and/or auxiliary piers.
For Nanpu and Yangpu Brisges, two auxiliary piers are located in the both side span at 94.5m and 144m away from the tower, respectively. For XupuBridge there are four auxiliary piers in the both side span.

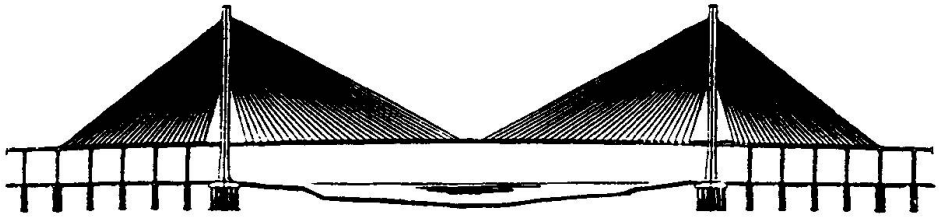

Fig.1 Elevation of Xupu Bridge

2. Lateral Seismic response of Side Piers and Auxiliary piers.

In order to investigate the effect of transvers restraint of auxiliary piers on seismic response of structures four cases are considered:

Case	Seismic Response	Side Pier #1	#2	Auxiliary #3	Pier #4	#5	Tower
I	Relative Displacement	166	0	0	0	0	0
	Bending Moment	3.71×10^4	1.51×10^5	1.19×10^5	8.84×10^4	5.77×10^4	4.46×10^5
II	Relative Displacement	512	392	0	176	0	
	Bending Moment	3.68×10^4	2.94×10^4	3.26×10^5	2.95×10^4	2.70×10^5	5.55×10^5
III	Relative Displacement	522	402	0	183	97	
	Bending Moment	3.67×10^4	2.92×10^4	3.33×10^5	2.94×10^4	2.95×10^5	5.91×10^5
IV	Relative Displacement	440	345	250	162	88	
	Bending Moment	3.41×10^4	2.68×10^4	2.70×10^5	2.74×10^4	2.73×10^5	6.94×10^5

From this analytical results it can be found that the lateral seismic force will be shared by side pier and auxiliaty piers when the transverse restrain all existed between the top of auxiliary piers and girder.

3. The Disaster Lessons of Higashi Kobe Bridge

The Higashi Kobe Bridge located in Kobe city, is a steel cable-stayed bridge with double deck. The center span of the bridge is 485m. The pendel type bearing pin at the end chore pier in bridge side sapn on Kobe side have dropped off(Fig. 2). It seems that the main cause is the effects of combine action by vertivcal and transverse earthquake shaking.

Generally, the pendel type bearing at the anchored pier is designed to restrain displacement in the longitudinal and withstand the vertical up-action but no to withstand the seismic force in the transverse direction. In transverse seismic response analysis of Yangpu Bridge, we found that the transverse seismic response of anchored pier is very large, therefore, a steel bar of which the ultimate tension force is 2000KN is erected between the top of anchored pier and main girder.

For cable-stayed bridges, under the longitudinal seismic action the bottom sections of tower are critical, under the lateral seismic action the critical section will appear at the bottom of anchor pier and/or auxiliary piers. Therefore, the designer must pay great attention to out-plane seismic response analysis for long-span cable-stayed bridges.

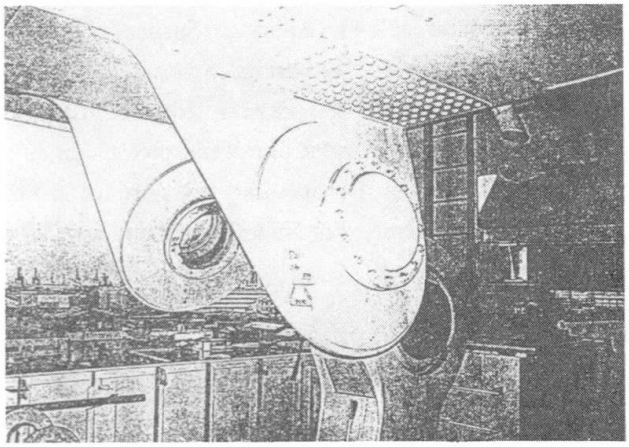

Fig. 2 Higashi-Kobe Bridge damage of pendel type bearing